SUM4Re

Creating materials banks
from digital urban mining

D10.1 Strategic planning and data collection report part 1

VERSION 1.0

28 October 2025

PUBLIC

Associated with document Ref. 101129961

Funded by the European Union. Views and opinions expressed are however those of the author(s) only and do not necessarily reflect those of the European Union. Neither the European Union nor the granting authority can be held responsible for them.

Funded by the European Union

SUM4Re

Creating materials banks from digital urban mining

Deliverable ID	10.1
Deliverable name	Strategic planning and data collection report part 1
Lead partner	TECN
Contributors	MOYUA, UVIGO, OLAR, EAGLE

PUBLIC

Funded by the European Union

DOCUMENT INFORMATION

Document name	D10.1 Strategic planning and data collection report part 1
Version	1.0
Due date	31/10/2025
Report date	28/10/2025
Number of pages	108
Lead Author	Jose Carlos Jimenez Fernandez (TECN)
Other Authors	Pablo J. Arauzo (OLAR), Jesús Balado (UVIGO), Jon Ander Iturrioz (TECN), Ourania Patsia (EAGLE)
Dissemination level	Public

REVISION HISTORY

Rev.	Date	Description of revision
0.1	01/10/2025	Initial draft version
0.2	16/10/2025	Revised draft version
1.0	28/10/2025	Final version (approved)

DOCUMENT APPROVAL

Written	Jose Carlos Jimenez Fernandez (TECN)	01/10/2025
Revised	Francisco Senna Vieira (VTT), Emil Lindberg (NORSKE)	15/10/2025
	Ana Sánchez (UVIGO)	28/10/2025
Approved	Pedro Arias Sánchez (UVIGO, Project Coordinator)	28/10/2025

EXECUTIVE SUMMARY

Deliverable D10.1 (Task 10.1) reports on the definition, preparation and initial validation of the SUM4Re pilot demonstration strategy. It establishes the methodological framework, site selection, instrumentation plans and evaluation protocols that will guide the implementation of pilot activities across SUM4Re. This work is central to work package (WP) 10, as it translates the technological advances of WPs 2–9 into real-world environments, enabling validation under operational conditions and supporting the project's exploitation pathway.

The initial phase of the deliverable focused on pilot site characterisation. Candidate infrastructures were surveyed in collaboration with local stakeholders, including transport authorities, contractors and facility managers. The final selection includes both civil engineering assets and building-scale rehabilitation sites, ensuring a diverse representation of use cases. Each site was mapped in terms of geometry, material composition, environmental exposure and accessibility. Stakeholder workshops were conducted to align monitoring needs, rehabilitation strategies and regulatory requirements.

The second phase concentrated on the preparation of pilot instrumentation and data acquisition strategies. For each site, a tailored sensor deployment plan was developed, combining fibre optic sensing (FOS), MEMS-based accelerometers, and vision-based inspection systems. Data management workflows were also designed, ensuring interoperability with the SUM4Re data lake and compliance with FAIR principles. Risk assessments and health and safety protocols were established in collaboration with site operators, with special attention to installation constraints in operational environments.

The third phase outlined the validation and evaluation methodology. A phased implementation roadmap was produced, starting with baseline monitoring, followed by intervention stages (rehabilitation or retrofitting) and concluding with post-intervention evaluation. This roadmap ensures traceability of results and comparability across pilots.

GLOSSARY

Terms, Abbreviations, and Acronyms

AI	Artificial Intelligence
AR	Augmented Reality
BIM	Building Information Modelling
C-BIM	Circular-BIM
CIELAB	CIE 1976 L*a*b*
EC	European Commission
EU	European Union
GDPR	General Data Protection Regulation
GNSS	Global Navigation Satellite System
GPR	Ground penetrating radar
HMD	Head Mounted Display
HMLS	Handheld Mobile Laser Scanner
HPR	Hidden Point Removal (algorithm)
IMU	Inertial Measurement Unit
iMMS	Indoor Mobile Mapping System
LiDAR	Light Detection and Ranging
MLS	Mobile Laser Scanning
RTK	Real-Time Kinematic
SUM4Re	Creating material banks from digital urban mining (project name)
TLS	Terrestrial Laser Scanner
VIS	Visual Inertial System
WA	Work Area
WP	Work Package
XRF	X-ray Fluorescence

TABLE OF CONTENTS

LIST OF TABLES

LIST OF FIGURES

1. RESEARCH CONTEXT AND APPROACH

1.1. SUM4Re

1.1.1. The project

"SUM4Re is the acronym of "Creating materials banks from digital urban mining".

The SUM4Re project is co-funded by the European Commission and aims to reduce waste and promote circular construction practices. It proposes an integrated approach to the creation of material banks from built-up areas, combining urban mining, automated in situ data acquisition technologies and the identification of building components and materials with value for new uses.

The project will include the implementation of three pilot demonstration projects linked to construction projects, and a strategy to improve the qualification of the construction workforce and facilitate the uptake of solutions developed by companies and professional groups with interests in the sector." (website SUM4Re).

SUM4Re aims at adding value to existing construction entities and materials paving the path to an increased supply and use of secondary materials and components by means of developing smart digital solutions, by means of AI and other digital techniques and supported by blockchain solutions, for faster and less labour-intensive identification, analysis and digitalisation of materials and elements in the built environment. The challenges in data integration, material identification and marketing adoption will be addressed during this project. The three main activities of the SUM4Re project are:

1. Identification
2. Analysis
3. Contribution to circularity

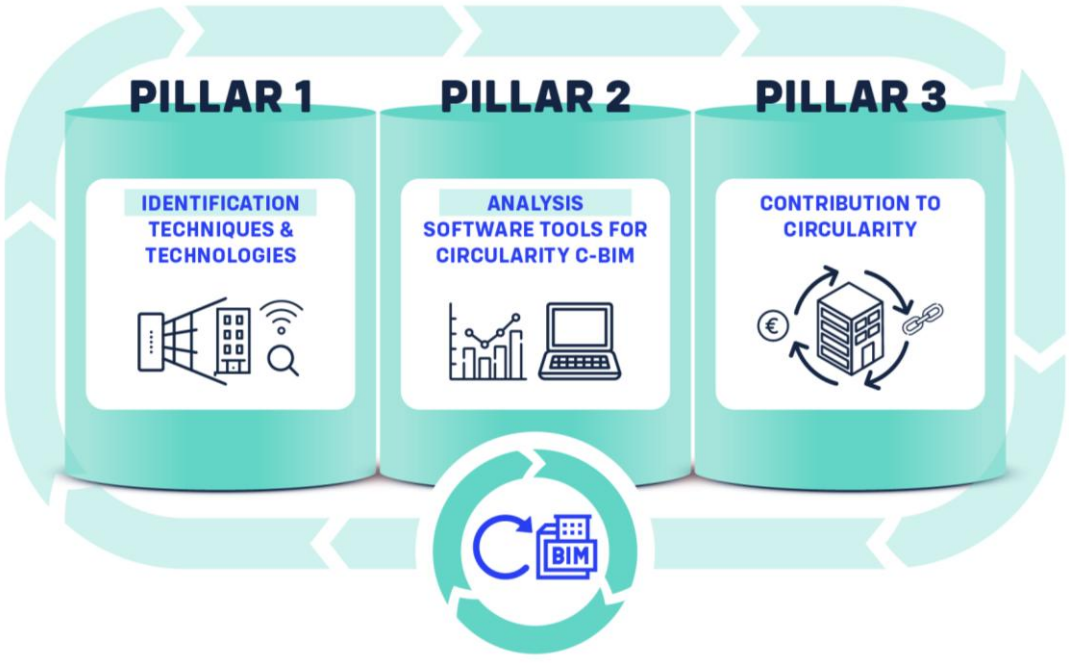

Figure 1. SUM4Re main pillar activities

1.1.2. The consortium

*"Researchers from **nine countries** are leading this European project, aimed at reducing and recycling construction materials from the predemolition phase.*

*The consortium, led by UVIGO, is composed of **17 entities from the construction sector** in Norway, the Netherlands, Spain, Germany, Belgium, France, Finland, Estonia and Switzerland,*

"A clear indicator of the interest in the project, which we hope, will help to stimulate the business sector so that the EU continues to be a benchmark in this field on a global scale", says the project's PI, who stresses the importance of starting waste reduction, recycling and by-product recovery at an early stage and before the demolition or dismantling of existing built infrastructure.

1.1.3. About the pilot sites

"SUM4Re's results will be demonstrated in 3 different pilot sites linked to singular construction projects in EU regions (North, Norway; Centre, The Netherlands; South, Spain), considering existing buildings with different uses or typologies (residential, tertiary, industrial & infrastructure assets) and targeting different products & materials (concrete, timber, asphalt, structural steel, and reinforced concrete), to validate the methodology and a strategy for skill development to upskill the workforce in the construction sector and facilitate the uptake of the solutions developed.

This strategic choice will prove relevant in the pathway to standardisation from a technical (different technologies for various materials), economic (availability and maturity of marketplaces) or regulatory framework (local policies) to widen the impact in the construction sector." (website SUM4Re)

1.1.4. Horizon Europe

"The European Commission, the funding body of the SUM4Re project

The SUM4re project is funded by Horizon Europe, the EU's key funding programme for research and innovation.

It tackles climate change, helps to achieve the UN's Sustainable Development Goals and boosts the EU's competitiveness and growth.

The programme facilitates collaboration and strengthens the impact of research and innovation in developing, supporting and implementing EU policies while tackling global challenges. It supports the creation and better diffusion of excellent knowledge and technologies.

It creates jobs, fully engages the EU's talent pool, boosts economic growth, promotes industrial competitiveness and optimises investment impact within a strengthened European Research Area." (website SUM4Re)

1.2. Baseline Assessment and Strategic Planning for Pilot Implementation and Testing

1.2.1. Research goals and activities WP10

"Assessment of the baseline condition at the Pilots sites. Strategic plan for the implementation of pilot & testing activities will be created, together with a general protocol to use techniques & technologies for identification, analysis, digitalization of the demonstrators. Making a basic inventory of materials at the pilot site, including registering data in the Digital Materials Databases CIRDAX and CONCULAR (or other applications)."

1.2.2. Research task 10.1: Case study 1 - Tertiary building & urban asset, Spain

"This task will prepare the on-site data acquisition for earthworks, the dismantling of the asphalted access roads, the removal of a historic masonry wall, demolition of old building (reinforced concrete and steel components), and the construction of large structural beams made by reusing concrete from CDW. Case study 1 involves data acquisition for: AR iMMS-RGB scan for material identification and C-BIM generation [UVIGO], XRF for concrete and asphalt characterization [OLAR], GPR-ECT for rebar detection [EAGLE], FOS for steel structural components quality testing [TECN], and the installation and assembly of TRACLINE on site [TECN]."

1.3. Objectives for the Baseline Assessment

Table 1. Source: Page 5 SUM4Re proposal

O7: To demonstrate SUM4Re in a real construction case that focuses on the structural potential for reuse of asphalt, reinforced concrete (steel & concrete) and automated CDW characterization schemes.	
Improvements to labour productivity	KPI18: Reduction of **10% of time needed for circular assessment** of the construction project (SUM4Re's solutions vs manual approach).
Efficient analysis in terms of circular potential	KPI19: Increased **supply of secondary materials** in pilots in **25%** and **reduction in construction CDW** in **25%** (SUM4Re's solutions vs manual).
Relation to the Work Programme:	Expected outcomes: EO1, EO2, EO3, EO4, EO5;
	Scope: S1, S2, S3, S4, S5
Key results:	UC1, iMMS & RGB and scan-to-BIM
	UC3, XRF for harmful and mineral composition
	UC5, GPR & ECT for reinforced structures, wood conditions and hidden element detection
	UC6, FOS for structural condition
	UC7, multisensor TRACLINE for CDW material composition

Table 2. Source: Page 5 SUM4Re proposal

O3: To develop on-site and off-site smart digital solutions to rapidly identify construction entities (including complex or concealed elements) with the additional ability to analyse their properties and characteristics.

Ability to digitally obtain structural and non-structural information from construction entities (on-site) that can be linked to circularity-driven BIM models	**KPI7:** SUM4Re will combine various techniques for characterization before physical intervention: visible (AR-iMMS-RGB) with time reduction of 50% for 3D models generation and materials identification; hidden components and geometric modelling (MFT), harmful materials and chemical-mineral composition (XRF), reinforced concrete structural-mechanical identification (GPR & ECT), and timber pathologies detection (AHS) with an increase of productivity of 90% (real time vs. sample collection and laboratory analysis). **KPI8:** The reuse of large structural components will be assessed through the structural condition index (FOS in combination with transfer learning) to detect structural alterations, reducing time for assessing mechanical behaviour by over 60%, when involving repetitive structural patterns. **KPI9:** One plugin to extend GENIA platform for data acquisition & integration of all the techniques included and for the assessment of structural components in accordance with their recyclability potential.
Quality control of CDW using AI-based multisensory system	**KPI10:** For heterogeneous CDW composed by multiple mineral fractions, all-in-one TRACLINE will characterize material composition and mineral stream. It is composed by LIBS, Raman, RGB-D, NIR, UV. AI will be used to process (identify, quantify and classify) construction materials and assets for a C-BIM. CDW quality control process and/recycled materials with with capacity to process 1-3 t/h will be developed and tested in a real case study.
Relation to the Work Programme:	Expected outcomes: EO1, EO5;
	Scope: S1, S2, S3, S4, S5, S7, S8
Key results:	UC1, iMMS & RGB and scan-to-BIM
	UC3, XRF for harmful and mineral composition
	UC5, GPR & ECT for reinforced structures, wood conditions and hidden elements detection
	UC6, FOS for structural condition
	UC7, multisensor TRACLINE for CDW material composition

1.3.1. Use cases

Table 3. Source: Page 5 SUM4Re proposal

UC	Use Case Description	Use Case Product/Result
1	3D geometric models of buildings for visual **inspection** and **integration of georeferenced** information collected from various sensors.	**iMMS & RGB image AR prototype and Scan-to-BIM software prototype** for massive and faster 3D geometric modelling.
3	Detection of harmful materials, compounds, or coatings in construction products such as concrete and asphalt for their recyclability	**XRF and software prototype** for real-time identification of concrete and asphalt materials.
5	Detection of hidden elements (reinforcements) in concrete structures for reuse/repair.	**GPR & ECT integration and software prototype** for characterization of reinforced concrete structures, wood

		condition and detection of hidden elements in buildings.
6	Characterization of structural health for reuse (beams and pillars) and to reduce the need for new ones	**Distributed FOS prototype** for structural condition characterization of structural components (steel-reinforced concrete)
7	Optimum CDW upcycling through the analysis of chemical composition, mineralogy, humidity, particle size-morphology and identification of pollutants	**TRACLINE multi-sensing prototype** for the identification & classification in real time of CDW mineral fractions (onsite and in-line)

1.3.2. Expected outcomes

Table 4. Source: Page 20 & 21 SUM4Re proposal

EO1: Faster and less labour-intensive identification, analysis and digitisation of materials and products from existing built works.	
SUM4Re will answer to the call scope through several smart innovative solutions (UC) developed in the project work plan for on-site and off-site faster smart digital identification of construction entities (O3), with a traceability system (O1) and cost-effective methodology aligned with open standards (O4), supported by a framework on circular construction uses (O2) and tested in several case studies (O7, O8, O9) that will contribute to: i) scientific advancements (section 1.1.4.) of these technological innovative solutions answering various scopes (UC1-S1; UC2-S4; UC3-S2; UC4-S5; UC5&UC6-S3/4; UC7-S2/4) implemented on WPs (2, 3, 4, 5) and KPIs (7, 9, 10); ii) improvements by means of new cost-effective products/services to the market and contribution to standardization (UC9-S7/8-WP1/5/7) (KPIs1/8/11);iii) societal benefits derived from an increased supply of secondary materials and reduction in CDW (KPIs4/18/19).	At least, **5%** scale of the community working with the technologies leveraged by SUM4Re's technology service providers & multipliers (stakeholders); **10 potential users** (demolition/recycling companies) for the CDW technology; 50 users of CIRDAX, CONCULAR, GENIA.
SUM4Re will decrease resources needed for building characterization (pre-demolition) in more than 20% in time and minimizing human presence, involving less personnel requirements (working hours) and avoiding human exposure in risky environments (some buildings to be demolished). CDW is one of the heaviest and voluminous waste streams generated in EU27, 330Mt/year excluding excavation waste. CDW recovery rates vary in EU, assuming the Spanish scenario, the project proposes a potential retrieval over 3,7Mt/year CDW.	
EO2: Increased supply of secondary materials and construction products for reuse, thus reducing the resource- and energy-intensity of the construction sector	
SUM4Re's framework will facilitate circular use of construction components & secondary materials (O5), considering LCA for improving quality of secondary materials increasing the availability and quality characteristics of such products (UC11-S4-WP6) (KPI12). Contribution to generate new knowledge based on a strategy for skill development (e.g., guidelines on circularity assessment) (O6), fostering a circular economy model in the marketplace considering traceability (e.g., blockchain), improved prediction of material flows & societal benefits from reduction of resources, energy	At least, 6 stakeholders in the community (industry, municipalities, investors) follow the guidelines of SUM4Re; 30 new agents in the marketplace & 50 references traceable beyond the partner database systems (CONCULAR, CIRDAX).

intensity and toxic free by removing hazardous materials. Know-how in CDW management (UC15-S7/9/11-WP8/9) (KPI17).	
SUM4Re will implement solutions for reducing CDW generation in buildings up to 640 Kg/m2; and additionally, recovering as secondary materials abt: >90 Kg/m2 cement-based materials, 8 Kg/m2 steel, and >10 Kg/m2 timber. Potential CO2 emission savings from improved management of CDW material fractions are (kg CO2-eq.per tonne CDW): 95.2 (ferrous), 41.1 (non-ferrous), 32.7 (mixed metal, cables), 18.5 (concrete), 11 (wood). Dominating mineral CDW fraction (305 Mt EU27 in 2020), better management of mineral waste leads to 5.6 Mt CO2. Followed by 1.3 Mt CO2 savings (2020) for reusing-recycling of ferrous CDW (13.6 Mt). Concrete CDW improved management means recycling aggregates and reuse of shell of building, or precast elements.	
EO3: Reduction in construction and demolition waste	
Aligned to EO2, a special focus will be put to minimize CDW generation, increase efforts to 5Re, in order to avoid landfilling and reducing energy demands for transportation out of the local areas and costs (thus minimizing carbon footprints for transport and construction logistic), facilitating the circular use of construction components (applied in the renovated/transformed buildings and infrastructures) by preserving the maximum value of the built environment (O5). For that, different go-to-the-market strategies will be considered to optimize the added value of secondary construction materials (UC12-S6-WP1/4) (KPI13).	At least, 5% scale of the working community on these fields in the countries of the pilots; 15 potential users (5Re companies) working with these CDW technologies; 20% energy demand reduction.
SUM4Re will implement solutions to reduce CDW, based on the ability to identify and calculate existing building components and materials to be reused, 50% of these components/materials do not have to be disposed as waste and transported out of the local areas. CDW accounts for more than 32% was landfilled, only 6.5% was treated in energy recovery operations. Alternative recycling and reuse options exist for CDW streams, mineral waste can be recycled up to 96 % compared to current recovery rate about 74%. In terms of CO2 savings, reuse of concrete waste is by far to the highest saving potential, followed by recycling of steel, asphalt, wood, PVC, EPS-insulation. SUM4Re will adapt the Integrated Action Plan for Resourceful Cities, which have recently been presented to the European Commission in the Interreg project URBACT, referring to the real example from the City of The Hague.	

1.3.2.1. Scope

Table 5. Source: Page 6 & 7 SUM4Re proposal

S	EU horizon call	Alignment of SUM4Re to the topic
1	*New techniques and technologies to identify materials, construction products and components of existing or demolished built works*	SUM4Re will exploit various smart digital solutions (**UC1-UC7**) comprising different remote and embedded data acquisition systems combined with advanced data analysis methods (AI), for data segmentation and classification of construction materials. These will be based on the requirements and methodologies established (UC8, UC10-UC13).
2	*Solutions that rapidly analyse the properties and characteristics of materials, products, and components*	Methods for data analysis will be based on AI systems allowing close to real time analysis for extraction of properties (geometry and materials) during on-site inspections (**UC1-UC6**). Algorithms for structured and

		systematic data labelling for class assessment, basic strength estimation, dimensions, etc, will be developed (UC8-UC9).
3	*Solutions to digitally record, categorise, tag existing materials, construction products & elements for their use on the market, inclusion in relevant software tools & databases. Support of the development of existing tools & databases, co-creation with relevant actors across the construction ecosystem, SSH*	SUM4Re will facilitate circular use of construction entities from an added value perspective and a cost-effective methodology for data sharing during the asset life cycle based on a detailed classification, categorization, and labelling system and supported by blockchain solutions for robust identification and possible market transactions. SUM4Re will address the challenges of a paradigm shift from traditional BIM modelling towards Cdriven BIM (UC8). Data segmentation and classification will be constrained to the information needed to characterize materials and components, that can be salvaged, reused, or recycled at the end of the building's life cycle (**UC1-UC7**). An approach based on co-creation will be considered due to the different profiles of the partners, including SSH expertise, reinforced by activities envisaged beyond the consortium in the Dissemination and Exploitation Strategic Plan (UC14-UC15).
4	*Solutions that analyse the suitability of identified elements for use in a circular economy, or conversely to label them as waste including the necessary separation and sorting.*	SUM4Re will develop a comprehensive methodological framework for assessment of the actual potential to make circular use of construction components through circularity indicators for material flow tracking (UC10, UC13) with the aim of improving the facility for circular use (UC11). This will provide the requirements for the extension of CIRDAX and CONCULAR database systems (UC9).

1.4. Relevance to the other research goals and -activities

The research at the pilot site aligns with the three pillars of SUM4Re: Identification, analysis and contribution to circularity. This deliverable reports the identification-activities: planning the collection of data, collecting the baseline data of the buildings at the pilot site (off-site and on-site, manually and by using different scan technologies) and create a starting point for further research.

Figure 2. *R*elation between the actions in the pilot case in Spain and the other work packages

After this “baseline assessment”, the results will be evaluated (T11.1 and pillar II Analysis) and used to develop a building renovation and re-use plan (T12.1 and Pillar III Contributing to circularity).

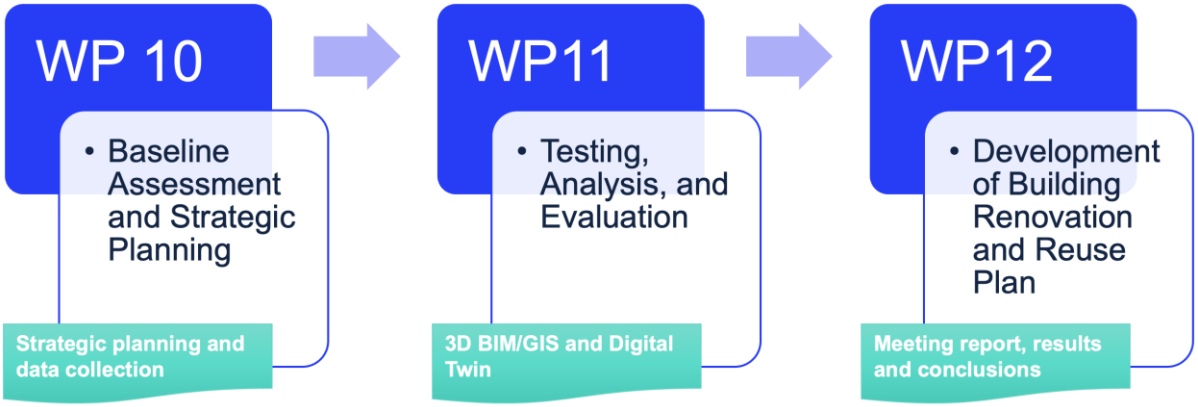

Figure 3. WA6 relation between each work package

With regards to Task 10.1, the integration of sensing technologies such as iMMS, XRF, GPR, FOS, and TRACLINE is directly linked to the overall framework of entity classification and Digital Product Passport (DPP) requirements. The classification of construction entities defines which elements must be characterized and how they should be described in digital workflows, while the DPP requirements establish the attributes to be collected, ranging from geometry and composition to lifecycle traceability. In this sense, the sensors play complementary roles: iMMS provides the geometric information, XRF reveals material composition and hazardous substances, GPR identifies concealed elements such as insulation or embedded utilities, FOS monitors the structural behaviour of selected components, and TRACLINE ensures the lifecycle tracking of construction products. Special attention is given to challenging waste streams such as hazardous or multi-component materials, where XRF and GPR become essential tools.

The outputs of Task 10.1 feed directly into WP2, where pre-demolition data collection is consolidated. iMMS captures 3D dimensions and generates point clouds; XRF provides data on the chemical properties of materials, highlighting hazardous or valuable fractions; GPR detects subsurface features that are not visible through conventional scanning; FOS supplies quantitative information about strain and structural condition; and TRACLINE guarantees component traceability along the value chain. This rich dataset not only supports pre-demolition audits but also aligns the collected information with the required fields of the DPP.

In WP3, the acquired data is processed with AI algorithms to automate C-BIM generation. iMMS and GPR contribute to automated geometry modelling, while XRF enhances AI-based material classification. FOS data is used for predictive modelling of the structural condition of materials and components, and TRACLINE metadata is integrated to link physical objects with their digital identities, ensuring robust traceability.

The transition from data collection to circular strategies takes place in WP4 to WP6. WP4 relies on sensor outputs to design pre-demolition and renovation plans: XRF and GPR identify hazardous areas and reusable materials, iMMS estimates volumes and geometrical constraints, and FOS validates the structural condition of elements. WP5 uses the results from XRF, FOS, and TRACLINE to populate Digital Product Passports with material properties, performance, and traceability information. WP6 then integrates these enriched DPPs into the C-BIM environment, ensuring that both geometry and material data are accessible and interoperable for circular economy decision-making.

Finally, in WP7 to WP9, the integration and dissemination of these results are ensured. Data derived from Task 10.1 are normalized and uploaded into platforms such as GENIA, CIRDAX, and CONCULAR, enabling interoperability and visualization. Stakeholder engagement in WP8 validates the applicability of sensor-based classification and DPP information for practitioners, while WP9 transforms the lessons learned into training activities, best practices, and replication strategies. In this way, Task 10.1 provides the technological foundation that links

physical sensing with digital circularity workflows, bridging pre-demolition assessment, AI-driven modelling, DPP development, and C-BIM integration.

Table 6 summarizes the relation of each technology, in the context of task 10.1, with the rest of the SUM4Re work packages.

Table 6. Task 10.1 technologies relation between each work package.

Technology	Main Role	WP2 (Data Collection)	WP3 (AI/C-BIM)	WP4 (Plans)	WP5 (DPP)	WP6 (Integration)	WP7–WP9 (Platforms & Uptake)
iMMS	3D geometry & dimensions	Capture geometry/point clouds	Automated Scan-to-BIM	Volume & geometry for audit	Structural info in DPP	IFC integration in C-BIM	Upload to GENIA/CIRDAX
XRF	Material composition, hazardous detection	Identify chemical properties	AI-assisted material classification	Hazardous material mapping	DPP material properties	Linked to C-BIM entities	Data visualization in CONCULAR
GPR	Subsurface/hidden element detection	Reveal concealed elements	AI for complex geometry recognition	Locate insulation/utilities	DPP enrichment on composites	Model concealed structures	CIRDAX integration
FOS	Structural response & strain monitoring	Data from load/strain sensors	Condition prediction models	Safety assessment in demolition	DPP durability/condition fields	C-BIM structural enrichment	GENIA database link
TRACLINE	Lifecycle traceability of components	ID & track components	Metadata for AI linking	Track reuse potential	Core traceability field in DPP	C-BIM–DPP synchronization	CONCULAR interoperability

1.5. Research approach

1.5.1. Methods and activities

The research approach for this deliverable combines **qualitative and quantitative methods**, ensuring that both the conceptual framework and empirical evidence are addressed. The methodology is structured around the following interconnected activities:

- **Desk research**: A comprehensive review of literature, international standards, and best practices was undertaken to provide the theoretical foundation of the study. This included regulatory frameworks for hazardous materials management, technical standards for Digital Product Passports (DPPs), and advances in material identification and structural assessment using digital technologies. The desk research also highlighted existing gaps and constraints, positioning SUM4Re's contribution within the wider context of circular economy strategies in construction. These activities contribute to EO1 (faster and less labour-intensive identification and digitalisation of materials) by aligning SUM4Re with cutting-edge knowledge and regulatory requirements.
- **Baseline requirements**: The next step involved identifying the fundamental technical, legal, and environmental constraints influencing data acquisition and reuse potential. Technical requirements relate to the accuracy, resolution, and limitations of the applied technologies (iMMS, XRF, GPR-ECT, FOS, and TRACLINE). Legal aspects focus on compliance with EU waste directives, building codes, and safety regulations, especially when dealing with hazardous substances. Environmental constraints were analysed in terms of potential CO_2 savings, minimisation of waste, and the sustainability benefits of reuse. These requirements define the conditions against which all pilot activities are benchmarked, directly supporting EO2 (increased supply of secondary materials) and EO3

(reduction in CDW) by ensuring that regulatory and environmental aspects are integrated from the outset.

- **Scan plan**: A structured and detailed plan was developed to ensure systematic data acquisition across the pilot sites. This plan assigns roles to each technology: iMMS for 3D geometry and point cloud generation, XRF for chemical and mineral composition, GPR-ECT for the detection of reinforcement and concealed elements, FOS for structural health assessment of steel and concrete components, and TRACLINE for material traceability and classification of heterogeneous CDW streams. The scan plan also specifies the calibration procedures, the sequencing of measurements, and the strategies for cross-validation and data fusion between technologies. This activity underpins KPI7 (time reduction of 50% in 3D modelling and materials identification) and KPI10 (quality control of heterogeneous CDW streams) by formalising how each sensing technology contributes to efficiency and data reliability.
- **On-site data collection**: The implementation of the scan plan at the Anoeta Metro Station and Jolastokieta Urbanization pilots was carefully documented to ensure reproducibility. Each technology was deployed according to defined prerequisites, considering accessibility, environmental conditions, and safety requirements. Detailed logs were maintained for equipment calibration, scanning protocols, and sampling methods. Cross-verification was performed to validate the consistency of results across technologies—for example, comparing iMMS point clouds with GPR subsurface scans or linking XRF measurements with TRACLINE classifications. This process produced a robust and multi-layered dataset covering geometry, material composition, structural behaviour, and traceability. By securing accurate and validated datasets, this activity responds to EO4 (digital recording, categorisation, and tagging of materials) and EO5 (analysis of suitability for circular use).
- **Assessment of labour productivity impact**: A key dimension of the research approach is the evaluation of how digital data acquisition improves efficiency compared to conventional manual methods. Quantitative metrics, such as time savings, reduction in manual sampling, and accelerated generation of BIM-ready datasets, were analysed. In parallel, qualitative insights from practitioners were gathered to evaluate changes in workflow, skill requirements, and acceptance by end users. This dual assessment enables the measurement of SUM4Re's contribution to productivity gains, expressed through KPI18 (10% reduction in time needed for circular assessment), KPI19 (25% increase in secondary material supply and 25% reduction in CDW), and KPI8 (reduction of >60% in structural assessment time using FOS and transfer learning).

1.5.2. Reading guide

This deliverable is structured to provide a clear and systematic overview of the research context, pilot applications, technological foundations, and results of Task 10.1. Readers are encouraged to follow the sections sequentially, as each is built upon the previous one:

- Section 1 – Research Context and Approach: Introduces the SUM4Re project, the objectives of Work Package 10, and the specific scope of Deliverable 10.1. It outlines the methodological framework combining qualitative and quantitative approaches, including desk research, baseline requirements, scan plan, on-site data collection, and labour productivity assessment.
- Section 2 – Pilot 1 "Jolastokieta Urbanization": Presents the selected pilot site and its relevance as a demonstrator. It describes the characteristics of the urbanization, the context of intervention, and the challenges it poses for data acquisition, circularity assessment, and material recovery strategies.
- Section 3 – State of the Art: Reviews existing literature, standards, and best practices related to material identification, structural assessment, and circular economy principles. Special attention is given to the application of sensing technologies (iMMS, XRF, GPR-ECT, FOS, and TRACLINE) in construction and demolition contexts.

- Section 4 – Prerequisites for Data Acquisition: Details the technical, legal, environmental, and economic constraints that influence the application of advanced sensing technologies. It sets the baseline requirements for data quality, accessibility, safety, and regulatory compliance.
- Section 5 – Baseline Assessment: Summarises the outcomes of the on-site implementation of the scan plan. It presents the preliminary datasets obtained from the technologies deployed, discusses the complementarity of results across methods, and highlights the challenges encountered in capturing material and structural information.
- Section 6 – Evaluation: Assesses the effectiveness and efficiency of the data acquisition process. The section reflects on the impact of digitalisation on labour productivity and its contribution to SUM4Re's Expected Outcomes and KPIs.
- Section 7 – Conclusions and further research: Synthesises the main findings of the deliverable and their relevance for circular construction strategies. It highlights the contribution of multi-sensor data to DPP development and C-BIM enrichment and outlines future research directions, including improvements in data integration, platform connectivity, and replication across other construction contexts.

This structure ensures an easy navigation from the project's context and objectives, through the technical and methodological foundations, to the obtained results, evaluation, and strategic recommendations for future developments.

2. Pilot 1 “Jolastokieta Urbanization”

From the SUM4Re proposal: *“The old school area in San Bartolome (San Sebastian) will be renovated and converted into a new shopping centre. The case study has two buildings. The main building (2000 m2 with 4 floors) will be set into the hillside of the former San Bartolome school and will have 9 floors, 4 for the shopping centre and 5 below ground for the car park. Building interventions include demolition, renovation, and recycling. The buildings contain: clay tiles, wooden and glass windows, masonry walls, concrete walls, protective coating, and plaster, reinforced concrete beams and columns, steel beams and asphalt on access roads. The main building presents pathologies inherent to concrete such as loss of cohesion of the structure, cracks and fractures, spalling, efflorescence, excessive deformation in structural components, and corrosion in reinforced concrete and structural steel components.*

***SUM4Re will contribute to the conservation of the historical heritage of this building**, while improving the economic and social impact of the area. The task conducted in this case study will be: (1) virtual replica generation of road-structural element; (2) real-time monitoring data (FOS); (3) application of inverse techniques for mechanical performance assessment; (4) XR virtual interaction; (5) decision making; (6) material bank integration. “*

Due to unforeseen changes in the timeline by the public administration, the originally selected pilot site, the San Bartolome commercial centre, is no longer available for SUM4Re intended use. To address this issue and ensure the successful implementation of the project objectives, it was proposed a modification to the pilot site plan. It was identified two alternative sites that, when combined, can fulfil the requirements and objectives set forth in the original proposal.

2.1. General aspects

2.1.1. Demolition Site: Anoeta Metro Station

Location: Euskotren Metro Station, Anoeta

Description: This urban tertiary building will be demolished to create a new entrance/exit for the metro station. The site features concrete and steel components, providing an opportunity to utilize Construction and Demolition Waste (CDW). However, it lacks masonry walls and asphalt, and there is no opportunity to reuse the steel components.

Figure 4. New demolition pilot case

2.1.2. Reuse and Material Recovery Site: Jolastokieta Urbanization

Location: Herrera

Description: This project involves the demolition of existing warehouses and the urbanization of the area. It is a private development by MOYUA HOMES, a subsidiary of Moyua Group. This site includes steel components and asphalt, offering significant opportunities for both steel reuse and CDW utilization. While it is not an urban tertiary building, it aligns well with the project´s goals for material recovery and reuse.

Figure 5. New reuse pilot case

2.1.3. Combined Pilot Site Approach

By combining these two sites, we can achieve a comprehensive pilot case:

- **Anoeta Metro Station** will serve as the urban tertiary demolition site.
- **Jolastokieta Urbanization** will provide the opportunity for material recovery and reuse, particularly steel components, which can be subjected to stress tests before demolition.

2.1.4. Pros of the New Situation

- Enhanced material recovery: The inclusion of the Jolastokieta site allows for a broader range of material recovery, especially steel, which can be reused effectively.
- Diverse scenarios: Combining two different types of sites (an urban tertiary building and a private development) provides a more diverse set of data and scenarios, enhancing the robustness of our findings.
- Increased opportunities for CDW utilization: Both sites offer significant opportunities for the utilization of CDW, aligning well with the project's goals of promoting sustainable construction practices.
- Mitigation of schedule risks: By selecting two sites, we reduce the risk associated with potential delays from a single site, ensuring project timelines are maintained.

2.2. Scan technology used

In Task 10.1 of the SUM4Re project, a multi-technology approach is employed to capture comprehensive structural and material data for existing and rehabilitated structures. The objective is to generate high-resolution geometrical, material, and structural information to support structural health monitoring, retrofitting strategies, and digital twin development.

The scanning and sensing framework includes:

	Tertiary building & urban asset	Urban district transformation	Residential building
Timber		AHS	AHS GPR+ECT
Steel	FOS		
Concrete	XRF GPR+ECT	MFT	
Asphalt	XRF GPR+ECT		
CDW	TRACLINE*		
3D Model	iMMS+RGB	MFT iMMS+RGB	iMMS+RGB
*TRACLINE (LIBs+Raman+RGB-D+NIR+UV)			

Figure 6. Scanning technologies used

Table 7. Task 10.1 Scan technologies summary

Technology		Used for	Partner	Contact person
iMMs+RGB	Indoor Mobile Mapping Systems	3D models generation and materials identification (UC1)	UVIGO	Jesús Balado Frías jbalado@uvigo.gal
XRF	X-ray fluorescence	Material/chemical composition, detection of hazardous chemical elements	OLAR	Pablo Arauzo pj.arauzo@olar-solutions.com
GPR+ECT	Ground penetrating radar system	Material characterization and hidden element detection	EAGLE	Alex Novo alex.novo@screeningeagle.com
FOS	Fiber Optic monitoring System	Structural elements condition assessment	TECN	Jose Carlos Jimenez Josecarlos.jimenez@tecnalia.com
TRACLINE	Multi-sensory classification system	characterisation and classification of demolition waste	TECN	Jon Ander Iturrioz jonander.iturrioz@tecnalia.com

3. State of the art

3.1. iMMS point cloud

3.1.1. State of the art

Indoor Mobile Mapping Systems (iMMS) have rapidly advanced as efficient tools for capturing dense georeferenced point clouds in indoor environments, leveraging SLAM techniques, LiDAR, IMUs, and high-resolution cameras. Compared to traditional terrestrial laser scanners (TLS), iMMS systems significantly accelerate data acquisition and improve spatial coverage, as demonstrated in case studies using systems like NavVis VLX2 achieving better than 2.5 cm accuracy and low noise levels in complex indoor settings [1].

Parallel to this advancement, the usage of Augmented Reality (AR) for 3D data acquisition evolved significantly, increasing the number of applications in different range of fields from immersive environments to robotic perception. A key step is Simultaneous Localization and Mapping (SLAM), which allows AR systems to map environments while estimating their own position. SLAM-based AR is now widespread in mobile devices and headsets. For example, LaMAR benchmark is one of the most used for evaluating AR-based localization [2].

Recent developments have explored collaborative capture using multiple mobile AR devices. For instance, Bortolon et al. [3] employs synchronized multi-user smartphones to scan dynamic scenes. Focused on 3D indoor environment reconstruction, Manni et al. [4] propose a method that use Android app tracking to capture image for each object and infer each depth to create the 3D reconstruction. In medical field, AR technology is also used to reconstruct 3D images about hepatic and biliary structures to superimpose these virtual images and plan the surgery [5].

These AR-based 3D acquisition systems are evolving toward higher accuracy, dynamic scene adaptability and different kinds of data. As the underlying hardware continues to improve, especially in mobile platforms, we can expect broader adoption of real-time 3D acquisition in everyday AR applications.

3.1.2. iMMS point cloud limitations

Nowadays, there are several advances in LiDAR-generated point clouds due to the number of applications that use this information such as BIM creation, object detection, instance segmentation, among others. Consequently, the number of different LiDAR devices is constantly incrementing. For instance, portable LiDAR devices (iMMS), such as smartphones and tablets, further enhance accessibility by allowing real-time damage detection and data sharing through cloud-based platforms [6]. AR devices like HoloLens 2 are also used, which integrate multiple sensors (LiDAR, IMU, …). All these portable devices are cheaper than more sophisticated technologies like HMLS or TLS and at the same time, they are easy to handle as they are generally not very heavy [7]. However, the accuracy depends on calibration and fusion, and errors in one sensor can compromise the mapping precision. Furthermore, these systems often require extensive post-processing like bundle adjustment or manual cleaning of noisy data. Moreover, the usage of AR systems for 3D reconstruction, demand the user to devote attention and time during scanning [8]. Following in this same line, indoor scenarios often contain occlusions, which limits visibility, and the result remains incomplete [9].

With the introduction of AI models, a new limitation appeared. Most of the Deep Learning (DL) models are trained for specific sensors or environments, thus these are not generalized well [10].

3.1.3. Beyond the state of the art

Augmented Reality (AR) is rapidly transforming from a visualization tool into a powerful platform for real-time 3D reconstruction and progress monitoring in construction. One clear

trend is the shift toward real-time or near real-time reconstruction directly on site, using edge computing and optimized SLAM pipelines. For instance, SCFusion algorithm [11], performs incremental volumetric scene reconstruction with semantic completion, enabling geometry to be filled in on the fly as new data is acquired.

Similarly, recent developments in AR photogrammetry pipelines are targeting this pain point by automating model generation and alignment directly from handheld AR captures. For example, in heritage brick reconstruction tasks, the novelty lies in the step to calibrate and align the model instantly on site, reducing the post-processing time to just a few minutes [12].

To address the challenge of aligning large-scale scans in complex construction sites, some systems use hybrid AR + LiDAR methods with real-time spatial anchoring, leveraging cloud backends to stitch and synchronize point clouds incrementally as new data is uploaded from mobile or drone-based devices. This reduces delay in generating usable 3D reconstructions and facilitates faster progress monitoring.

Together, these innovations are overcoming the classic trade-off between processing time, and field usability. The trajectory is clear: toward on-device, real-time, semantically rich reconstruction, eliminating the long delays that have historically impeded agile AR use in construction.

The SUM4Re project will develop an application based on AR hardware that allows 3D geometric data to be collected, while minimizing the limitations in the accuracy of 3D data generated by virtual markers positioned in real time. These markers will serve as notes, labels, or reference points for algorithms implemented in subsequent phases to identify and segment structural and/or recyclable elements.

3.2. XRF

3.2.1. State of the art

For the purpose of determining the presence of major and minor elements, as well as hazardous trace metals in concrete, asphalt, brick, and glass, pXRF has been demonstrated to offer a rapid screening method. This approach facilitates on-site sorting, identification of hazards, and decisions regarding recyclability, thereby supporting compliance checks that are aligned with the EU Waste Framework Directive and associated product regulation workflows [13]. As outlined in the proposal, the XRF is to be used for the explicit purpose of detecting harmful materials and characterising the chemical and mineral composition of concrete and bitumen. The ICP-OES is to be used as the quantitative laboratory reference.

As XRF is surface-sensitive and matrix-dependent, the most effective approach in the context of CDW is to adhere to the following best practices: The procedure is initiated with surface cleaning and smoothing. Subsequently, the thickness and moisture content are controlled (dry, ≥10 mm if possible, or grind/press pellets for laboratory workflows). Thirdly, matrix-matched or FP-aided calibrations are performed, using Compton normalisation where appropriate. Finally, the validation is periodically reviewed against ICP-OES/ICP-MS to anchor detection limits and accuracy for regulatory or passporting needs. It is evident that EPA Method 6200 and its associated guidance documents are extensively referenced in the field of pXRF QA/QC. This encompasses critical aspects such as sample homogenisation, replicate shots, blanks/CRMs, and action-level-focused calibration ranges.

In the specific context of SUM4Re, the following three objectives are delineated: (1) the construction of an extensive XRF library for concrete and asphalt; (2) the analysis of these samples by ICP-OES for the purpose of high-accuracy bulk composition; and (3) the training of machine learning regression models to predict properties and contaminants, with subsequent deployment on-site. The proposal also commits to the establishment of relationships between XRF's surface-sensitive signals and ICP-OES bulk values, and to the utilisation of these models in pilots (WP10). This is connected to a more extensive multi-

sensor/AI stack (for example, TRACLINE with LIBS-Raman-NIR-UV-Vis) for the purpose of data fusion and automated CDW classification.

3.2.2. XRF limitations

Basics of XRF

X-ray fluorescence (XRF) is based on the photoelectric effect, whereby a primary photon ejects a core (K/L/M) electron if its energy exceeds the shell binding energy. De-excitation proceeds via either radiative emission (characteristic X-rays) or non-radiative Auger processes, with line families (Kα, Kβ; L, M) set by the specific shell transitions and element Z [14]. Fluorescence yield increases with Z, which underpins the challenges of low-Z detection, while the photoelectric cross-section scales strongly with Z and inversely with photon energy. These interactions are standardly reviewed in the fields of X-ray physics and XRF fundamentals.

Modern XRF instruments are predominantly either wavelength-dispersive (WDXRF) or energy-dispersive (EDXRF). WDXRF uses analysing crystals to diffract characteristic wavelengths and achieves superior spectral resolution (≈0.6% at Mn Kα), favouring laboratory-grade, high-precision work. EDXRF measures photon energies directly with solid-state detectors, also referred as drift detectors (SDDs [15]), enabling fast acquisitions and portable form factors; typical SDD energy resolutions are ≈120–150 eV at Mn Kα with high count-rate capability and Peltier cooling (no LN_2).

The extent of the information obtained is determined by the excitation/fluorescence attenuation within the matrix. For silicate-like matrices and common lab/field energies, effective information depths are on the order of micrometres to sub-millimetres for heavier elements, extending up to ~1–2 millimetres for lighter elements in low-density matrices [16]. This inherent surface bias in XRF is a consequence of the need for surface cleaning/levelling or coring/grinding for heterogeneous CDW. Calculations are routinely made from mass attenuation coefficients (e.g., NIST) or empirical tables for micro-XRF [17].

Quantification is limited by matrix effects, which include absorption and enhancement, as well as spectral overlaps. These effects couple analyte intensities to bulk composition and geometry. State-of-the-art workflows have been developed to mitigate these effects using fundamental parameters (FP) models derived from Sherman's equation (and/or empirical calibrations with matrix-matched CRMs. In pXRF, Compton normalization (utilizing the tube's Compton peak as an internal standard) is a widely adopted technique for partial correction of matrix variability in low-density materials (soils, plastics, wood), though the necessity for stringent control of moisture and thickness persists (i.e., drying to ≥10 mm thickness).

XRF applied to construction and demolition

Whilst portable X-ray fluorescence (pXRF) has revolutionised the realm of rapid, non-destructive field analysis, it is important to acknowledge the inherent limitations imposed by its physical detection limits. These limits give rise to systematic biases when attempting to estimate bulk composition. In essence, pXRF is a surface-sensitive technique, with the depth of information being constrained by the attenuation length of both incident and fluorescent X-rays. For heavier elements in dense matrices, the effective penetration is often only tens of micrometres, whereas for lighter elements in low-density materials it can reach up to 1–2 millimetres [18]. This surface constraint poses a significant challenge in the context of construction and demolition waste (CDW), where the presence of coatings, paint layers, carbonation crusts, and weathered surfaces can dominate the detected signal, thereby masking the underlying bulk composition.

A second major limitation is presented by matrix effects. It is evident that both X-ray absorption, whereby low-energy fluorescence is reabsorbed by the matrix prior to reaching the detector, and secondary enhancement, wherein the fluorescence of one element excites another, resulting in the distortion of true concentrations. The severity of the phenomenon is contingent

upon the mineralogy, density, and moisture content of the sample in question. In the field of construction materials, the extent of these matrix effects can vary significantly, with an order of magnitude difference possible. In the absence of rigorous matrix-matched calibration, compositional bias can persist even when employing advanced fundamental parameter (FP) correction models.

A well-known challenge for pXRF is its poor sensitivity to light elements (below Mg, and particularly for C, O, Na, and Al), whose low-energy fluorescent photons are absorbed either in the sample itself or in the air path to the detector. This limitation has a direct impact on the assessment of CDW, as these elements are frequently pivotal in differentiating between material types. To illustrate this point, one may consider the task of distinguishing high-alumina refractory bricks from Portland cement concrete, or the identification of specific insulation materials.

Furthermore, surface roughness and heterogeneity have been demonstrated to compromise reproducibility. Rough surfaces have been observed to scatter incident X-rays in a manner that is difficult to predict, resulting in a decrease in the apparent concentrations of heavier elements and an increase in the relative standard deviations. In concrete and asphalt, the heterogeneous distribution of aggregates and binder means that a single pXRF spot may disproportionately sample a particular phase, resulting in a bias in the result compared to the homogenized bulk measured by ICP-OES.

From a workflow perspective, calibration gaps and time delays represent additional limitations. Current industry practice relies on periodic calibration using Certified Reference Materials (CRMs) or historical site data. In the field, calibration models are seldom updated dynamically during the course of field campaigns. This may result in the occurrence of model drift, a phenomenon characterised by the systematic deviation of data points due to alterations in material types across a demolition project. Furthermore, ICP-OES, while the accepted bulk reference method, requires the collection of samples, their drying, grinding, and digestion (frequently involving multiple acids). The samples must then be transported to a laboratory for analysis. Despite the implementation of accelerated processing protocols, the duration of this process can extend between 24 and 72 hours, during which field decisions are contingent upon unvalidated pXRF estimates.

It is evident that the majority of contemporary pXRF–ICP-OES correlations are dataset-specific, constructed under controlled calibration conditions that may not be applicable to new sites or material streams without recalibration. This issue is further compounded by the absence of uncertainty quantification in numerous pXRF workflows. Frequently, people who use these devices are provided with a point estimate, devoid of confidence intervals or applicability metrics, which renders it challenging to substantiate decisions within regulatory frameworks. In heterogeneous CDW environments, this absence of quantified uncertainty undermines both the traceability of results and their acceptance in digital product passport frameworks now emerging in EU circular economy policy.

3.2.3. Beyond the state of the art

Recent advancements have elevated the use of portable X-ray fluorescence (pXRF) from quick screening tools to semi-quantitative instruments capable of reliably estimating bulk composition, a development that is further enabled by the calibration of such instruments against laboratory-grade techniques, such as ICP-OES. A case in point is a study conducted around the Tar Creek Superfund site in Oklahoma, where in-situ pXRF readings were rigorously compared with lab-processed ICP-OES analyses following homogenization, air-drying, sieving, and acid digestion. The outcomes were noteworthy, correlation coefficients of $r^2 \approx 0.96$ for lead, ≈ 0.91 for zinc, and ≈ 0.93 for cadmium were attained, following the implementation of adjustments for moisture and organic matter. The findings support the hypothesis that pXRF is a suitable preliminary screening tool, with ICP-OES providing precise, confirmatory bulk-level composition results [19].

That research has demonstrated comparable fidelity between pXRF [20] and lab-based methods across a diverse array of samples. A meta-analysis encompassing 235 studies found strong agreement (with correlation coefficients between ~0.82 and 0.98) for elements such as As, Ca, Cr, Cu, Fe, K, Mg, Mn, Ni, P, Pb, Si, Ti, and Zn. This finding serves to reinforce the generalisability of pXRF calibration across a variety of material matrices.

In materials that are more directly comparable to construction components, such as cementitious binders, energy-dispersive XRF (EDXRF) methods have been validated against ICP-OES with near-perfect agreement. A specialised study on cement-based binders, blended with fly ash, zeolite and bentonite, demonstrated excellent correlation when analysed by EDXRF and verified by ICP-OES [21]. The accuracy of the measurements is attributed to the rigorous calibration protocols that are in place. These include the use of fused glass disks and Certified Reference Materials (CRMs) that are traceable to ISO and NIST standards. This enables quick and reliable routine analysis using XRF.

An evaluation by the Louisiana Transportation Research Center (LTRC) of the use of a portable Olympus Vanta C pXRF to measure materials such as Portland cement, fly ash, and aggregates is of particular interest. In the case of cement, the pXRF reliably quantified heavier oxides (e.g. SiO_2, CaO, Fe_2O_3), with correlation coefficients of up to ~0.7 (Type III cement), while aluminium oxide exhibited significantly lower R^2 (~0.12), indicative of detection limitations for lighter elements. The results of the fly ash analysis similarly demonstrated underestimation for SiO_2 and Al_2O_3, though Fe_2O_3 aligned more closely with laboratory values, albeit with lower variance. Nevertheless, for crushed stone aggregates, pXRF exhibited remarkably high correlations ($R^2 > 0.85$) for SiO_2, Al_2O_3, Fe_2O_3, and CaO, thereby substantiating its robust predictive capacity when physical form and composition are conducive to such analysis.

These studies underscore two pivotal insights: pXRF demonstrates remarkable efficacy for heavier oxides and dense aggregated phases when meticulously calibrated yet encounters challenges with lighter elements and heterogeneous binders. The necessity of matrix-specific calibration and verification is emphasised, with the recommendation being ICP-OES analysis as the optimal method. This is deemed essential in achieving reliable bulk compositional prediction in construction matrices.

Innovative solutions XRF

The most promising pathway beyond current practice is to replace static, linear XRF→ICP-OES calibrations with AI-driven, matrix-aware models that learn non-linear corrections from paired datasets. Recent studies have indicated a shift in community preference towards Random Forests, SVMs, Cubist and even CNNs, as these models have been found to be more effective in handling factors such as heterogeneity, moisture, thickness and surface coatings. These factors are known to complicate the analysis of pXRF in construction matrices. Large comparative studies and reviews have reported consistent accuracy gains of machine learning (ML) over linear baselines for element prediction from spectra. This supports a methodological upgrade for on-site quantification (e.g., random forest (RF) and convolutional neural networks (CNNs) outperforming partial least squares regression (PLSR) for elemental/property prediction from spectra). In soils (a relevant analogue for mixed mineral matrices), RF and neural approaches have been shown to routinely improve predictive metrics over GLM/PLSR for key analytes. Recent calibration-set design studies have quantified how sample diversity and size govern model generalization, which is useful when planning UC3's sampling campaign. Collectively, these findings substantiate UC3's strategy of training non-linear regressors on paired XRF–ICP-OES data to infer bulk composition from surface-sensitive readings in real time [22].

A second frontier pertains to multi-sensor fusion, wherein pXRF is complemented by techniques that contribute orthogonal information, most notably LIBS for light elements and depth-resolved micro-ablation, and hyperspectral imaging (HSI) for spatial mineralogy. Recent reviews and studies in analytical chemistry and geoscience demonstrate that the integration

of LIBS with XRF/Raman/HSI, followed by the application of data-science pipelines, results in enhanced classification accuracy and more robust quantification than any individual method alone. The practical integration constraints that have been identified are now well understood. For example, LIBS should be implemented subsequent to XRF in a measurement sequence i to avoid surface modification that could potentially bias the XRF step. Furthermore, fusion can be implemented at either the feature or decision level. It is evident that UC3 has the capacity to utilise these patterns to construct a realistic on-site workflow. This workflow is comprised of three stages: firstly, the rapid analysis of pXRF; secondly, the optional utilisation of LIBS/HSI in cases where ambiguity arises; and thirdly, the employment of machine learning fusion as a means of arriving at a definitive conclusion.

A third lever is to tighten the field-lab loop so that bulk truth from ICP-OES can feed models quickly enough to matter operationally. Although ICP-OES remains a laboratory technique, there are now rapid digestion playbooks (microwave or hot-block) that have been validated for solids and wastes. Coupling small representative micro-samples (obtained through on-site coring or grinding) to these accelerated digestions can reduce turnaround times from days to hours, enabling frequent re-anchoring of the XRF models during pilots. EPA Method 6200 continues to provide the QA/QC backbone for pXRF (replicates, CRMs, Compton normalization, moisture/thickness control), while standard digestion methods and vendor application notes codify accelerated prep for ICP-OES reference analyses. The innovation at the core of this study lies in the formalisation of a closed calibration loop by UC3. This innovation involves the scheduling of periodic micro-sampling, the prioritisation of elements or models exhibiting the most significant drift or uncertainty, and the automatic re-fitting of regressors in response to the arrival of new ICP-OES truth.

Finally, it is imperative to acknowledge the critical role of uncertainty-aware deployment in ensuring compliance decisions on CDW. Contemporary machine learning (ML [23]) pipelines facilitate the output of not only point estimates but also calibrated uncertainties, achieved via ensembles or quantile regression. Additionally, they enable the encoding of rule logic that flags predictions as borderline or out-of-domain, thereby facilitating their subsequent confirmation through ICP-OES. Concurrently, HSI-guided mapping has the capacity to pre-screen surfaces to identify coatings, weathered layers, or filler "hot spots" prior to the pXRF shot. This process serves to reduce systematic bias from near-surface anomalies. Evidence derived from mining and core-scanning studies suggests that automated mineral mapping utilising an integrated approach of infrared/hyperspectral imaging (IR/HSI) [24] combined with X-ray fluorescence (XRF) and/or laser-induced breakdown spectroscopy (LIBS) is sufficiently reliable to inform the methodology and parameters of measurement. This finding directly translates to demolition environments characterised by heterogeneous substrates. The integration of these steps results in two key benefits: enhanced system speed and improved defensibility of accuracy. This aligns with regulatory expectations and the quality standards of digital passport data.

3.3. GPR + ECT

3.3.1. State of the art

Ground penetrating radar (GPR) has matured into one of the most versatile tools for non-destructive testing (NDT) and is used in numerous applications such as concrete building inspection, bridge health monitoring, utility mapping, road inspection, archaeology, geological applications amongst others [38]. It is used to characterize materials, detect and map layers and hidden objects, find anomalies and assess overall the health of structures/layers. The broad adoption of GPR is due to its many advantages such as that it is non-invasive, allows fast data collection and high-resolution.

GPR operates by transmitting electromagnetic (EM) waves into the ground (or other medium) with a transmitting antenna and recording reflections from interfaces between subsurface materials with a receiving antenna. For EM waves to be reflected, a contrast in the dielectric

properties between materials is required. These properties are material properties and are used to characterize the materials. The frequency range in which GPR operates is between 10 MHz to 5 GHz, with lower frequencies offering deeper penetration at the cost of resolution and higher frequencies providing higher resolution for shallow applications. Lower frequency systems are used for utility mapping and geological/technological applications whereas high frequency is suitable for concrete scanning and pavement assessment.

Since its initial applications in the 1970s, the technique has evolved considerably. For many years now, advances in antenna design, computational power and signal processing have significantly improved the resolution, penetration depth and portability of GPR systems. Today, commercial systems are lightweight, often handheld or cart-based and integrated with GNSS or total stations for accurate positioning. Advances have also been made to the antenna shielding, reducing the external interference.

Furthermore, on the hardware side, stepped-frequency continuous-wave (SFCW) GPR commercial systems have been developed in recent years [39] due to technological innovations that made it possible, whereas previously only pulsed GPR systems could be found.

In addition to the single channel systems which are still widely used, in the recent years, the technological advancements have enabled the development of multichannel systems [40], both in cart and as vehicle mounted multichannel GPRs, which consist of multiple antennas. These allow for rapid data collection over large areas (many Kms), reducing significantly the survey delivery time since a wider area can be scanned with a single pass compared to a single channel system which would require many passes to scan the same area.

There are now GPR systems available that can be controlled wirelessly avoiding the need for multiple cables and systems that can be controlled simply by an iPad application. Calculating and visualizing time/depth slices live on-site is now possible, which was not available a few years back along with real-time position visualization and slice display on background maps on site.

In practice, GPR data which are collected without GPS are performed by laying out survey grids and collecting parallel lines with a certain spacing in both directions whereas collection with a positioning device allows for free path movement as the position is handled by the positioning system. Data from measured lines are presented in the form of B-scans (or 2D radargrams) with the vertical depth axis and horizontal distance axis and as time/depth slices which are formed from combining B-scans. Basic data processing can be done also from the data acquisition software, however for more advanced processing, dedicated post-processing software exist from each manufacturer or independent.

Apart from the hardware innovations, developments have also been made in the data processing with advanced signal processing methods (such as 3D and reverse-time migration, full waveform inversion and wavelet analysis) have been implemented for assisting in interpretation in addition to AI algorithms such as automatic rebar detection [41].

Finally, significant developments have been made in modelling techniques, where now it is possible to model in 3D, complex structures, full antennas, complex heterogeneous materials but also irregular geometry objects [42] and generate thousands of complex synthetic realistic scenarios for training AI models. Being able to model real scenarios found in GPR surveys, generate and study realistic synthetic data can assist greatly in the analysis and interpretation of the real GPR data.

Regarding the ECT technology, some hardware innovations that have been made in recent years are wireless connection over Bluetooth to an iPad app and fully standalone probe versions without need for cart and iPad app. For software, it is now possible to visualize signal strengths and heat maps directly on the data acquisition app and perform neighbouring rebar corrections as the measurements from a rebar are influenced by neighbouring rebars. This can be now performed for both the first but also for the second rebar layer. Rebars can be also

exported as dxf files directly from the data acquisition app. Finally, cloud storage with direct upload of the data from the field app is now supported.

3.3.2. GPR + ECT limitations

Despite all the advancements made in hardware and software, as with other technologies, GPR still faces challenges.

Although GPR is a powerful tool, its effectiveness strongly depends on the environmental conditions and technical factors. A key limitation is the penetration depth which decreases in media with high conductivity such as media containing clay or water, which attenuate the GPR signals rapidly and thus limit attenuation. Conversely, in dry sandy or concrete media, the penetration is good but can be also limited by the frequency of the antenna used as mentioned earlier high-frequency systems have high resolution but small penetration.

Another challenge is clutter from within the medium or noise from external sources which affects the data clarity and makes the interpretation difficult. Although filtering can help reduce these effects, there are still many cases where these are persistent.

GPR is also sensitive to survey design and data density. Sparse data collection may fail to capture complex features and thus miss important targets of interest. Higher data density can be a solution to this problem but based on the system used can also be time-consuming.

Although some improvements were made, another challenge that needs to be addressed is how to handle the increasingly larger data including the loading, processing but also the interpretation which can take significant time for large projects.

Finally, data interpretation remains a major bottleneck as the GPR data can be quite complex and require expert users to interpret those. The results often remain dependent on operator expertise and subjective interpretation. However, even experienced operators can struggle to distinguish between true targets and false positives, especially when the data are complex.

Regarding the ECT technology, one of its disadvantages is the depth limitation for rebar diameter estimation as beyond a certain depth although it is still possible to estimate the concrete cover, rebar diameter estimation is not possible. In addition, this method is highly affected by all metallic objects nearby, even above ground and thus care should be given to remove those or scan at a further distance when possible.

A major limitation of this method is the requirement for conductive objects to be present. Without metallic rebars existing inside concrete slabs, this method could not be utilised.

3.3.3. Beyond the state of the art

Although in recent years, SFCW GPR systems have been commercially used and are increasingly favoured over impulse systems, there are still improvements to be made to achieve the best trade-off between resolution and depth. In the case of multichannel GPRs, the next generation of systems should aim to optimize the penetration and resolution (possibly with higher channel density) while increasing the mobility and system stability.

While there has been limited research, future solutions could be to integrate GPR systems in robots where human operator will not be always required or drone-mounted, which will enable rapidly mapping larger areas. Amongst others, this will require the stability challenges to be addressed.

Hybrid workflows combining GPR with additional sensors of other NDT technologies could be the next step to combine the strengths and acquired information of each method but also reduce survey time. This approach will provide a more robust interpretation, particularly in complex environments as there are data from different sources for verification.

Although recently there have been extensive research on AI algorithms for processing and interpretation of GPR data, the commercial use is very limited. One of the challenges is

generalization beyond the training dataset but also developing models that work well for data from different GPR sensors as the data are strongly dependent on the GPR antenna used and thus each sensor can produce quite different data even for the same exact area.

AI-driven interpretations are the most promising path for the future with models assisting in object detection, object classification and material characterization [43, 44]. This will decrease significantly the time delivery of a GPR project as the data analysis is faster and this automated process decreases (but does not remove the need of) the time needed for experienced operators. When it comes to large data from multichannel systems, AI models will be particularly useful for faster interpretation, but also more powerful computer hardware and efficient software needs to be developed to handle storage and processing of terabytes of data per survey.

A long-term vision is the development of national or even global underground and above ground digital infrastructure databases using different sensors including GPR for large-scale underground network mapping.

As investigated also as part of the SUM4Re project, combining GPR with ECT sensor can maximize the information for the health of concrete as with a single pass using both sensors, metallic rebars can be detected, their diameter, the cover depth but also other non-metallic features and voids in addition to characterizing concrete itself.

3.4. FOS

3.4.1. State of the art

Fiber optic sensing (FOS) technologies have become a reference for structural health monitoring (SHM) because of their high sensitivity, immunity to electromagnetic interference, and capability to cover long distances with a single sensing line. In the last decade, civil engineering has moved from pilot implementations to widespread deployments, with applications in bridges, tunnels, dams, and transport infrastructures. The ongoing developments are not only technical, focusing on higher spatial resolution, increased robustness, and improved signal interpretation, but also methodological, as they are progressively integrated into digital workflows for condition assessment and predictive maintenance [25, 26].

The main technologies can be broadly grouped into point sensors and distributed approaches. Fiber Bragg Gratings (FBG), including advanced forms such as π-FBG and ultra-weak FBG arrays, allow for discrete or quasi-distributed measurements of strain and temperature with very high temporal resolution, making them suitable for modal testing, fatigue monitoring, and local load evaluation [27]. Recent advances in multiplexing enable the deployment of thousands of sensing points along a single fibre, which extends their applicability to large-scale structural systems [28]. Distributed fibre optic sensing (DFOS) complements this by providing continuous measurements along the fibre. Rayleigh scattering techniques, such as Optical Frequency Domain Reflectometry (OFDR), achieve millimetre-scale resolution over tens of meters, and are particularly effective for detecting crack initiation, localized strain anomalies, and segment joint behaviour in concrete structures [29]. Brillouin-based methods, such as BOTDA and BOFDA, offer lower spatial resolution but extend the range to tens of kilometres, which makes them suitable for global monitoring of long-span bridges, tunnels, and pipelines [30]. Raman scattering, though less common, is used for distributed temperature sensing in applications such as fire detection, thermal stress monitoring, and leakage detection in hydraulic infrastructures. In parallel, Distributed Acoustic Sensing (DAS), based on phase-sensitive OTDR, transforms existing optical fibres into dense vibration arrays capable of detecting acoustic and dynamic events over tens of kilometres, which has opened new perspectives for traffic monitoring, railway condition assessment, impact detection, and security along linear assets [31].

Civil infrastructure applications illustrate the diversity of benefits. In bridges, FOS technologies are deployed to capture dynamic modal parameters, assess live-load responses, and identify early signs of cracking or fatigue. Tunnels represent another strong field of application, where distributed sensing has been used to monitor lining deformation, detect segment displacements, and evaluate long-term settlement behaviour. Dams and massive concrete structures benefit from fibre optics for simultaneous thermal and mechanical monitoring, enabling early detection of crack propagation and leakage risks. Along transport corridors, DAS provides continuous coverage to monitor rail and road conditions, enabling detection of train passages, scour events, and structural impacts in real time.

The interpretation of fibre optic data has evolved significantly. Current practice often combines measurements with finite element model updating to reduce uncertainties and obtain a calibrated representation of structural behaviour. Machine learning techniques are increasingly being used for damage detection and anomaly classification, although their effectiveness strongly depends on robust feature selection and the availability of representative training datasets [32]. Integration with digital twin frameworks is now emerging as the natural next step, where fibre optic monitoring data serve to update and validate virtual models of infrastructure, enabling predictive condition assessment and lifecycle management.

3.4.2. FOS limitations

Despite the maturity of the technology, several challenges remain. The long-term durability of optical fibres in concrete is still an active research area, with issues related to strain transfer, chemical attack, and micro-bending requiring appropriate protective sheathing and careful installation procedures [33]. Calibration and traceability also continue to be critical, since the translation of raw optical signals into standardized structural indicators is not yet harmonized across civil codes [34]. At the same time, the large volume of data generated by distributed and acoustic sensing requires scalable algorithms for automated analysis and event classification [35]. Standardization efforts are progressing, with IEEE and IEC having recently published specifications for FBG and DAS interrogators, providing a reference framework for device performance and acceptance testing [36].

3.4.3. Beyond the state of the art

Fibre optic sensing (FOS) for structural monitoring has reached a stage where it can be regarded as a mature and field-proven technology for condition assessment, offering unique advantages in terms of distributed coverage, high sensitivity, and seamless integration with digital tools. Current applications already demonstrate its robustness under operational and environmental loads, as well as its capacity to complement or replace conventional strain gauges and accelerometers.

Beyond this well-established use, the SUM4Re approach extends the application of FOS by exploiting its potential in combined static and dynamic structural condition assessment. In this context, FOS measurements are used not only to capture load-induced strain and vibration signatures but also to provide rich datasets that can be directly employed in the calibration of finite element models (FEM). This integrated use of FOS ensures that numerical models are updated with real-world behaviour, increasing their predictive accuracy and reliability for both structural safety verification and reuse planning.

A further advancement lies in the reuse and reemployment of structural elements. Within circular construction workflows, elements such as beams or slabs may be dismantled from one site and considered for integration into a new structure. FOS offers a unique advantage in this process, as sensors can be installed on the element without the need for dismantling after testing. Once instrumented, the structural element can be monitored during its current service, tested under controlled static and dynamic loads, and then relocated and re-employed in a new construction project while retaining its sensing capacity. This continuity of monitoring

across different service lives represents a major step forward compared to conventional methods, where condition assessment is often limited to single-use inspections.

At the research frontier, these developments place FOS at the centre of digital twin environments, where data streams from sensors continuously inform the digital representation of the asset. By combining long-term monitoring, FEM calibration, and multi-life assessment of structural elements, FOS moves condition assessment from reactive inspection toward proactive and predictive asset management. In doing so, the approach directly contributes to EO5 (analysis of suitability for circular use) by providing reliable structural condition data that supports reuse decisions, and to KPI8 (reduction of >60% in structural assessment time using FOS and transfer learning) by accelerating the evaluation process through automated, sensor-based measurements.

3.5. TRACLINE

Figure 7. TECN's multi-sensor system

3.5.1. State of the art

In recent years, the development of multisensory systems for the inspection and characterization of heterogeneous waste streams has gained increasing attention. A central challenge in this field is the ability to perform remote and continuous inspection of materials under conditions that emulate real industrial processes, where waste moves dynamically through conveyor systems. To address this, research initiatives have proposed the integration of continuous transport systems with embedded multisensory modules, enabling in-line inspection and continuous sampling of residual flows.

A representative example is the TRACLINE platform (Figure 7), specifically designed for the remote and online inspection of concentrates derived from complex residual streams. Its core innovation lies in the integration of several advanced spectroscopic subsystems into a single analytical module. Unlike conventional inspection methods used in industrial waste management, TRACLINE incorporates techniques such as Raman spectroscopy and Laser-Induced Breakdown Spectroscopy (LIBS), which are rarely applied in routine industrial environments but offer high analytical power. This makes TRACLINE uniquely positioned to generate large volumes of high-resolution spectral data while remaining fully compatible with industrial-scale deployment.

From an analytical perspective, multisensory approaches aim to extract comprehensive information about several key parameters of residual materials, including:

- Elemental composition and detection of toxic elements above regulatory thresholds.
- Mineralogical and crystalline structure of the residual matrix.
- Organic matter content, providing quantitative insight into compositional variability.
- Moisture content, a critical factor in both material quality and sensor response.

The strength of this approach resides in the complementarity of the sensing techniques. Table 8 illustrates the relative sensitivity of four widely used spectroscopic methods—LIBS, Raman, NIR, and UV-Vis—against the main quality parameters of interest represented as the number of asterisks being 1 minimum sensitivity, 5 maximum:

Table 8. Sensor specifications

Sensor / Parameter	LIBS	Raman	NIR	UV-Vis
Elemental composition	*****			**
Toxic elements	*****			**
Mineralogical composition	*	*****	***	***
Organic matter		***	*****	***
Moisture	*		*****	***

As shown in the table, relevant information for each parameter can be extracted by more than one sensing technique. This redundancy ensures not only the robustness of the system but also enables the synergistic combination of outputs across sensors. By leveraging these complementarities, multisensory platforms such as TRACLINE can build comprehensive analytical models that surpass the limitations of single-sensor approaches. The result is a system capable of addressing multiple dimensions of material quality simultaneously, laying the groundwork for reliable and scalable industrial implementation.

3.5.2. TRACLINE limitations

Despite the innovative integration of four spectroscopic techniques (Raman, NIR, UV-Vis, and LIBS) within the multisensory TRACLINE device, several limitations constrain its current performance. The most significant restriction lies in the fact that the system only enables punctual measurements, meaning that the information obtained is limited to discrete spots on the sample rather than continuous surfaces or volumes. This approach can limit representativeness, especially when dealing with highly heterogeneous Construction and Demolition Waste (CDW) materials.

Another critical limitation arises from the heterogeneity of acquisition parameters among the sensors. Each spectrometer operates with different integration times and signal-to-noise requirements, with Raman spectroscopy being particularly demanding. Raman requires substantially longer integration times to acquire a consistent and interpretable spectrum, and its performance is highly dependent on the intrinsic properties of the material being measured (e.g., crystallinity, fluorescence background, or mineral composition). In contrast, NIR and UV-

Vis typically offer faster acquisitions, while LIBS generates instantaneous signals, leading to significant discrepancies in acquisition rates between sensors.

Even when all sensors are directed to measure the same region of interest, technical challenges remain. The most notable is the risk of misalignment between measurement spots: the first point acquired with one sensor may not exactly overlap with the corresponding spot measured by the next sensor, particularly if the surface morphology is irregular. Furthermore, each sensor operates with a different spot size (diameter of the laser or illumination footprint), which means that even nominally co-located measurements may correspond to slightly different sample volumes. This divergence complicates the direct comparison and fusion of spectra across modalities, since variations in spot size can lead to differences in signal intensity, resolution, and sensitivity to local heterogeneities.

In summary, the current multisensory device demonstrates strong potential but faces practical constraints related to punctual-only acquisitions, heterogeneous integration times, material-dependent performance, and spatial mismatches across sensors. These limitations highlight the need for improved alignment systems, harmonised acquisition protocols, and future exploration of spatially resolved measurement approaches to ensure more robust and representative multisensory data fusion.

3.5.3. Beyond the state of the art

The multisensory approach developed in this task goes beyond the current state of the art by explicitly bridging the gap between controlled laboratory research and industrial-scale applications. While existing systems have demonstrated the potential of Raman, LIBS, NIR, UV-Vis and HSI technologies for material characterization, their use has been largely confined to static or semi-controlled environments. The TRACLINE platform represents a step forward by providing a flexible architecture that allows sensor parameterization under laboratory conditions and subsequent extrapolation to real processing environments.

The first stage focuses on laboratory testing, where each sensor can be calibrated and benchmarked under controlled conditions. This ensures that optimal acquisition parameters (e.g., integration times, illumination, background correction) are identified and linked to clear analytical outputs such as moisture content, mineral composition, or elemental impurities. Once these parameters are established, the next step is to transfer them to dynamic conditions that more closely resemble industrial operations, such as continuous conveyor belts and variable feed streams.

However, one of the critical insights of this work is that not all sensors may remain suitable for direct industrial deployment. Raman spectroscopy, for example, provides highly informative compositional data but requires long integration times and precise alignment, making it less robust for high-throughput applications. Similarly, UV-Vis spectroscopy is highly dependent on surface colour and brightness, which can be strongly affected by dirt, dust, or uncontrolled moisture in real plants. By contrast, NIR and LIBS show more promise for rapid, robust, and scalable acquisition, particularly when combined with RGB imaging for spatial segmentation. This pragmatic evaluation allows TRACLINE to go beyond theoretical demonstrations and to define sensor combinations that are not only analytically powerful but also technically and economically viable for recycling plants.

The practical added value lies in the fact that the system does not assume that every sensor must be deployed in industrial conditions. Instead, it follows a staged approach:

- Laboratory phase: full use of all sensors for exhaustive parameterization and data fusion.
- Industrial adaptation phase: selection of the most robust and cost-effective sensors (e.g., NIR + LIBS + RGB) for deployment in conveyor-based processes.
- Data integration: combining the industrially viable sensors with predictive models trained on richer laboratory/industrial datasets, thereby retaining analytical depth without compromising on operational speed.

4. Prerequisites for data acquisition

4.1. Prerequisites for iMMS point cloud acquisition

4.1.1. Properties of the iMMS scanner

The main device used for data acquisition was the Head Mounted Display Microsoft HoloLens 2. To capture the data, a custom application called Reality Mesher was developed. It can acquire not only environment information, but also operator's position, virtual markers and referenced RGB pictures. HoloLens 2 specifications are obscured by the manufacturer. However, it is known that its LiDAR range goes up to 5 m and its battery can last up to 2 h of continuous use. Furthermore, a performance analysis was conducted to determine the limits of the AR device in different environmental conditions. HoloLens 2 integrates a LiDAR depth sensor, visible light cameras, hand tracking capabilities, and an inertial measurement unit (IMU).

For data verification and geolocation, a second sensor was used: CHCNAV RS10. This device performs a fast, accurate scan that can contain colour. A real-time previsualization of the data can be seen on its tablet application, along with the route followed by the operator. However, data export is slow and must be done in a licensed computer. And finally, to make a comparison between the 3 main different sensors devices we also use a Leica RTC360. This device obtains an accurate version of the scenario, but it is considerably slower than the other because more than one scan is required.

More information about the sensors can be found in Table 9 and in Deliverable D2.1.

Table 9. Technical specifications of Microsoft HoloLens 2, CHCNAV RS10 and Leica RTC360

Image or drawing of the scanner	 **Figure 8. Hololens 2**	 **Figure 9. CHCNAV RS10**	 **Figure 10. Leica RTC360**
Size	40 cm x 25 cm x 16 cm	20 cm x 20 cm x 30 cm	12 cm x 24 cm x 23 cm + tripod
Weight	2.9 kg	1.9 kg	5.35 kg
Placement method	Head Mounted Display	Handheld Mobile Laser Scanner	Terrestrial Laser Scanner
Other properties to consider	Mixed Reality capabilities	GNSS integration, automatic colourization	3D spherical vision cameras, automatic colourization, automatic recording of movement from one station to another

4.1.2. Expected output data and measurements needed

The output data of the sensors are point clouds and, if desired, pictures. HoloLens 2 can also provide informative markers that are referenced with the environment point cloud. These markers can provide information about the route followed by the operator or any other characteristic from the building that the user provided during the scan from a given list, including identification of structural elements, materials and purpose of the room.

To perform measurements, the user must walk through the environment with the sensors working. HoloLens 2 has a range of 5 m and can only acquire elements in front of it. RS10 can measure elements up to 120 m away, with a horizontal angle of 270º. People and occluding elements must be avoided as much as possible. In the case of the RTC360, the user must select different locations to carry out the different scans and the result obtained is a full-dome scan (360º horizontal x 300º vertical).

4.1.3. Prerequisites pilot buildings

Both buildings are scanned from indoor perspective, considering the range limitations of HoloLens 2. RS10 was employed also in the visible outdoor perspective.

4.1.4. Practical and technical scan requirements

Use of the scanner:

- HoloLens 2
  - Distance: 5 m maximum
  - Battery: 2 h of continuous use
- RS10
  - Distance: between 0.5 m and 120 m
  - Battery: 1 h (can be switched during the scan)
  - Speed: 320 000 points/s
- Leica RTC360
  - Distance: between 0.5 m and 130 m
  - Battery: 4 h (use two batteries)
  - Speed: 2.000.000 points/s

Facilities needed:

- Ladder to reach the attic
- LAN network and computer for in-site data export
- Power for charging batteries

4.1.5. Strategic planning

As the final prerequisite analysis performed by this technology, Table 10 summarizes the strategic planning developed prior to the data acquisition on site, to allow for a efficient and optimal activity on site.

Table 10. Strategic planning

Access to building	To get access to the different building the previous days, manage the access to the buildings was needed. Moreover, follow the previously defined protocols delineated with coordinators for safety reasons.
Practical needs	To complete the scanning part using the 3 different HW. We also needed to bring a torch to scan using HoloLens 2 during the night in Anoeta train station due to the lack of illumination. Also, safety equipment.

What to scan where	In San Sebastian there are two buildings to be scanned. Anoeta was split into the outside part and the inside part due to its different conditions. Jolastokieta building was scanned in one day. For both buildings the most important thing is to scan accessible part of the layout of the buildings: walls, floor, ceiling, columns, doors, among others.
What to scan for renovation plan	All the structural elements are important for BIM modelling; especial interest was devoted to TECN beams and OLAR concrete.
How many hours needed for acquisition	Both scans were done in two days, one day for each building. Specifically, for Anoeta train Station, the scanning phase was divided into two different moments: morning for outside part due to the light, and during the night for indoor part due to the abundance of people (no-working metro lines). To sum up, the number of hours needed for acquisition was around 10 hours per case study.
Requirements input	Plans were requested to ascertain the geometry in advance and estimate the time required to access the works and battery load.

4.2. Prerequisites for XRF acquisition

4.2.1. Properties of the XRF scanner

The portable XRF device utilised at the San Sebastián pilot locations was the Oxford Instruments X-MET 7500, a handheld spectrometer equipped with a rhodium (Rh) anode X-ray tube, a high-resolution silicon drift detector (SDD), and an automatic five-position filter changer. The instrument has been designed to cover a broad elemental range, from magnesium (Mg) to uranium (U), and allows measurement of both major oxides and trace elements relevant to construction and demolition materials. The acquisition of each spectrum requires approximately sixty seconds of live time, during which the device collects spectra that are processed in real time and stored in standard CSV or PDF formats for subsequent integration into the project's material database. The scanner is characterised by its rugged IP54-rated housing and a rechargeable battery capable of sustaining eight to ten hours of operation.

4.2.2. Expected output data and measurements needed

The anticipated results of the acquisition campaign encompass quantitative data on the concentrations of major elements such as calcium, silicon, aluminium, iron, and magnesium, which play a pivotal role in the characterisation of concrete and aggregates. Furthermore, the XRF measurements furnish data concerning trace elements in hazardous metals, including lead, chromium, zinc, nickel, and copper. This data is expressed either in ppm or as a percentage of the weight. It is evident from these results that key ratios such as Ca/Si and Ca/Al can be derived, which are pertinent to the assessment of binder composition and carbonation depth in cementitious structures. To ensure the reproducibility of the results, replicate scans were carried out at selected points, and relative standard deviations were calculated to evaluate measurement precision.

4.2.3. Prerequisites pilot buildings

Daily activities in the building that must be considered

Two pilot sites in San Sebastián were selected for the purposes of the study: Anoeta Station and the former OTIS industrial factory. At Anoeta Station, the scans were focused on accessible structural elements such as asphalted areas, concrete platforms At the OTIS site, no active daily operations interfered with scanning; however, safety considerations (unstable surfaces, corroded metal elements) required adherence to occupational safety protocols.

Location of the XRF scan activities

At Anoeta Station, p-XRF scans were conducted on the asphalt surfaces of the top platform and in the circular concrete entrance area The measurement of intact and degraded surfaces (efflorescence, coatings) was undertaken. At the OTIS factory, scans concentrated on vertical structural elements (walls, columns, pool) and horizontal concrete slabs, with additional measurements targeting areas exhibiting visible corrosion or deposits. In both sites, measurement points were documented photographically and logged into the acquisition database with associated metadata (time, operator, environmental conditions).

4.2.4. Practical and technical scan requirements

Table 11. Scan requirements

Requirement category	Description
Instrument type	Oxford Instruments X-MET 7500 portable XRF (Rh tube, SDD, 5-position filter)
Measurement duration	~60 s live-time per scan (plus ~1–2 min for positioning and metadata)
Detection range	Elements from Mg to U; major oxides (Ca, Si, Al, Fe, Mg) and trace metals (Pb, Cr, Zn, Ni, Cu)
Output data	Elemental concentrations (% or ppm); derived ratios (Ca/Si, Ca/Al); replicate measurements for reproducibility
Power supply	Rechargeable Li-ion battery, 8–10 h runtime; field-replaceable
Ruggedness	IP54-rated, suitable for outdoor/industrial environments
Calibration/QA	SOILS-LE fundamental parameters (FP) calibration; CRMs measured at start/end of runs
Field conditions	Requires flat, accessible surfaces; remove coatings/dust where possible; avoid unstable structures

4.2.5. Strategic planning

As the final prerequisite analysis performed by this technology, Table 12 summarizes the strategic planning developed prior to the data acquisition on site, in order to allow for a efficient and optimal activity on site.

Table 12. Strategic planning

Access to building	Prior to the initiation of a scanning campaign, it is imperative that access protocols are thoroughly delineated with site managers, safety coordinators, and, where pertinent, local authorities. This encompasses the identification of structurally sound areas for entry, the scheduling of scans outside of peak construction and demolition activity, and the assurance of

	safe working distances from hazardous operations. Furthermore, access planning should ascertain whether permits are required for restricted zones or for working at heights, and whether scaffolding, lifts, or confined-space entry equipment will be needed.
Practical needs	When scanning high façades or ceilings, using lightweight pXRF units with extended-reach mounts can reduce operator fatigue and safety risks. In renovation contexts, combining pXRF with complementary sensors (e.g. moisture meters and thermal imaging devices) provides a fuller condition profile.
What to scan where	The focus may be on accessible wall surfaces, floor screeds, coatings, window frames and roof elements, as these are areas where hazardous substances (such as Pb, As, Cr and Hg) are more likely to be present. A systematic grid approach ensures representative coverage. For example, a spacing of 2–5 m is used for large areas, while denser grids are used in high-risk zones.
What to scan for renovation plan	This means not only targeting suspected hazardous areas but also sampling representative 'clean' sections for comparison purposes. For instance, the absence of heavy-metal glazes could be confirmed by scanning façade bricks, while Pb-based pigments in interior plasters could be checked before sanding or recoating.
How many hours needed for acquisition	The acquisition time depends on the number of points, the dwell time per measurement and the accessibility. A standard pXRF reading takes 20–60 seconds for most construction materials. Allowing for setup, repositioning and recording metadata, an operator can process 40–60 points per hour under optimal conditions. A thorough hazardous-material survey of a multi-storey building with a floor area of ~500 m² may take 8–12 working hours with one trained operator, or proportionally less with a two-person team. Difficult access (e.g. high façades) can double acquisition time due to setup and repositioning.
Requirements input	Efficient planning requires site blueprints, renovation/demolition plans, historical building material records and previous hazard surveys. This information enables likely 'hot spots' to be mapped in advance and scanning zones to be defined. All measurement locations should be logged with coordinates or floor plan markers for traceability and possible re-measurement.

4.3. Prerequisites for GPR+ECT acquisition

4.3.1. Properties of the GPR+ECT scanner

4.3.1.1. GPR sensor

For the GPR scanning, the Proceq GP8800 GPR sensor was used. This is a step-frequency continuous-wave (SFCW) GPR system that has a modulated frequency range 400-6000 MHz. This system with its small sized antenna is a high-frequency system, meaning that it has a high resolution and can resolve quite small features. Its maximum penetration depth is approximately 65 cm; however, the penetration depth depends also on the material conditions of the area to be scanned.

The GP8800 system is a single channel system and includes two antennas, the transmitter Tx and receiver Rx antenna which are enclosed in the same case. The total size of this probe is 8.9 x 8.9 x 7.6 cm and it weights approximately ~500 g. Its operating temperature conditions are between 5° and 40°. Furthermore, the probe has a replaceable skid plate attached for

protecting the antennas from damage. Additionally, it is equipped with an adjustable wheel, which apart from acting as a distance encoder, it allows for scanning with both normal and cross-polarization mode. Which mode to use depends on the targets sought, with each mode allowing to detect certain targets better than the other.

Regarding powering the probe, there are different ways that can be used. It can be powered by a removable Lithium-ion battery pack, a removable pack of 4 AA (NiMH) battery pack or with an off-the-shelf 10000 mAh power bank. The sensor is controlled from an iPad using an application called GP app. The connection between the application and the sensor is established wirelessly via Wi-Fi or via a USB-C cable. From the same app, apart from controlling the system for acquisition, data visualization and basic signal processing can be performed. When an internet connection is available in the iPad, the data can be uploaded from the app to the cloud to our platform called Workspace.

The GP8800 system has been designed for operating in direct contact with the ground, wall or other surface to ensure maximum penetration. The main application of this probe is concrete inspection where it is used to characterize concrete (e.g. moisture content) and locate structural elements such as rebars, post-tension cables, conduits but also for inspecting wooden poles and other applications where high-resolution is needed. An image of the GP8800 system is shown in Figure 11.

Figure 11. The Proceq GP8800 probe along with some of its features annotated

4.3.1.2. ECT sensor

For the ECT scans, the Proceq Profometer PM8000 was used. This system is based on electromagnetic conduction and consists of different coil arrangements which generate magnetic fields when charged by electrical pulses. This way, eddy currents are induced in the surface of conductive materials such as rebars. The applications of PM8000 are rebar detection in concrete, cover depth and rebar diameter estimation.

The ECT sensor can measure the rebar diameter with a high accuracy if the rebars are located in the first 6 cm, whereas the concrete cover can be measured up to approximately 16 cm depending on the conditions.

The probe along with its encoder cart has dimensions of 25 x 13 x 4.5 cm and a weight of 690 g. Figure 12 shows the PM8000 sensor along with the encoder cart. The system can be powered with a pack of 2 x AA (NiMH) rechargeable or non-rechargeable batteries with 8 hours autonomy or a USB-C power bank.

Similarly to the GPR probe, the Profometer is controlled from an iPad using an application called PM app from which data collection, visualization and basic processing happens. This app also supports uploading the data to the Workspace cloud.

Figure 12. The Proceq Profometer PM8000 sensor

4.3.2. Expected output data and measurements needed.

The output data from the GPR sensor are signal amplitude values versus time (or depth) which can be represented as radargram (B-scan) or time/depth slice images. The GPR data apart from images, they can also be exported as SEGY, standard geophysical format or even point clouds. Markers called tags placed on the data to mark objects of interest can be exported as docx or csv with information regarding the position and depth of the tag and the dielectric value being also exported. The csv export has further information regarding the signal amplitude at the location of the tag.

After interpretation, the dielectric values at different scanning locations could be estimated and provided as material properties but also the locations and depths of hidden elements and layers in a structure. Qualitative information can also be provided based on the data interpretation for characterizing materials.

From the ECT sensor, the output data are signal strengths; however these are used to calculate the rebar location and diameter and concrete cover depth, which can be exported as csv or docx files whereas the rebar location and extent themselves can be also exported as a dxf file. Images of the signal strengths, the cover depth heatmap or the detected rebars could also be exported.

To perform the measurements, the users need to secure a grid paper to the scanning location and place the sensors in direct contact with the ground. The scans are performed by collecting lines in the x and y direction of fixed length to form the area scan. Each line is marked on the grid paper and the collection starts first from the x direction followed by the y direction.

4.3.3. Prerequisites pilot buildings

All the data collection activities with the GPR+ECT sensor will take place indoors in the Jolastokieta building. Since this is an abandoned building that is not currently being used, apart from access permit to the site, there is no daily activity that might get disrupted that needs to be considered. However, all the safety protocols required for accessing and scanning this building should be followed.

4.3.4. Practical and technical scan requirements

Table 13. Practical and technical scan requirements for the GPR and ECT sensors

	GPR	ECT
Instrument	Proceq GP8800	Proceq PM8000

Control software	GP app installed in an iPad	PM app installed in an iPad
Encoder wheel	Integrated to the sensor but is adjustable	Sensor needs to be mounted to a cart
Measurement duration	~20 minutes	~20 minutes
Penetration depth	65 cm	Up to 63 mm for rebar diameter estimation Up to 180 mm for cover depth
Power supply	Removable and rechargable Lithium-ion battery pack with 8h autonomy (can be replaced in the field if needed)	Pack of 2 x AA (NiMH) rechargeable with 8h autonomy (can be replaced in the field if needed)
Calibration	Not needed	Required before start measuring Recommended every 5 minutes
Field requirements	Ideally flat surfaces with ease of access and no obstacles	Ideally flat surfaces with ease of access and no obstacles. Conductive objects should not be in close proximity to the sensor/ scanning location (>400 mm away)

4.3.5. Strategic planning

As the final prerequisite analysis performed by this technology, Table 14 summarizes the strategic planning developed prior to the data acquisition on site, to allow for an efficient and optimal activity on site.

Table 14. Strategic planning

Access to building	Prior to the data collection, access permit to visit the site must be obtained along with information on the access protocols specifically for this building that need to be follow.
Practical needs	Apart from the hardware itself, only safety equipment is needed for data collection.
What to scan where	With the GPR and ECT sensors, the Jolastokieta building will be scanned, where both walls and floors will be inspected with focus given on reinforced structures. Due to accessibility reasons, the scans will be performed internally. Areas where variation is observed/expected should be scanned and compared (e.g. a dry concrete area and a wet concrete area). The ECT sensor, requires the presence of metallic bars and thus can only be used in reinforced areas.

What to scan for renovation plan	All hidden structural elements are important for the renovation plan with focus given on identifying the metallic rebars in concrete that can be reused.
How many hours needed for acquisition	The data acquisition time depends on the number of areas scanned and the density of the lines. The setup of the control application, grid paper and the data collection itself for GPR for a small dense area scan should take about 20-30 minutes for a trained operator. Similar time is required for conducting a small dense area scan for calibrating and acquisition with the ECT sensor.
Input requirements	To plan better what areas will be scanned, how many scans to perform and density of the lines, prior information on the site such as photos, blueprints or information from previous surveys would be beneficial.

4.4. Prerequisites for FOS acquisition

4.4.1. Properties of the FOS

The fibre optic sensing (FOS) system deployed in this task is based on HBM newLight sensors coupled with the QuantumX MXFS optical interrogator. These sensors rely on fibre Bragg grating (FBG) technology, which provides precise strain, vibration, and temperature measurements along optical fibres.

Table 15 summarizes the main technical details of both deformation sensors (FS62) and vibration sensors (FS65):

Table 15. Properties of the FOS sensors

Sensor	Type	Capabilities	Key Properties
newLight FS62 / FS62CSS	Deformation / Strain sensor (FBG)	Precise, stable strain measurement. Exact numerical strain range isn't shown in the Spanish page due to internal error, but generally, FBG strain sensors are capable of micro-strain resolution and large dynamic range. *newLight* line promises high long-term stability.	Uses fibre Bragg grating (FBG) technology. Robust construction, resistant to humidity, corrosion, salty environments. Offers stability and repeatability over long periods.
newLight FS65	Optical accelerometer (vibration)	Measures accelerations up to ±10 g, at low frequency range (0-50 Hz).	FBG-based accelerometer, so optical and passive (no electrical signals at sensing head). IP68 protection, safe in harsh environmental conditions (humidity, salinity). Linearity < 2% over the measurement range. Can be used in monoaxial mode; multiple

			sensors allow multi-axis measurement.

Following the sensors description, it is highlighted the optical interrogator properties (QuantumX MXFS [36]). The QuantumX MXFS module acts as the interface between FBG sensors and the digital acquisition system. Its technical features include:

- Channel capacity: Up to 8 optical connectors, each supporting up to 16 FBG sensors, resulting in a maximum of 128 simultaneous channels per module.
- Sampling rates:
  - Normal speed mode: up to 100 samples per second per channel, suitable for long-term monitoring of slow changes such as creep or temperature drift.
  - High-speed mode: up to 2,000 samples per second per channel, suitable for dynamic monitoring such as vibration and transient loads.
- Measurement types supported: Strain, temperature, acceleration, load, and tilt, depending on the sensor configuration.
- Accuracy and resolution: Wavelength measurement resolution of a few picometers, corresponding to high sensitivity in strain and temperature readings.
- Integration and interfacing: Fully compatible with catman® software (v5.4 or higher) for real-time visualisation, analysis, and reporting. It also allows synchronisation with other QuantumX modules, enabling hybrid optical/electrical acquisition and open interfaces with LabVIEW and APIs.

Figure 13. QuantumX optic interrogator

4.4.2. Expected output data and measurements needed

- Strain profiles along structural elements (FS62) with high resolution and low drift over time.
- Vibration signatures and acceleration data (FS65) especially for low frequency phenomena (0-50 Hz), for example vibrations induced by traffic, occupancy loads, or nearby construction.
- Temperature compensation or measurements to correct strain readings (for those sensors that include dual FBGs for temperature).
- Time series data for static testing are synchronized with load cell measurements, to link the load applied with the deformation response.

4.4.3. Prerequisites pilot buildings

Daily activities in the building that must be considered

Since the selected pilot building is abandoned and not in active use, there are no daily operations, occupants, or ongoing activities that need to be coordinated with during FOS installation and monitoring. This eliminates potential interferences such as vibrations from occupancy, accessibility restrictions, or scheduling conflicts with users. However, the absence

of maintenance or active services also requires additional planning for power supply, security, and safe access to the site.

Location of the FOS activities

All FOS acquisition activities will take place inside the building, with priority given to structural elements representative of the building's load-bearing system. The indoor location ensures protection from direct environmental exposure, although humidity, dust, and debris typical of abandoned structures must be considered when preparing surfaces and protecting optical fibres.

4.4.4. Practical and technical scan requirements

- Mounting and orientation: FS62 sensors must be bonded or affixed along the axis of expected strain (beam, slab, joint). Adequate surface preparation needed to ensure adhesion and accurate reading. For FS65 accelerometers, orientation relative to expected vibration vector matters (monoaxial or multi-axis). Multiple sensors may be needed to capture multidirectional vibrations.
- Protection: Because FS65 has IP68 rating, ensure installations respect environmental sealing, protect cable runs and connection points. For FS62, ensuring cable protection against mechanical damage, moisture ingress, etc.
- Interrogation system: Optical interrogator HBM's QuantumX optical modules capable of reading FBG sensors at required wavelengths and sampling rates. Calibration needed to establish baseline (zero strain / reference temperature).
- Long-distance deployments: Because of compatibility with telecom fibre, plan for cable lengths, losses, and connectors; ensure overall signal budget (fibre attenuation, connector/coupler losses) is respected.
- Data logging: Sampling frequency must cover the 0-50 Hz range for accelerometers; for strain sensors, sampling can be lower but continuous. Storage and power for interrogator, possibly using battery or mains with safe routing.

4.4.5. Strategic planning

As the final prerequisite analysis performed by this technology, Table 16 summarizes the strategic planning developed prior to the data acquisition on site, to allow for an efficient and optimal activity on site.

Table 16. FOS strategic planning table

Access to building	Coordinated with MOYUA to ensure safe and timely access during programmed activities for testing.
Practical needs	Scaffolding/ladders for elevated components; protective covers for fibres; power supply for interrogator unit.
What to scan where	Representative steel beams at Jolastokieta Urbanization; load-bearing elements most relevant to reuse assessment that presents a good structural condition.
What to scan for renovation plan	Structural elements identified for potential reuse, focusing on their condition and long-term durability.
How many hours needed for acquisition	Approximately 4–6 hours per element, depending on accessibility and complexity, including preparation and calibration.

Requirements input	Baseline structural drawings, FEM models, safety permits, and coordination with other scanning activities (iMMS, GPR-ECT).

4.5. Prerequisites for TRACLINE acquisition

4.5.1. Properties of TRACLINE

The TRAZIA system is a multisensory inspection platform designed for the semi-industrial characterization of Construction and Demolition Waste (CDW), particularly mixed fraction materials. It combines a continuous conveyor mechanism with an integrated multi-sensor head, enabling the simultaneous acquisition of both spatial and chemical information under dynamic conditions.

The system incorporates a variable-speed conveyor belt (0.2–0.6 m/s), which ensures continuous transport of the waste stream through the inspection zone. At the inlet, a motorised roller with adjustable height compacts the material and homogenises its surface layer, guaranteeing consistent conditions before analysis.

At the core of the device lies the sensor platform, consisting of a motorised structure that translates and positions the multi-sensor head transversely to the direction of material flow. This design allows precise alignment of the sensing optics with the conveyor stream and facilitates flexible measurement strategies across different waste distributions.

The multi-sensor head integrates four punctual spectroscopic techniques—Raman Spectroscopy (RS), Laser-Induced Breakdown Spectroscopy (LIBS), Near-Infrared Spectroscopy (NIRS), and Ultraviolet-Visible Reflectance Spectroscopy (UV-Vis)—together with a linear RGB camera. Raman and LIBS modules provide detailed information on mineral phases and elemental composition, while NIR and UV-Vis are sensitive to moisture content, organic matter, and optical reflectance properties. The RGB line scan camera complements this data with spatial and morphological information (colour, particle distribution, surface texture), creating a synergistic dataset that combines both spectral and imaging domains. The sensor head is protected by a forced-ventilation enclosure equipped with filters, safeguarding optical components from dust and ensuring measurement stability in semi-industrial environments.

All light sources, optical instrumentation, and power electronics are integrated into a sealed instrumentation cabinet, which maintains robustness and safety. In parallel, a dedicated control cabinet manages the entire line, housing the programmable logic controller (PLC), safety relays, and power modules. Special attention is given to safety requirements, as the integration of class IV lasers and high-power UV sources follows the IEC-60825-1 standard to protect operators during operation.

Data acquisition and processing are managed by a dedicated computer, which governs three main functions: (i) preprocessing of all spectra, including noise filtering, baseline correction, standardization, or referencing to calibration standards (Spectralon and others); (ii) structured storage of the processed spectra into datasets, ensuring that acquisition frequency and test duration are configurable; and (iii) communication with the PLC via Ethernet, enabling real-time coordination of alarms, safety controls, and module activation.

Finally, the system features a graphical user interface (GUI) implemented on a touch display. This interface provides operators with complete control of the platform, including system start-up and monitoring of all sensors, calibration using reference materials, adjustment of acquisition frequencies and conveyor belt speed, and real-time access to alarm states.

Altogether, TRAZIA is characterised by its ability to combine punctual spectroscopic measurements with spatial imaging techniques in a moving waste stream, producing high-resolution spectral and visual datasets under conditions close to real industrial operation. This

integration makes the system a powerful tool for bridging laboratory-based material characterization with scalable, semi-industrial applications in CDW recycling.

4.5.2. Expected output data and measurements needed

The multisensory platform produces a variety of outputs depending on the sensing modality, each of which contributes complementary information to the characterization of grey fraction (for this use case) CDW materials.

The punctual spectroscopic sensors (Raman, LIBS, NIR, and UV-Vis) generate two-dimensional spectra in which peaks and valleys correspond to specific chemical or mineralogical features of the material. For instance, Raman provides vibrational bands associated with carbonates or silicates, LIBS delivers elemental emission lines linked to oxides or impurities, NIR highlights water-related absorption bands, and UV-Vis reflects the optical response of the surface. Given that each acquisition campaign can yield thousands of spectra, direct use of raw data is impractical. Instead, the system is configured to extract and return diagnostic features—such as the presence, intensity, or ratio of specific peaks—so that each measurement can be translated into interpretable chemical information rather than storing complete raw spectra. This strategy dramatically reduces data redundancy while preserving its analytical value. It is necessary for a technician specialized in programming and applying ML and DL models to extract the desired characteristics from the extracted data.

The RGB line-scan camera provides high-resolution spatial images over a user-defined length of up to 500 mm. These images capture particle morphology, colour, texture, and distribution, enabling segmentation into regions of interest. When combined with LIBS or Raman shot positions, the RGB data can be used to directly link chemical spectra with specific particles or zones in the material stream.

In terms of measurements needed, several layers of data are required to achieve reliable material classification and industrial applicability:

- Spectral fingerprints: identification of characteristic peaks (e.g., carbonates in Raman, Ca/Si/Al emission in LIBS, water absorption in NIR) that can serve as reference markers.
- Moisture content indicators: systematic measurement of absorption bands at 1400–1900 nm (NIR/HSI), critical for distinguishing between wet and dry conditions.
- Particle-level mapping: extraction of morphological descriptors from RGB images, such as size, shape, and clustering of aggregates.
- Cross-modality correlation: linking punctual spectroscopic features with spatial segmentation from RGB (and HSI when available) to provide chemical + visual characterization at the particle level.
- Quality control parameters: aggregation of measurements into statistics (mean spectra, variance, feature distributions) to detect anomalies such as gypsum, wood, or impurities in the recycled aggregate stream.

Altogether, the expected output of TRAZIA consists not only of raw spectra and images, but of a structured dataset of features and descriptors that can be directly used in predictive models. This enables a transition from simple spectral inspection to actionable quality indicators, paving the way for integration into industrial-scale sorting, material passports, and smart recycling workflows.

4.5.3. Prerequisites pilot buildings

The transition from laboratory-scale characterization to semi-industrial pilot buildings requires careful consideration of both methodological and infrastructural prerequisites. While the laboratory setup enables controlled measurements of prepared samples—ensuring homogeneity, stable illumination, and optimised sensor configurations—the reality of pilot environments introduces additional comple

xity. Material flows are continuous, particle distribution is irregular, and environmental factors such as dust, variable humidity, and vibration can affect data quality. For this reason, pilot buildings must meet certain requirements to guarantee that the multisensory methodology developed in laboratory conditions can be effectively transferred and validated at an industrial scale.

One of the primary aspects concerns the environmental conditions in which the sensors will operate. Spectroscopic sensors such as Raman and LIBS are highly sensitive to dust, alignment, and optical interference, making it essential to control airborne particles through forced ventilation and protective filters in the measurement area. For imaging sensors (RGB and UV-Vis), ambient lighting must be minimised or controlled to avoid variability in reflectance, ensuring that the signal depends only on the material properties and not on external light fluctuations. Additionally, vibration control of the conveyor and mechanical stability of the sensor head are essential to maintain consistent measurements during continuous operation.

Equally important are the requirements of the material flow. Unlike laboratory-prepared samples, which are homogenised, sieved, and classified, real CDW streams in pilot buildings will present variable granulometry, random moisture levels, and occasional impurities such as gypsum or wood. To ensure representativeness, a minimum volume of material per fraction must be processed, and compacting rollers or feeding mechanisms should be used to homogenise the layer height before inspection. This reduces the risk of shadowing, misalignment, or unrepresentative spectra from isolated clasts.

The adaptation of sensor parameters also plays a critical role. Integration times and acquisition parameters optimised in laboratory conditions (e.g., Raman's long integration times) may not be directly transferable to pilot environments, where throughput and measurement speed are key. For this reason, robust sensors with fast acquisition times (e.g., NIR, LIBS, RGB) are prioritised for dynamic use, while Raman or UV-Vis may be reserved for specific checkpoints or laboratory validation. Calibration standards and procedures validated under static conditions must be replicated in pilot environments to confirm reproducibility under motion.

Finally, infrastructure and safety considerations must be carefully addressed when transferring the methodology to pilot buildings. Due to the high cost, complexity of realignment, and risk of damage during transport, the complete multisensory system cannot be moved from the laboratory to an industrial environment. Instead, individual sensors—selected based on laboratory testing and their robustness under dynamic conditions—should be deployed to replicate the functionality of the multi-sensor platform in situ. Each sensor must be equipped with its own illumination system, spectrometer, and power supply, ensuring independent operation and minimising integration risks.

In addition, dedicated enclosures are required to control environmental factors such as dust and ambient lighting, which can otherwise interfere with optical measurements. These cabins not only protect the sensors but also stabilise measurement conditions, increasing reproducibility. It is important to highlight that not all industrial environments will allow the integration of every sensing technique: while some, like NIR, LIBS, or RGB, are more robust and adaptable, others (e.g., Raman or UV-Vis) may face limitations in alignment, acquisition speed, or sensitivity to ambient conditions. For this reason, pilot implementation must be strategically planned, selecting the most suitable sensors for each scenario while ensuring compliance with industrial safety standards and maintaining operational feasibility.

In summary, pilot buildings must provide the structural, environmental, and operational framework that allows laboratory-developed methods to be tested under semi-industrial conditions. By addressing these prerequisites, it becomes possible to validate which sensor combinations are robust enough for real-world applications and to refine acquisition protocols for eventual large-scale deployment. The most adaptable method for this case is to apply industrial conditions to the laboratory system and see how the results differ from those

obtained under controlled conditions. After this, the sensors would be installed in the plant and tested in situ.

Key prerequisites for pilot buildings include:

- Controlled illumination and dust management in the inspection zone.
- Mechanical stability of the conveyor system and adjustable feed rollers for homogenization.
- Processing of minimum representative volumes of CDW fractions.
- Adaptation of laboratory-calibrated parameters (e.g., integration times) to dynamic conditions.
- Prioritization of robust sensors (NIR, LIBS, RGB) for high-throughput acquisition.
- Availability of power supply, ventilation, and protective infrastructure.
- Compliance with IEC-60825-1 laser safety standards, including protective barriers and interlocks.
- Simulation of semi-industrial situation in TECN facilities adapting the device to these conditions.

4.5.4. Practical and technical scan requirements

The implementation of multisensory measurements in pilot environments requires addressing a series of practical and technical scanning requirements to ensure data reliability and operational feasibility. Unlike laboratory conditions, where material preparation and acquisition parameters can be tightly controlled, industrial scenarios introduce variability in material flow, ambient conditions, and mechanical stability. For this reason, the following aspects must be considered:

- **Environmental conditions**: Dust and airborne particles represent a major source of interference, particularly for optical techniques such as Raman, LIBS, and HSI. Enclosures or dedicated cabins with forced ventilation and filtration are necessary to maintain measurement stability. Ambient lighting must also be controlled, as external illumination can distort signals in UV-Vis, RGB, and hyperspectral imaging. Vibrations and mechanical oscillations in conveyor systems should be minimized to ensure consistent acquisition.
- **Sensor-specific requirements**: Each spectroscopic and imaging modality has its own operational needs.
    - *Raman* requires relative darkness, precise alignment, and long integration times, which limit its applicability under continuous flow.
    - *LIBS* demands clean, stable surfaces for plasma generation and safety measures to manage gas and plasma emissions.
    - *NIR* is comparatively robust, though highly sensitive to water absorption bands and to sensor–sample distance.
    - *UV-Vis* depends strongly on colour and optical brightness, requiring stable and uniform illumination.
    - *RGB* imaging benefits from uniform, calibrated light sources and is essential for segmentation and spatial mapping.
    - *HSI* (if integrated) requires powerful illumination, controlled environments, and significant computational capacity due to the size of the generated datasets.
- **Acquisition parameters**: To adapt measurements to dynamic conditions, integration times must be shortened, and acquisition frequencies synchronized across sensors to avoid spatial misalignment. Material homogenization prior to inspection, through compacting rollers, is critical to stabilize layer thickness and reduce shadowing effects. Conveyor speed (0.2–0.6 m/s) should be adjustable to balance throughput with sensor

integration capacity. Calibration using reference standards (Spectralon, colour targets) remains essential to ensure reproducibility.

- **Flow control requirements**: While it is not feasible to fully adapt tones of real grey fraction waste to laboratory standards, partial conditioning of the material stream is necessary to ensure reliable characterization. Randomly wet samples, heavily dust-contaminated clasts, or mixed fractions arriving simultaneously make it extremely difficult to obtain reproducible measurements. For this reason, a practical protocol should be established in pilot buildings to regulate factors such as surface moisture, fraction separation, and dust reduction, bringing the flow closer to laboratory-like conditions without compromising its industrial representativeness.
- **Safety and infrastructure**: Given the use of class IV lasers and high-power UV sources, strict compliance with IEC-60825-1 standards is required, including protective barriers, interlocks, and emergency stop protocols. Adequate space must be provided for control cabinets, power modules, and operator access.
- **Data processing capacity**: Real-time operation requires immediate preprocessing of acquired spectra and images, including noise filtering, baseline correction, and reflectance normalization. Structured storage of data must ensure traceability across batches. Furthermore, sufficient computational power must be available to handle RGB and especially hyperspectral datasets without compromising throughput.

In conclusion, practical and technical scanning requirements extend far beyond the laboratory calibration of sensors: they involve the adaptation of acquisition protocols, infrastructure, and data processing pipelines to the realities of industrial CDW recycling environments. By considering these prerequisites, the methodology can be effectively scaled up while preserving measurement quality and operational robustness.

4.5.5. Strategic planning

The strategic planning of the pilot must address both the practical limitations of the demonstration site and the opportunities offered by the industrial network of the project partners. Since Construction and Demolition Waste (CDW) will not be generated directly at the pilot building, a contingency plan has been defined. In this plan, representative CDW samples produced during the pilot are transported to the facilities of TECN, where they can be analyzed under controlled conditions. This approach has the added value of enabling measurements on a wider range of material flows than those produced explicitly within the pilot, thus increasing the robustness and representativeness of the dataset. Importantly, it is not necessary to relocate the multisensory TRAZIA device itself, avoiding the costs and risks associated with transport, alignment, and recalibration.

In parallel, the industrial group to which the project partner MOYUA, responsible for waste supply belongs can provide access to CDW streams from different construction sites and with diverse origins. This extended access to heterogeneous material streams is strategically valuable, as it allows validation of the methodology across multiple real-world scenarios. By testing the protocols on CDWs of different provenance, the project ensures that the developed models and procedures are not limited to a single case study but are transferable and scalable to the wider sector.

Together, these strategies provide resilience to the pilot plan: the contingency pathway ensures continuity of testing in case of limited on-site material, while the broader industrial collaboration enhances the generalizability and applicability of the results to future large-scale implementations.

5. Baseline assessment – Preliminary results of material and data acquisition

5.1. AR iMMs-RGB by UVIGO

5.1.1. Process

The device used for data collection was the Microsoft HoloLens 2, where specific software was developed and implemented to capture the 3D environment, position virtual markers, and take referenced RGB photos. However, Microsoft does not provide technical specifications for this device, beyond indicating that it has a range of 5 m and a battery life of 2 hours. It was necessary to perform a performance analysis to determine the limits of the AR glasses in different light and atmospheric conditions (more information in Deliverable D2.1). The HoloLens 2 integrates various sensors necessary for data collection, such as a depth sensor (Time of Flight (ToF) LiDAR), an RGB camera, four cameras for hand tracking, and an inertial measurement unit (IMU).

In addition, a Handheld Mobile Laser Scanner (HMLS) CHCNAV RS10 and Terrestrial Laser Scanner (TLS) were used to obtain reference data in the evaluation of the quality of the point clouds generated by the HoloLens 2. The specifications for the HW used are depicted in Table 17.

Table 17. Overview of scan materials and programs used by UVIGO

	Microsoft HoloLens 2	CHCNAV RS10	Leica RTC360
Scan material			
Program used	Reality Mesher App developed by UVIGO	CHCNAV CoPre 2 LiDAR Processing Software	Cyclone Register 360 LiDAR Processing Software
Registration and data visualisation	CloudCompare (open source) Developed by Telecom ParisTech and the R&D division of EDF	CloudCompare (open source) Developed by Telecom ParisTech and the R&D division of EDF	CloudCompare (open source) Developed by Telecom ParisTech and the R&D division of EDF

The workflow consisted of the following actions. Starting with walking around and asses the to-be-scanned area and then acquire the data by using the three scanners: the HoloLens 2, Leica RTC360 and the CHCNAV RS10. The data is collected by walking around and through the different regions. For Leica RTC360 different scanning are required, starting from different points. After data collection, it was needed process the data to check the results in order repeat possible occlusions or missing parts.

Processing the data is in relation to UC1: 3D geometric models of buildings for visual inspection and integration of georeferenced information collected from various sensors.

5.1.2. AR iMMs-RGB results: Anoeta Station

The following figures show the point clouds generated with Microsoft HoloLens 2 (Figure 14), Leica RTC360 (Figure 15), and CHCNAV RS10 (Figure 16).

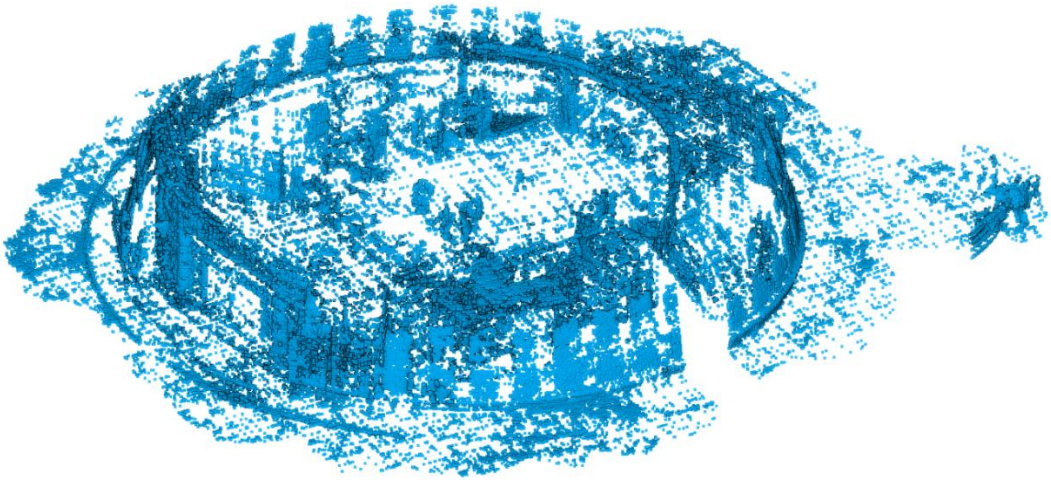

Figure 14. Point cloud obtained in Anoeta hall with Microsoft HoloLens 2 (indoor & outdoor)

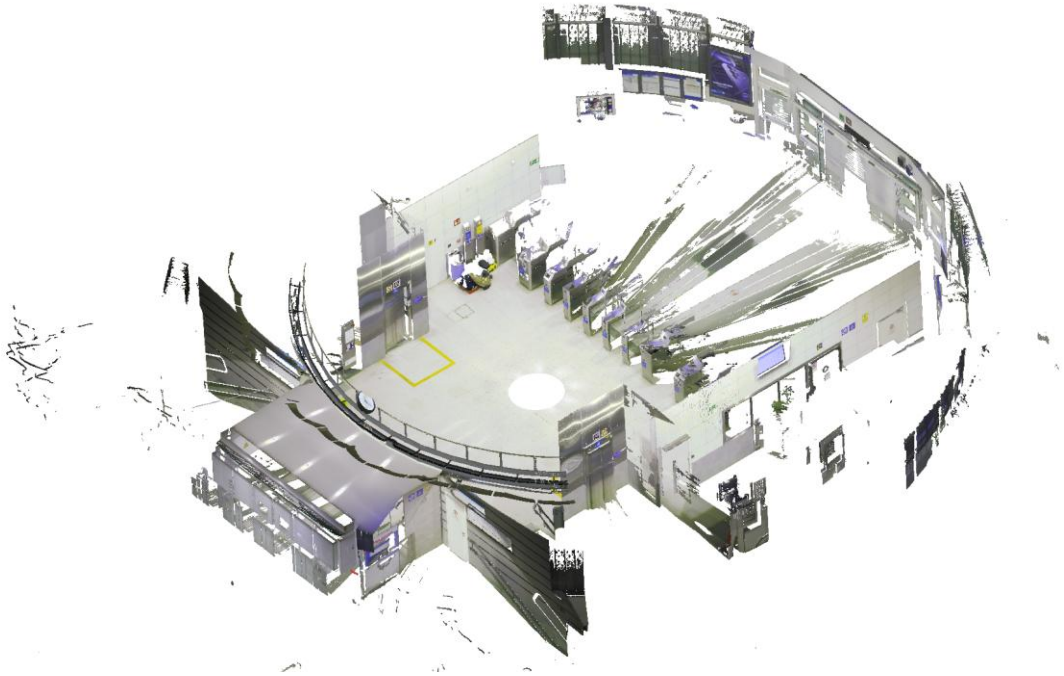

Figure 15. Point cloud (1 scan) obtained in Anoeta with Leica RTC360

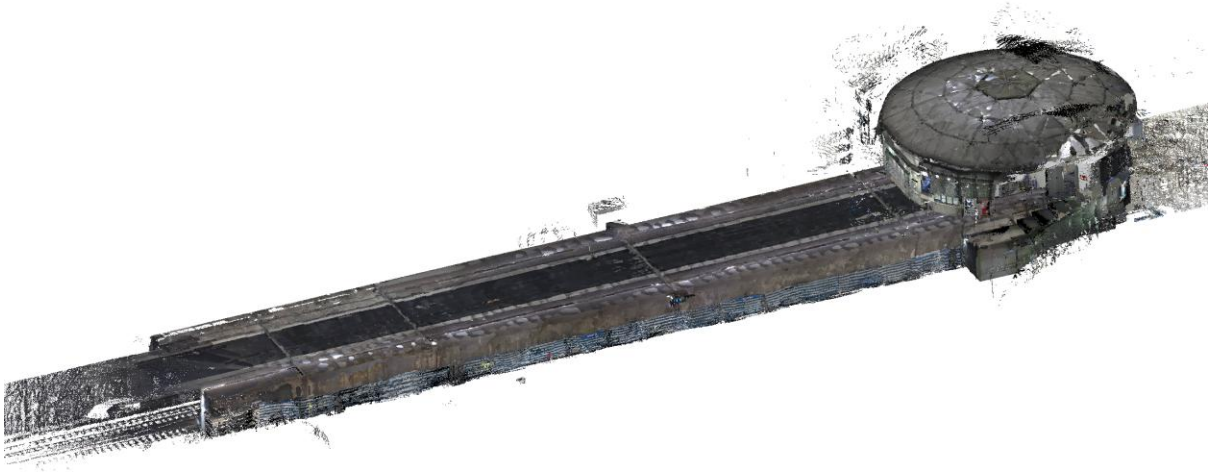

Figure 16. Point cloud obtained in Anoeta with CHCNAV RS10 (platforms area)

5.1.3. AR iMMs-RGB results: Jolastokieta

The following figures show the point clouds generated with Microsoft HoloLens 2 (Figure 17), Leica RTC360 (Figure 18), and CHCNAV RS10 (Figure 19).

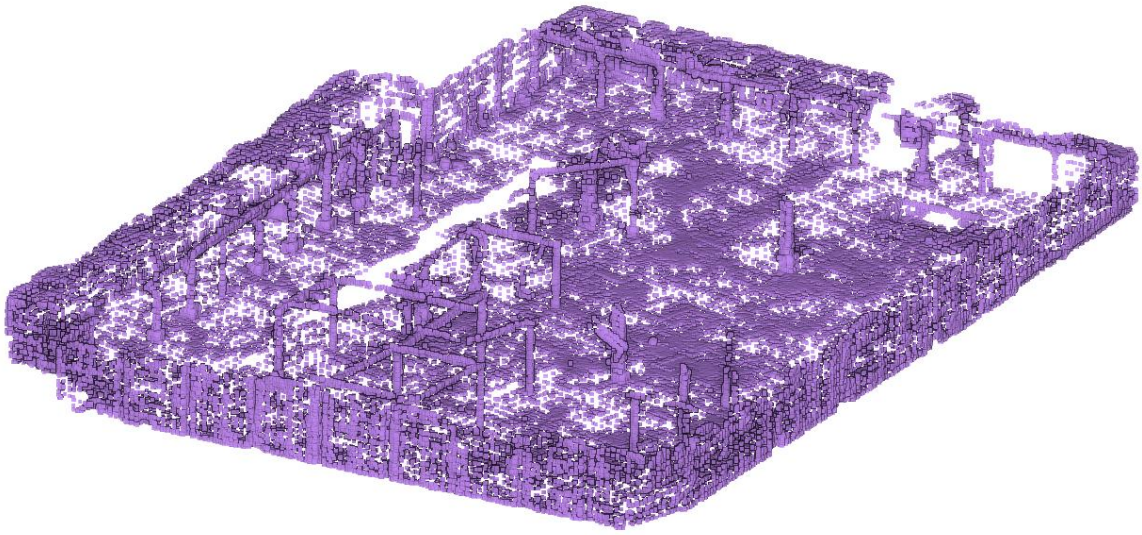

Figure 17. Point cloud obtained in Jolastokieta with Microsoft HoloLens 2

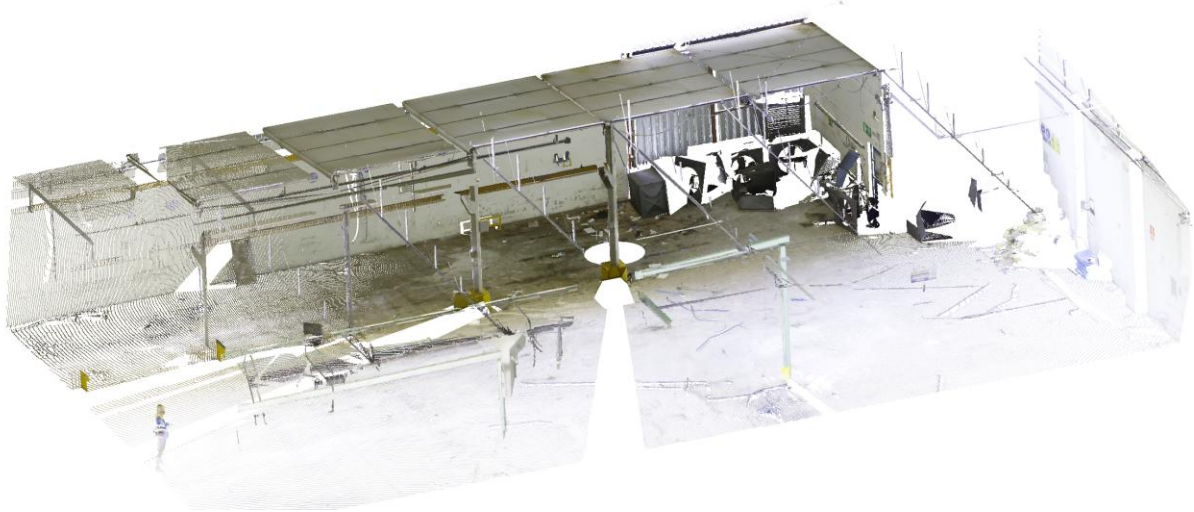

Figure 18. Point cloud (1 scan) obtained in Jolastokieta with Leica RTC360

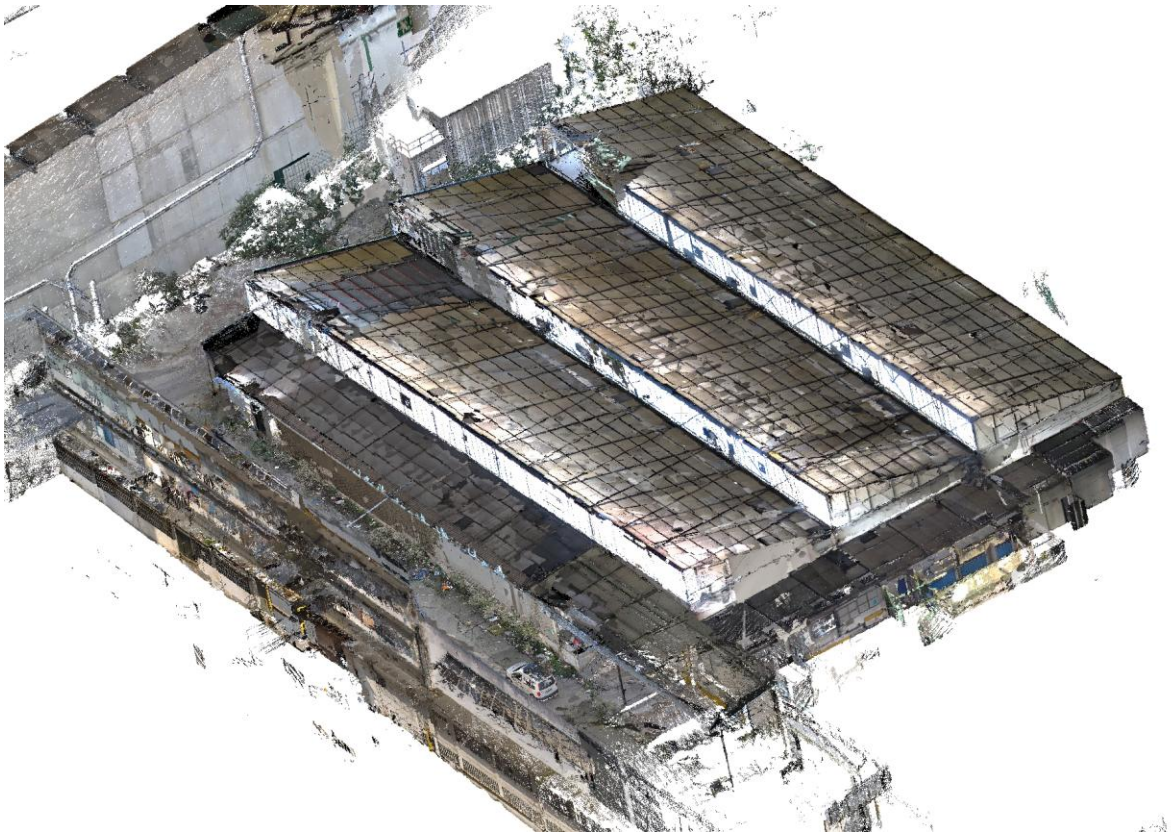

Figure 19. Point cloud obtained in Jolastokieta with CHCNAV RS10.

5.1.4. iMMS labour productivity

This baseline assessment establishes current performance metrics for the scanning task through workflow documentation and comprehensive cost analysis. Table 18 describes the overall workflow and quantifies costs across five key areas: tool transport, worker transport, labour hours, operational hours, and additional expenses. This systematic analysis provides the foundational benchmark for measuring future process improvements and enables informed cost-benefit analyses for scanning operation optimization.

Table 18. Details about the cost's quantification

Workflow	Geometric review of pre-visit plans On-site description data scanning On-site data verification (processing) Labelling and modelling in the office 3 workers
Cost – tool transport	Included on workers transport
Cost – workers transport	300€ travel + 1200€ accommodation + 500€ allowances
Cost – labour hours	8 hours x 4 days x 3 workers x 33.33€/h = 3200€
Cost – operational hours	6 hours x 2 days x 3 workers x 33.33€/h = 1200€

Amount of time for the whole scan process.

The overall scan process took two days to be done in both buildings with all scan techniques. The acquisition with the HoloLens 2 took more time than with CHCNAV RS10 but less than Leica RTC360 (this is including the marker positioning; putting virtual labels with the AR too), which was done in-real-time during the scan. The detailed summary about productivity is depicted in the following.

Table 19. Details about the scans with the different HW

SUM UP TIMES			
Anoeta Station			
	HoloLens 2	CHCNAV RS10	Leica RTC360
Acquisition time	74 minutes	12 minutes	93 minutes
Preprocessing time	*Not applicable*	20 minutes	90 minutes
Number of scans	1	2	10

Jolastokieta building			
	HoloLens 2	CHCNAV RS10	Leica RTC360
Acquisition time	58 minutes	8 minutes	72 minutes
Preprocessing time	*Not applicable*	7 minutes	90 minutes
Number of scans	1	1	24

5.2. XRF by OLAR

5.2.1. Location of the pilot measurements

The activity related to this task of OLAR solutions was accomplished on the April 11th, 2025, in the pilot testing of MOYUA in two different locations. These 29 in situ measurements were conducted at multiple spots across five distinct areas of the former OTIS elevator factory and one area within the Anoeta football stadium.

The selection of the spots for measuring the inorganic composition was done by the members of OLAR Solutions UG and the MOYUA. The main objective of the measurements was capturing the maximum material variability based on visual inspection and spatial distribution. The locations of the twenty-nine measurements in six different spots in two different locations is shown in Figure 20. These in situ measurements were done with the Oxford XMET 7500 portable X-ray fluorescence (pXRF) spectrometer.

5.2.2. Description of the equipment

Oxford XMET 7500 portable X-ray fluorescence (pXRF) spectrometer, equipped with a Rhodium (Rh) anode X-ray tube, a high-resolution silicon drift detector (SDD), and an automatic 5-position filter changer for optimized excitation conditions. The elemental quantification was conducted using the SOILS-LE calibration program, which employs the fundamental parameters (FP) method to correct for matrix effects. Each measurement consisted of a 60-second live-time acquisition, covering elements from magnesium (Mg) to uranium (U). Moreover, to ensure the data reliability, it was applied the following approaches: 1) Certified reference materials (CRMs) (BCR-032 #919 and GMB306-12) were pressed into 32-mm pellets and analysed at the beginning and end of each measurement run. 2) Instrument stability was verified through periodic recalibration and background checks.

Figure 20. From top left to bottom right. Area I: Spot measurements from right to left. Area II: Spot measurements from right to left (areas with salt efflorescence are visible all along the wall and corner). Area III: Spot measurements from right to left. Area IV: Spot measurements from right to left. Area V: Spot 1 yellow beam and spot 2 green beam. Anoeta asphalt measurement area.

Table 20 shows the elemental composition of the 29 spots analysed during the in-situ measurements (detailed XRF spectra are provided in Appendix A Figure. A1). The results approach 100% in total elemental weight (%).

Table 20. Elemental composition of the 29 spots analysed during the in-situ measurements

Sample location	Inorganic compound (wt.%)												
	Mg	Al	Si	P	S	Cl	K	Ca	Ti	V	Cr	Mn	Fe
otis-I.1	0.0 ± 0.0	2.9256 ± 0.1567	3.0369 ± 0.0621	0.5815 ± 0.0195	9.3693 ± 0.0418	1.5559 ± 0.0174	30.3782 ± 0.0761	47.6488 ± 0.1018	0.2133 ± 0.0098	ULLD	0.065 ± 0.0164	0.0667 ± 0.0142	3.2238 ± 0.0358
otis-I.1.humedo	0.0 ± 0.0	1.785 ± 0.1387	1.0802 ± 0.0418	0.5685 ± 0.018	16.474 ± 0.0514	1.6377 ± 0.0176	44.1078 ± 0.0913	30.8616 ± 0.0875	0.1143 ± 0.0084	ULLD	0.0403 ± 0.0134	0.0622 ± 0.0123	2.3833 ± 0.0291
otis-I.2	3.0332 ± 0.8049	2.8271 ± 0.1463	3.2041 ± 0.0614	0.6741 ± 0.0185	0.9468 ± 0.0136	1.3534 ± 0.0145	6.1036 ± 0.0303	76.6337 ± 0.0978	0.3115 ± 0.0103	ULLD	0.0486 ± 0.0155	0.0903 ± 0.0148	3.686 ± 0.0377
otis-I.3	0.0 ± 0.0	3.1411 ± 0.1551	4.0997 ± 0.0684	0.6517 ± 0.0191	3.4948 ± 0.0254	1.4108 ± 0.0152	11.4654 ± 0.0426	70.1804 ± 0.0978	0.3349 ± 0.0106	ULLD	0.0568 ± 0.0156	0.0939 ± 0.0149	4.0095 ± 0.039
otis-I.4	0.0 ± 87.7689	2.1994 ± 0.1539	3.4065 ± 0.0649	0.6007 ± 0.0197	0.6861 ± 0.0123	1.4239 ± 0.0149	4.1739 ± 0.0248	82.1692 ± 0.0988	0.3128 ± 0.0104	ULLD	ULLD	0.1293 ± 0.0134	3.7139 ± 0.0381
otis-I.5	0.0 ± 0.0	2.0379 ± 0.1603	2.8508 ± 0.0627	0.5443 ± 0.02	0.935 ± 0.0144	1.2124 ± 0.0144	5.5871 ± 0.0291	81.0928 ± 0.1003	0.315 ± 0.0106	ULLD	0.0688 ± 0.017	0.1054 ± 0.016	4.0422 ± 0.04
otis-II.1	0.0 ± 0.0	1.8105 ± 0.2725	2.4104 ± 0.0973	1.2568 ± 0.0432	20.0433 ± 0.0929	4.0669 ± 0.0457	1.2308 ± 0.0291	64.0763 ± 0.1421	0.214 ± 0.0176	ULLD	0.1805 ± 0.0341	ULLD	4.1862 ± 0.06
otis-II.2	0.0 ± 0.0	1.9287 ± 0.2086	2.1532 ± 0.0725	0.8462 ± 0.0285	21.8943 ± 0.0811	3.3963 ± 0.0343	1.0743 ± 0.0203	64.8307 ± 0.1206	0.1167 ± 0.0132	ULLD	0.0698 ± 0.0231	ULLD	2.9334 ± 0.043
otis-II.3	0.0 ± 0.0	3.7172 ± 0.245	12.2794 ± 0.1531	0.9229 ± 0.0355	2.8009 ± 0.0331	7.6874 ± 0.0488	3.6242 ± 0.0353	58.2515 ± 0.1124	0.7618 ± 0.017	ULLD	0.0925 ± 0.0246	0.1115 ± 0.0217	9.0003 ± 0.0716
otis-II.4	0.0 ± 0.0	2.4282 ± 0.2147	4.4283 ± 0.091	0.8287 ± 0.0276	12.8429 ± 0.0598	4.1378 ± 0.034	2.0152 ± 0.0241	67.3985 ± 0.1146	0.3478 ± 0.0139	ULLD	ULLD	ULLD	5.2016 ± 0.0539
otis-II.5	0.0 ± 0.0	2.04 ± 0.3643	2.2828 ± 0.1206	1.4273 ± 0.0555	16.6443 ± 0.1007	5.7269 ± 0.0623	1.6301 ± 0.0382	63.3176 ± 0.1668	0.304 ± 0.0238	ULLD	0.1451 ± 0.0403	ULLD	5.6468 ± 0.0822
otis-II.6	0.0 ± 0.0	2.8234 ± 0.3371	10.4787 ± 0.1799	1.0256 ± 0.0527	8.3285 ± 0.0669	4.1976 ± 0.0478	3.6124 ± 0.0449	58.093 ± 0.1347	0.8213 ± 0.0204	ULLD	0.1557 ± 0.0322	0.1108 ± 0.0272	9.8054 ± 0.089
otis-II.7	0.0 ± 0.0	1.1856 ± 0.2249	3.5738 ± 0.0914	0.6603 ± 0.0322	21.9241 ± 0.0793	2.9471 ± 0.0338	1.1512 ± 0.0245	63.8889 ± 0.1153	0.2075 ± 0.0124	ULLD	ULLD	ULLD	3.8083 ± 0.0465
otis-III.1	0.0 ± 0.0	0.8766 ± 0.157	0.8765 ± 0.0474	0.4355 ± 0.0197	0.5575 ± 0.0121	1.21 ± 0.0142	ULLD	81.9518 ± 0.0931	11.5709 ± 0.0398	ULLD	ULLD	ULLD	2.1716 ± 0.0297

otis-III.2	0.0 ± 0.0	0.7861 ± 0.1699	0.9346 ± 0.0513	0.5035 ± 0.0218	0.5601 ± 0.0129	1.2462 ± 0.0151	ULLD	81.7436 ± 0.0979	11.5396 ± 0.042	ULLD	ULLD	ULLD	2.2215 ± 0.0318
otis-III.3	0.0 ± 0.0	1.1208 ± 0.1464	0.9329 ± 0.0457	0.489 ± 0.0196	0.5902 ± 0.0121	1.1963 ± 0.014	ULLD	82.1474 ± 0.0942	11.4708 ± 0.0401	ULLD	ULLD	ULLD	1.6628 ± 0.0264
otis-III.4	0.0 ± 0.0	1.1842 ± 0.1606	0.8739 ± 0.0481	0.5107 ± 0.021	0.5841 ± 0.0127	1.3706 ± 0.0154	ULLD	81.2011 ± 0.0971	11.7208 ± 0.0419	ULLD	ULLD	ULLD	2.1894 ± 0.0315
otis-III.5	0.0 ± 0.0	3.5205 ± 0.2006	9.5334 ± 0.1201	0.8418 ± 0.0272	1.2446 ± 0.0196	2.2377 ± 0.0228	2.41 ± 0.0235	72.7689 ± 0.109	0.539 ± 0.014	ULLD	0.0981 ± 0.02	0.1822 ± 0.0218	5.8993 ± 0.0541
otis-IV.1	0.0 ± 0.0	2.656 ± 0.2633	5.7127 ± 0.1137	0.9299 ± 0.0342	3.0382 ± 0.0429	0.0 ± 0.0233	1.503 ± 0.0194	78.1331 ± 0.1014	0.5024 ± 0.0221	ULLD	ULLD	0.1685 ± 0.0275	6.4983 ± 0.0865
otis-IV.2	9.913 ± 1.56	4.7873 ± 0.2264	8.7476 ± 0.1288	1.2563 ± 0.0322	2.2151 ± 0.0361	0.0 ± 0.0235	2.2636 ± 0.0232	63.5829 ± 0.0904	0.3922 ± 0.0185	ULLD	ULLD	0.1529 ± 0.0244	5.3562 ± 0.0723
otis-IV.3	0.0 ± 0.0	2.305 ± 0.298	4.375 ± 0.116	0.8197 ± 0.0375	1.8282 ± 0.0396	0.0 ± 0.0259	1.2773 ± 0.0202	83.3001 ± 0.1146	0.4108 ± 0.0244	ULLD	ULLD	ULLD	4.8671 ± 0.0841
otis-V.1	0.0 ± 0.0	0.6672 ± 0.1737	0.8866 ± 0.0544	0.636 ± 0.0268	10.9128 ± 0.0973	5.7472 ± 0.0444	ULLD	1.5314 ± 0.0157	3.2566 ± 0.0313	0.8415 ± 0.1284	11.1284 ± 0.114	ULLD	29.4212 ± 0.1362
otis-V.2	0.0 ± 0.0	0.6743 ± 0.1534	1.2605 ± 0.0511	1.1025 ± 0.0245	0.4989 ± 0.017	3.8487 ± 0.0214	ULLD	16.1946 ± 0.0272	2.2836 ± 0.0105	ULLD	3.6689 ± 0.039	0.4489 ± 0.0305	65.4413 ± 0.1313
anoeta	4.648 ± 0.7814	2.9065 ± 0.1495	4.2788 ± 0.0728	0.7772 ± 0.021	1.4438 ± 0.0176	1.5671 ± 0.0165	ULLD	81.2918 ± 0.1007	0.283 ± 0.0106	ULLD	0.0688 ± 0.0163	0.0416 ± 0.0126	2.3261 ± 0.0312
anoeta2	0.0 ± 0.0	2.4055 ± 0.1605	3.2999 ± 0.0682	0.7529 ± 0.0223	1.3428 ± 0.0174	1.4481 ± 0.0163	ULLD	87.9949 ± 0.1076	0.2435 ± 0.011	ULLD	0.0598 ± 0.0186	ULLD	2.1672 ± 0.032
anoeta3	0.0 ± 85.5969	1.978 ± 0.1922	4.0117 ± 0.0833	0.7219 ± 0.0262	1.5826 ± 0.0209	1.6823 ± 0.0194	0.8164 ± 0.0149	85.3071 ± 0.1136	0.3668 ± 0.0134	ULLD	0.0842 ± 0.0204	ULLD	3.2027 ± 0.0411
anoetahoe	0.0 ± 0.0	3.8531 ± 0.2006	10.5503 ± 0.1177	0.6515 ± 0.0252	0.5111 ± 0.0135	1.5102 ± 0.0181	3.9628 ± 0.0276	72.1582 ± 0.1008	0.4862 ± 0.0123	ULLD	0.071 ± 0.0178	0.0786 ± 0.0158	5.836 ± 0.0492
anoetahoe	0.0 ± 0.0	4.7065 ± 0.2057	14.3708 ± 0.1356	0.5927 ± 0.0262	0.5361 ± 0.0148	1.6912 ± 0.02	5.2998 ± 0.0326	64.4235 ± 0.096	0.7073 ± 0.0129	ULLD	0.0621 ± 0.0163	0.0977 ± 0.0163	7.1623 ± 0.0527
anoetahoe	0.0 ± 0.0	4.3802 ± 0.1938	10.7223 ± 0.1124	0.6028 ± 0.0231	0.5169 ± 0.0129	1.353 ± 0.0164	2.3462 ± 0.0205	72.9636 ± 0.0946	0.5878 ± 0.0119	ULLD	ULLD	0.1271 ± 0.0127	6.0906 ± 0.0473

ULLD: Under lower limit of detection

5.2.3. General interpretation of the results.

It can be observed the presence of various inorganic compounds in the wall, floor, column and asphalt samples from the OTIS factory and the Anoeta site (Table 20). It can be explained through a combination of material science, construction history, and environmental exposure. Cement-based materials, such as concrete and mortar, are composed of a complex mixture of binders, aggregates, and additives. Each of these components contributes a distinct elemental signature to the overall composition of the material. In their hardened state, these materials retain the chemical markers of both their original components and any post-construction environmental influences.

These inorganic compounds, identified using XRF, provide important insights into the chemical history and potential reuse risks of the sampled materials.

Calcium (Ca), for instance, is a prevalent element in all concrete materials, derived from cementitious binders such as Portland cement. Its high concentration is characteristic of concrete walls and floors, particularly in older structures where the use of lime mortar may have been prevalent. The presence of silicon (Si) and aluminium (Al) has been observed to be associated with silicate and aluminate phases, primarily originating from aggregates such as sand and gravel, as well as supplementary cementitious materials including fly ash or slag. In the context of asphalt, these elements are also anticipated as components of the mineral filler or aggregate blend.

Chlorides (Cl) are frequently detected in external walls and floors. These chlorides are commonly introduced through marine aerosols, de-icing salts, or industrial chemicals like hydraulic fluids. Once absorbed by porous building materials, chlorides can lead to steel reinforcement corrosion. Chlorides are often concentrated in surface layers, particularly in structures exposed to coastal environments or historical industrial activity.

Sulfur (S) compounds are typically found in the form of sulfates, which may originate from gypsum ($CaSO_4 \cdot 2H_2O$) utilized in interior wallboard applications or from the degradation of rubber materials and fossil fuels. In industrial environments, sulfur can accumulate on the floors of facilities due to the deterioration of equipment such as conveyor belts or the combustion of fuel oils. Sulfates have been demonstrated to pose a long-term durability risk due to their potential to react with the cement matrix, causing expansion and cracking (known as sulfate attack).

The presence of lead (Pb) in wall samples is frequently associated with the historical utilization of lead-based paints, particularly in industrial buildings that predate the implementation of contemporary safety regulations. Lead was extensively utilized due to its corrosion-resistant and pigmentation properties. Floors and beams may also accumulate lead (Pb) through atmospheric deposition of leaded fuel exhaust or deterioration of painted components. Once incorporated into the matrix or settled in dust form, lead can persist over decades, especially in enclosed or unmaintained structures.

Zinc (Zn) has been detected in areas associated with industrial flooring and structural footings. The provenance of this substance may be traced back to its integration within galvanized steel components or its incorporation as a constituent of lubricants and anti-wear additives utilized in various mechanical systems. With the passage of time, the process of mechanical wear, coupled with fluid spills, can result in the transfer of zinc (Zn) into the surrounding concrete or floor slab. While elevated zinc (Zn) levels are not typically a structural concern, they may influence the reuse potential due to environmental leaching risks.

The presence of iron (Fe), manganese (Mn), copper (Cu), and nickel (Ni) has been identified as a common occurrence in the composition of structural steel alloys. These elements are frequently detected in corroded beams or reinforced concrete structures. Their presence is expected in areas where metallic components were embedded in or adjacent to construction

materials. The corrosion processes that ensue further mobilize these metals, enabling their diffusion into adjacent cement paste and mortar.

In asphalt samples, a relatively clean composition is expected, reflecting modern formulations using controlled aggregate mixes and bitumen binders. However, residual levels of elements like Pb, Zn, and S may still appear due to urban pollution, vehicle emissions, and road surface degradation.

5.2.4. Results of each measured area.

Moreover, each area investigated exhibits a distinct profile of inorganic elements, attributable to both original materials and subsequent environmental and industrial exposure.

5.2.4.1. Area I

It has shown elevated concentrations of chloride (Cl) and sulfur (S), particularly in samples from areas that are visibly moist. The Cl levels, which have been measured at over 1.4 wt.%, are likely associated with marine aerosol deposition, given San Sebastian's coastal location. This assertion is further substantiated by the presence of NaCl signatures in wet concrete. Hydraulic fluids utilized in elevator systems have the potential to serve as a source, as they have been observed to contain chloride-rich compounds on occasion. Sulfur, which manifests as sulfate, can have origins in deteriorated rubber conveyor belts or the residues of fuel oils that have been historically utilized in machinery. The presence of iron (Fe) variation in this area is indicative of the heterogeneous nature of industrial debris embedded in the wall.

5.2.4.2. Area II

The presence of sulfate is particularly pronounced in Area II, as evidenced by the elevated sulfur content, which exceeds 20 wt.%, as indicated in Sample II.1., Sample II.2 and Sample II.7. This finding suggests the possibility of contamination by gypsum wallboard or plaster, which are commonly used in interior partitions. The deterioration of rubber components and exposure to sulfur-rich fluids are possible factors contributing to the observed phenomenon. The elevated Fe concentration observed in II.6 (nearly 10%) is presumably attributable to corroded steel reinforcements or proximate metallic equipment. The presence of chlorides is consistent with the building's exposure to coastal air or potential leakage from historic hydraulic systems. As indicated by the findings, elevated lead levels are indicative of the utilization of toxic paints or coatings.

5.2.4.3. Area III

The analysis of Area III reveals a profile that is distinctly divergent from the typical characteristics exhibited by other regions. This area is characterized by a remarkably elevated concentration of calcium, with levels that consistently surpass 80 wt.%, while concurrently exhibiting minimal presence of contaminants. This suggests the use of lime-rich mortar or unmodified concrete. The absence of salts or pollutants indicates that the wall has been shielded from aggressive environments. The Fe content (2.17–2.22 wt.%) are consistent with natural aggregates rather than contamination. The presence of low lead content (i.e., under lower limit detection) indicates that repainting with compliant latex-based coatings occurred after the 1980s. Zinc (Zn) concentrations ranging up to 170 milligrams per kilogram (mg/kg) have been observed in association with protective zinc primers or galvanized anchors utilized during retrofitting processes.

5.2.4.4. Area IV

The composition of Area IV is notable for its moderate presence of silicon and aluminum, characteristics that are commonly observed in fly ash or slag inclusions utilized as supplementary cementitious materials (SCMs) in industrial flooring applications. The elevated zinc levels (up to 904 milligrams per kilogram) observed in Sample IV.2 indicate potential

contamination from machine lubricants or corroded galvanized steel. These compounds contain zinc-based anti-wear additives, which have been shown to leach into the concrete over time. The uniformity of calcium values across the area indicates that the floor is well-compacted and structurally sound, with no significant degradation from chemical attack.

5.2.4.5. Area V

The Area V is characterized by a prevalence of iron and lead, a phenomenon that can be attributed to the historical use of structural steel beams that were coated with lead-rich primers. In sample V.1, the lead content exceeds 30%, a level consistent with the historic red-lead paint used for rust prevention. As illustrated in Sample V.2, the presence of iron exceeds 65%, which is indicative of carbon steel. The presence of additional alloying elements, including Mn, Cu, and Ni, is indicative of the distinct characteristics inherent to steel grades. Chromium (Cr), despite its low abundance, can become toxic Cr (VI) under conditions of oxidation during corrosion, a factor that necessitates caution in waste classification and the implementation of speciation testing.

5.2.4.6. Anoeta

In contrast, Anoeta samples exhibited a consistent and benign composition, with Pb under lower detection limit and Cl levels below 2 %. This approach aligns with regional guidelines promoting reuse, thereby enhancing compliance with environmental regulations. The materials utilized in this study reflect contemporary asphalt formulations with controlled aggregates. Elevated levels of silicon (Si) and aluminium (Al) have been observed in the range of 3.3 –14.4% and 2.4–4.7%, respectively, in the context of engineered mineral filler blends. Calcium values ranging from 72 to 88% are indicative of optimized binder usage and effective formulation control. No hazardous materials were detected, thereby reinforcing its suitability for reuse in public works.

5.2.5. XRF labour productivity

This baseline assessment establishes current performance metrics for the scanning task through workflow documentation and comprehensive cost analysis. Table 21 describes the overall workflow and quantifies costs across five key areas: tool transport, worker transport, labour hours, operational hours, and additional expenses. This systematic analysis provides the foundational benchmark for measuring future process improvements and enables informed cost-benefit analyses for scanning operation optimization.

Table 21. Details about the cost's quantification

Workflow	Verification of the installations safety briefing, securing permits, identifying measurement points, 2 workers
Cost – tool transport	Included on worker's transport
Cost – workers transport	508.42 € travel + 739.02 € accommodation + 409.70 € allowances
Cost – labour hours	Included in the operation hour cost

Cost – operational hours	277.42 € per person/day * 3 days * 2 people = 1664.55€
Any other expense	N/A

Amount of time for the whole scan process:

Table 22. Details about the scans with the different HW

SUM UP TIMES	
Anoeta Station	
	p-XRF
Acquisition time	1h
Preprocessing time	1.5h
Number of scans	6
Jolastokieta building	
	p-XRF
Acquisition time	3.5h
Preprocessing time	2h
Number of scans	23

5.3. GPR-ECT by EAGLE

5.3.1. Process

At the pilot site, an initial site observation is required to get a clearer understanding and acquire information that might be useful in deciding the data collection locations but also assist in data interpretation. In general, the number of required samples depends on the variability of a site and the accuracy needed. When a site does not vary much, less samples are needed which can be assumed that are representative of the total structure. After visual inspection of the site, it was decided to conduct scans at four different locations:

- One on the driest concrete floor slab
- Two on wet concrete floor slab
- One on the wall column

Even if the driest part was also selected for scanning, from visual inspection it was quite clear that the concrete slabs have high degree of deterioration and high moisture content shown with the voids, cracks and rough spalling surfaces.

For each floor location, a 60 x 60 cm area was scanned with the GPR, which was subsequently also scanned by the Profometer. The measurements were collected with a spacing of 5 cm, both in the x and in the y direction resulting in a total of 26 measurement lines per area scan

at each location. Starting from the (0,0) point on the grid, measurements are collected first in the x direction followed by collecting all lines in the y direction. For each individual measurement line, samples were collected at 2 scans/cm.

For the wall a 40 x 40 cm area scan with 5 cm spacing was conducted. Although the floors were scanned by both the GPR and the ECT, the walls could only be scanned by the GPR sensor and not the Profometer, as there was no reinforcement present and ECT relies on electromagnetic conduction.

Each location was marked with a grid paper with marked line position for scanning as seen in the results below. The GPR and the ECT probe were both in direct contact with the surfaces for scanning. All conductive objects in a distance of 400 mm from the sensor, if any, were removed prior to the data collection. Before starting the data collection with the PM8000 at each location, calibration was required by holding the device in the air for a few seconds. After each scan, the data of both sensors were checked on-site with basic processing applied to ensure there were no issues or repeat if necessary. In addition, when internet connectivity became available, the data were upload to the cloud and shared with all operators as additional back-ups.

After the data acquisition, post-processing at the office was performed. For the GPR data, the following processing filters were applied in the order of reference:

1. Time zero correction: This filter is used for correct depth estimation and is usually the first filter applied on GPR data
2. Noise cancellation filtering: Used for removing noise in the data from nearby Wi-Fi or cellphone emitters.
3. Background removal: Used to remove the response from the surface which due to being strong masks other responses.
4. Gain: The GPR signals are getting weaker with depth due to losses (e.g. attenuation due to material conductivity) making deeper features not visible and thus gain is needed to amplify the deeper responses.

5.3.2. Results

5.3.2.1. First area

The location of the first-floor area is displayed in Figure 22a). Here a reinforcement layer was identified, which is in the form of hyperbolas in the B-scan GPR data (Figure 22. b)) at around 10-12 cm depth. From the B-scan in Figure 22b), it is shown that these hyperbolas and thus the corresponding rebars have slightly different depths. From the depth slice and isosurfaces at c) and d), respectively, at ~12 cm depth, it appears that there is a mesh grid at both x and y directions. The rebars in these data appear distorted which could be due the roughness of the concrete surface that did not allow for the sensor wheel to move freely and smoothly across the surface and thus cause issues in data positioning or due to degradation of the rebar grid, which is highly likely in this area.

Additional responses were identified deeper in the slab at 17-22 cm depth, which can be seen in Figure 22e) and f). These appear only at the left section of the area scan. The first one is a long target parallel to the y direction, possible some kind of reinforcement and the second one is smaller parallel to the x direction.

Via a process called hyperbola fitting, the dielectric constant (relative permittivity) and thus the velocity of the electromagnetic waves through this material can be estimated. This is a material property and apart from the material composition is related also to the water content. For this area, this was found to be between 9.5 and 10.5, which are typical values for wet concrete and were expected as this is further verified by the visual inspection. Typical dielectric constant

values for dry concrete are around 5-7. The estimated dielectric is used to calculate the velocity and thus the depth to the objects.

This area was also scanned with the ECT sensor. However, as also observed by the GPR data, the depth of the rebars is >10 cm which is deep for this sensor to make any accurate rebar diameter estimations. To obtain accurate diameters, the rebars need to be placed within the first 6.3 cm. Beyond this depth, the deep mode in the ECT sensor can only indicate the presence of rebars accurately. An example is shown in Figure 21, where the green vertical lines represent three of the rebars detected and the yellow curve shows the signal strengths. From this curve, it can be seen that the signals received are very weak to acquire useful information from the rebars. Same observations were also made for scan areas three and four which also correspond to reinforced concrete floor slab. Although ECT could not be used with success in this case, it can be used for other reinforced concrete slabs with shallow reinforcement successfully.

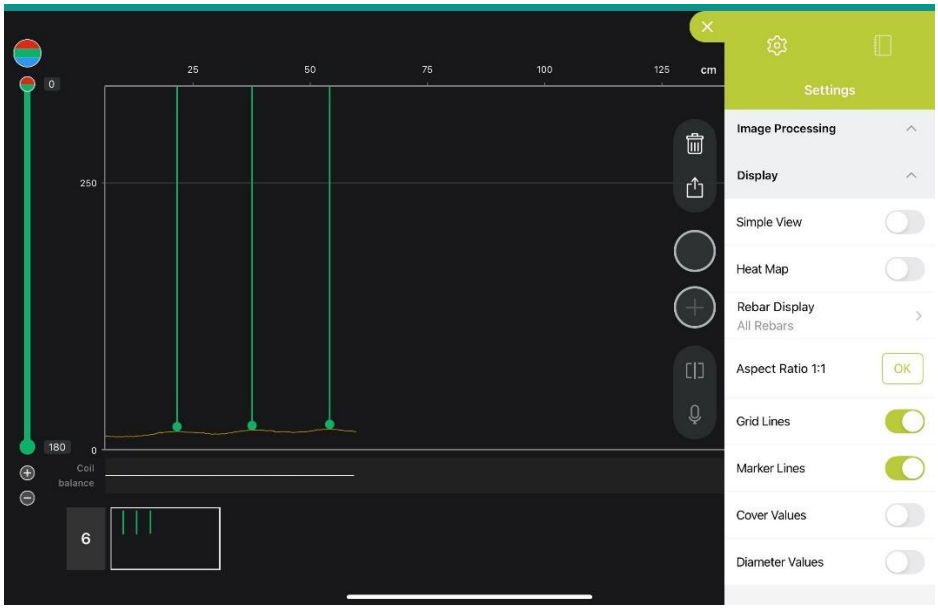

Figure 21. First area scan with PM8000 – line 6 which shows the detected rebars and low signal strengths.

5.3.2.2. Second area

The second scan was performed in a wall column, which also had high degree of moisture. The wall surface was quite rough due to the wall deterioration making it difficult to move the wheel for scanning similarly to the first area. Due to the length size of the area, a 40 x 40 cm grid was performed as it was not large enough to perform the full 60 x 60 cm scan. The location of this scan area is presented in Figure 23a) and b) during data collection.

Cracks, large voids and spalling were observed overall in all the walls. No reinforcement or other elements were expected to be found inside, which was further verified by the GPR data. From observing the GPR data, significant noise can be seen in both the x-directed and y-directed B-scans which is due to the external and internal cracks in the wall and high moisture content.

As mentioned earlier, the PM8000 could not be used in this location due to absence of reinforcement in the walls.

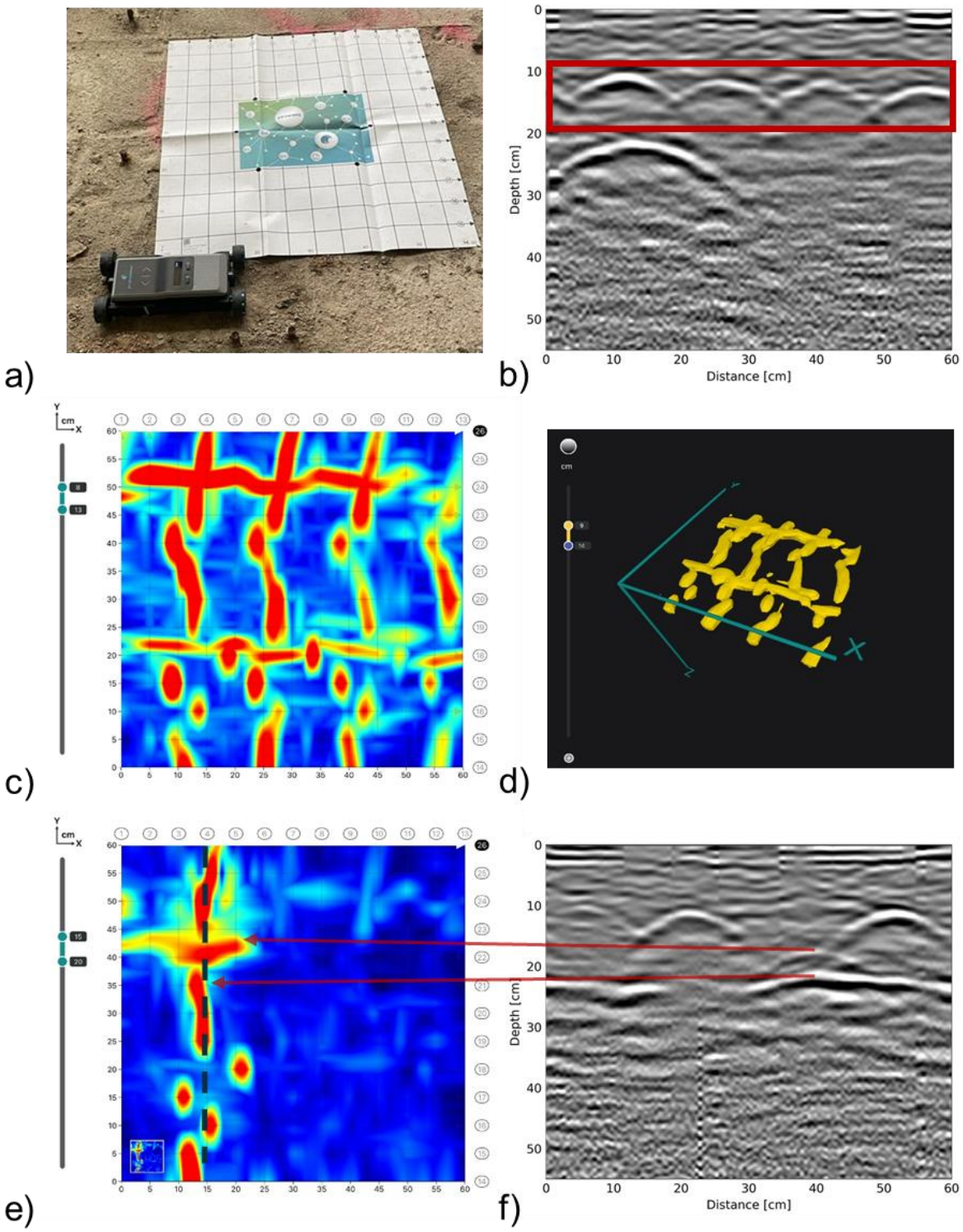

Figure 22. a) First area scan location, b) GPR B-scan showing the reinforcement, c) GPR slice at ~12 cm depth, d) Reinforcement as isosurfaces in 3D, e) GPR slice at ~17 cm depth and f) Line 4 B-scan.

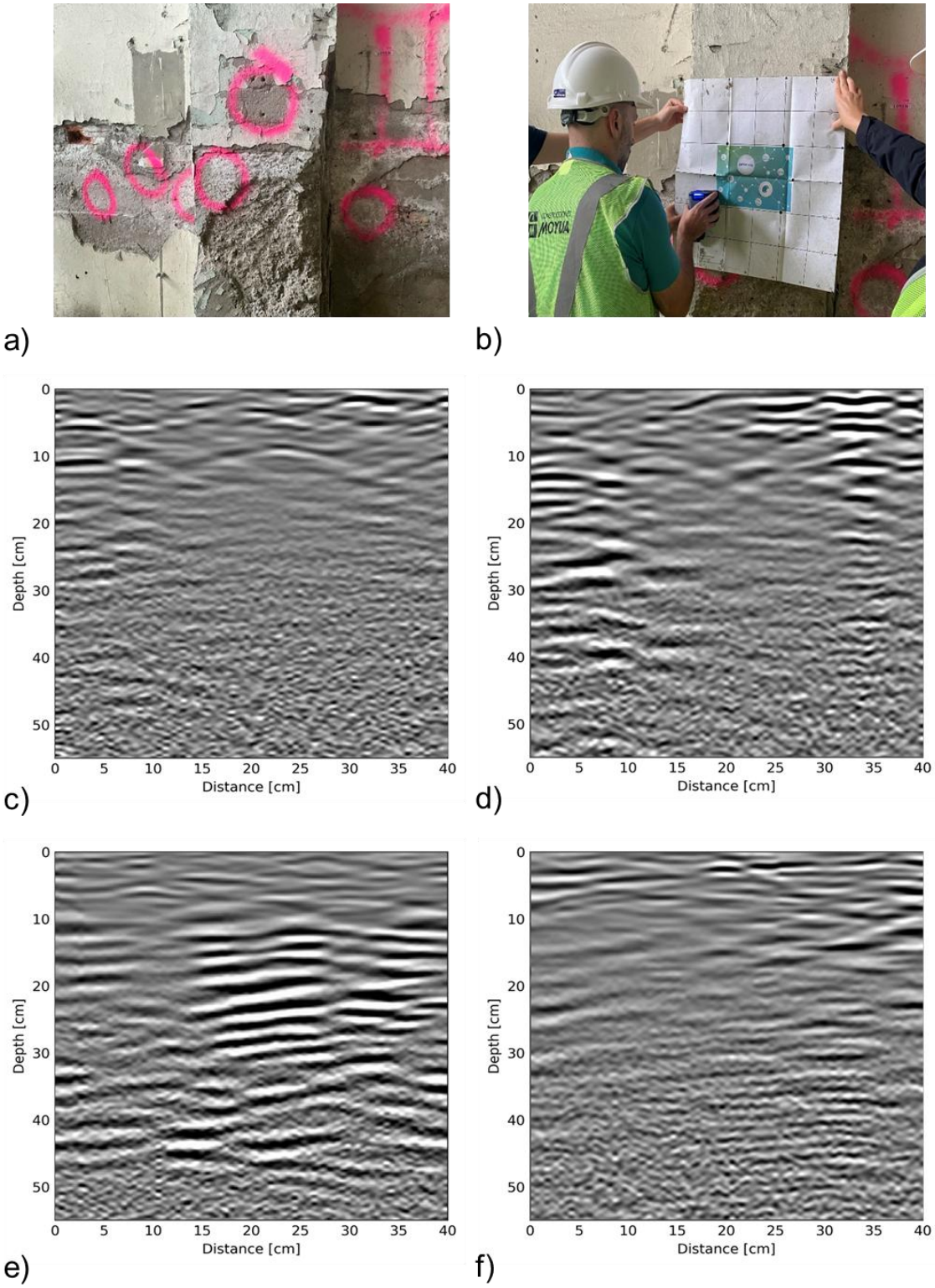

Figure 23. a) and b) Second area scan location, c) and d) Y-directed GPR B-scans, e) and f) X-directed GPR B-scans.

5.3.2.3. Third area

The third scan was conducted on a wet floor slab with a smooth surface, as shown in Figure 24a). The smooth surface allowed for easier movement of the wheel and therefore more precise scanning and data positioning. Looking at the data, a reinforcement layer could be located around 15-18 cm depth with the rebars located at slightly different depths, similarly to the first area. In this case, the reinforcing mesh can be seen clearer on the slice data and with the isosurfaces, as can be seen by the elongated responses in c) and d). However, it appears that there is inconsistent spacing between the rebars. Also, in some parts these are offset from each other.

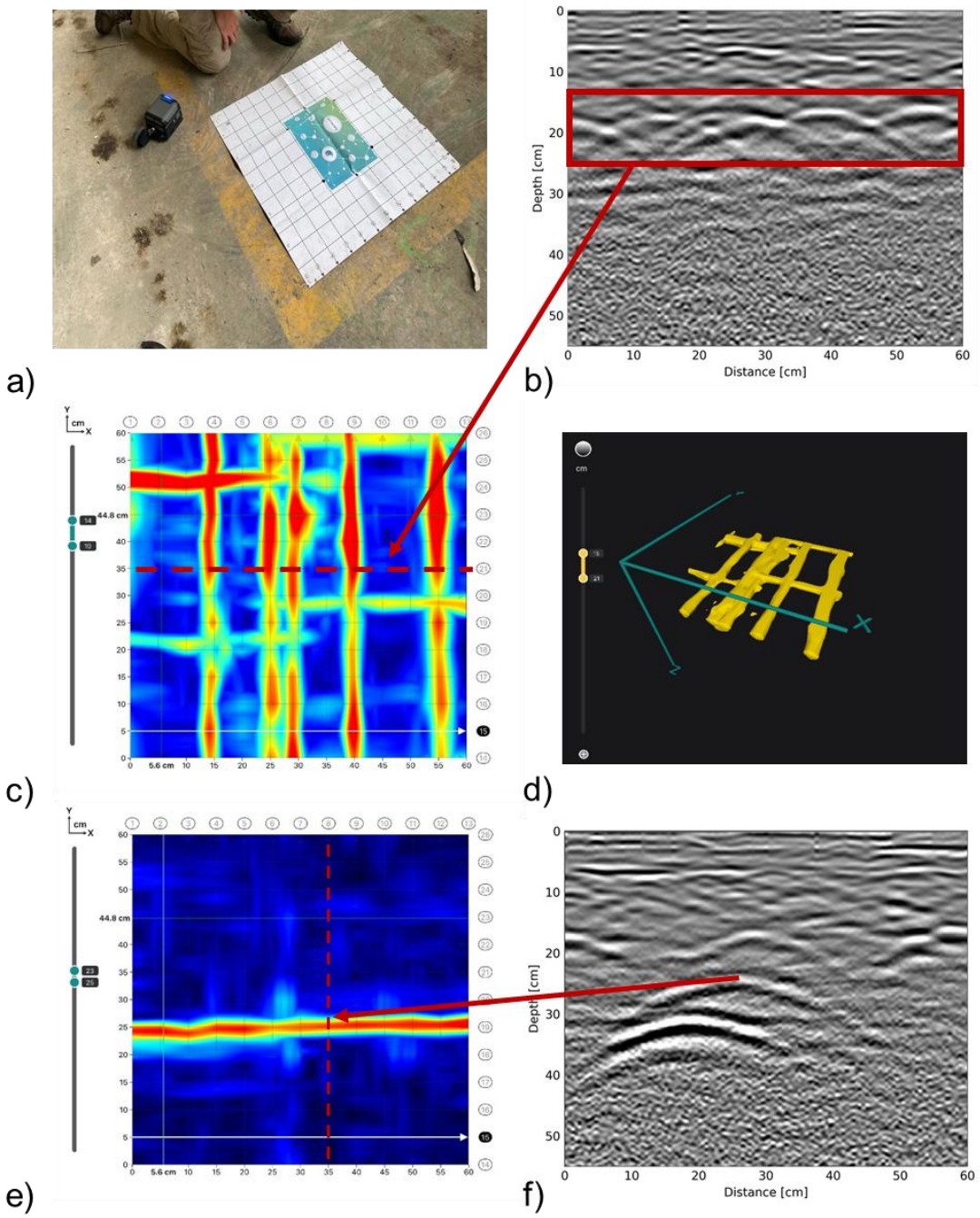

Figure 24. a) Third area scan location, b) GPR line 21, c) GPR slice at ~16 cm depth which also illustrated the position of line 21 with a dashed line, d) Isosurfaces of reinforcing mesh, e) and f) Detected element at ~24 cm depth.

Deeper in the slab, there was another strong elongated response identified at ~24 cm depth, as presented in Figure 24e) and f) which seems to correspond to some kind of reinforcement. In addition, a second strong response at ~30 cm depth was observed, which this time seems to be only local, as shown in the slice and as a hyperbola in the B-scan of Figure 25. This is probably a void inside the concrete slab.

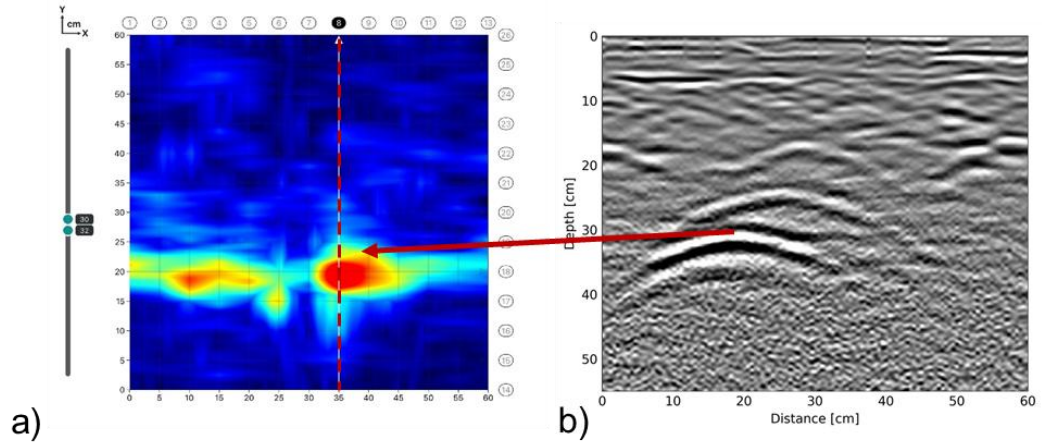

Figure 25. Target at ~30 cm depth in third area as shown in a) GPR depth slice and b) GPR B-scan line 8. Line 8 is also illustrated with a dashed line on the slice in a).

This floor slab seemed to have higher moisture than the first area as shown by hyperbola fitting, where dielectric values between 10.5 and 12 (typical wet concrete) were estimated across this area. In addition, significant clutter is present at the data above the reinforcement layer, as illustrated in the B-scans from lines 2 (y-directed) and 17 (x-directed) in Figure 26, which indicate the presence of moisture and/or voids. The high dielectric values along with the clutter observed show high likelihood of deterioration in this area.

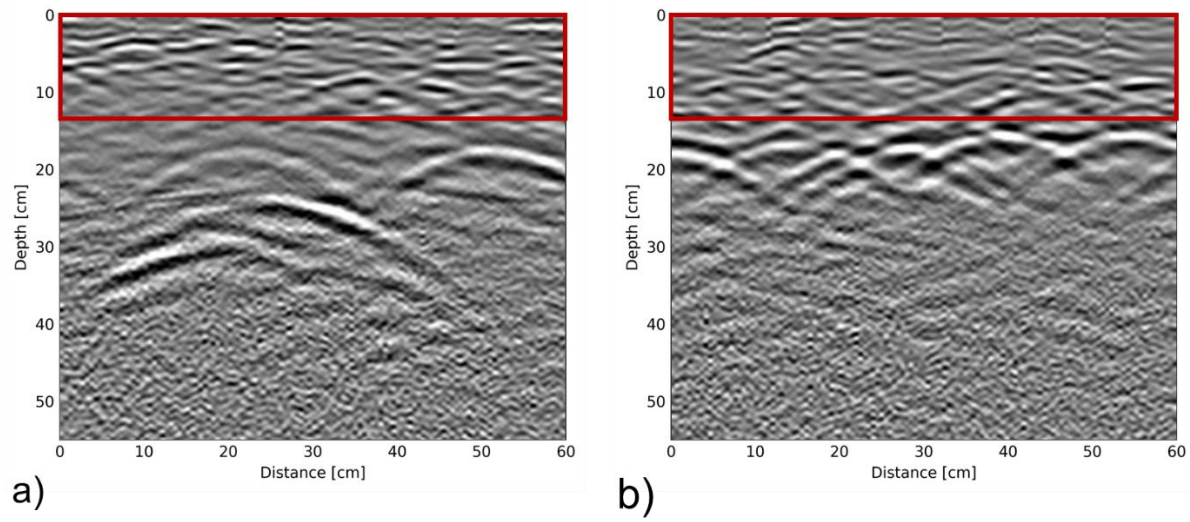

Figure 26. Third area a) Line 2 B-scan and b) Line 23 B-scan with the clutter region highlighted at the top.

5.3.2.4. Fourth area

The fourth area scan was also conducted on a wet floor slab. In this area, around 5 cm depth, elongated elements at both directions were identified (Figure 27b)), which could be a certain type of reinforcement or cabling; however, is not the main reinforcement layer observed in the previous floor scans. The main reinforcement layer appears also in this scan deeper at ~20

cm depth as shown by the series of hyperbolas in Figure 27c) and the rebar mesh in the slice and as isosurfaces in Figure 27d) and e), respectively. Most rebars in this case appear to be at the same depth in contrast to the previous cases and there is consistent spacing between the rebars.

Around 13 cm depth, there is another unidentified strong response, which can be seen in Figure 28a) and b). This response has an irregular shape as seen in a) and could potentially correspond to a void.

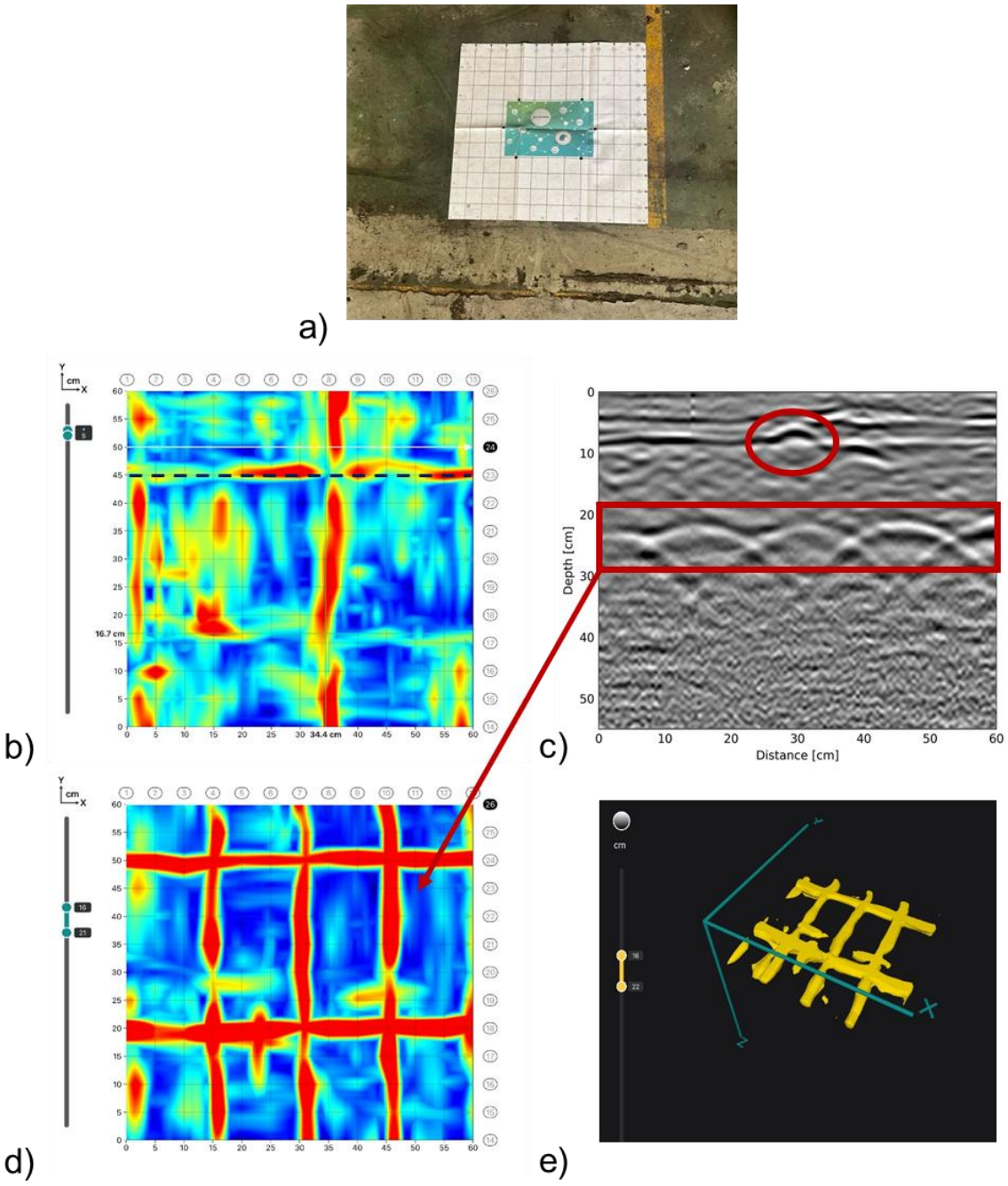

Figure 27. a) Fourth area scan location, b) GPR slice at ~5 cm depth, which also illustrates the position of line 23 with a dashed line, c) GPR line 23, d) GPR Slice at ~19 cm depth and e) Isosurfaces of reinforcing mesh.

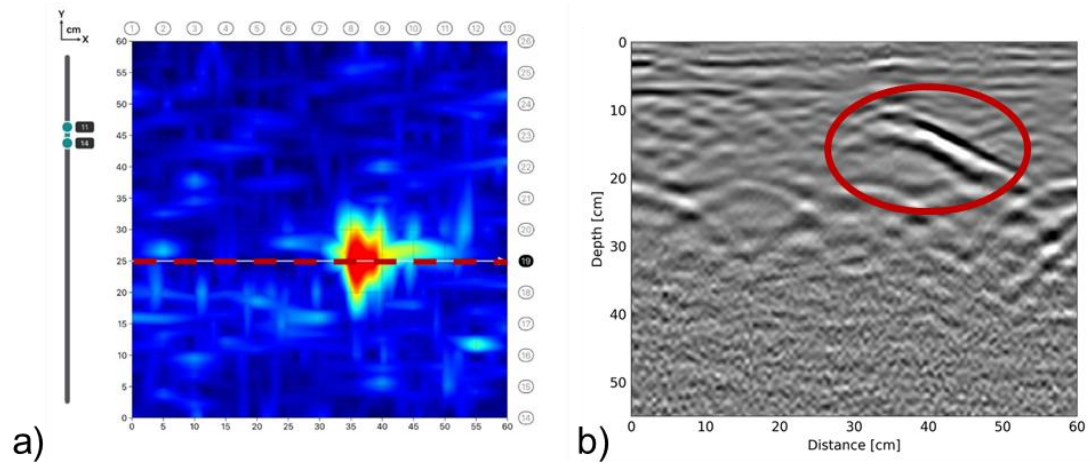

Figure 28. Unidentified response around 13 cm depth as seen in a) GPR slice and b) GPR B-scan line 19 where it is marked with an ellipse.

Furthermore, across most B-scans from both directions, there is a flat response observed at around 6 cm depth as highlighted in Figure 29a) with an arrow. Since this response is found in both directions and as a flat response, it corresponds to an interface between layers or between a layer and another layered feature. Tracing this response across the full area, it was observed that it has some strong and some weaker amplitude regions as shown by the signal amplitude heatmap in Figure 29b). The values are represented as normalized amplitude values, with the maximum amplitude observed being 0.89 and the minimum 0.3. Smaller amplitudes usually indicate weaker areas in a structure. The potentially weaker areas are shown with a red colour in b), whereas the stronger healthier parts are shown with green and yellow.

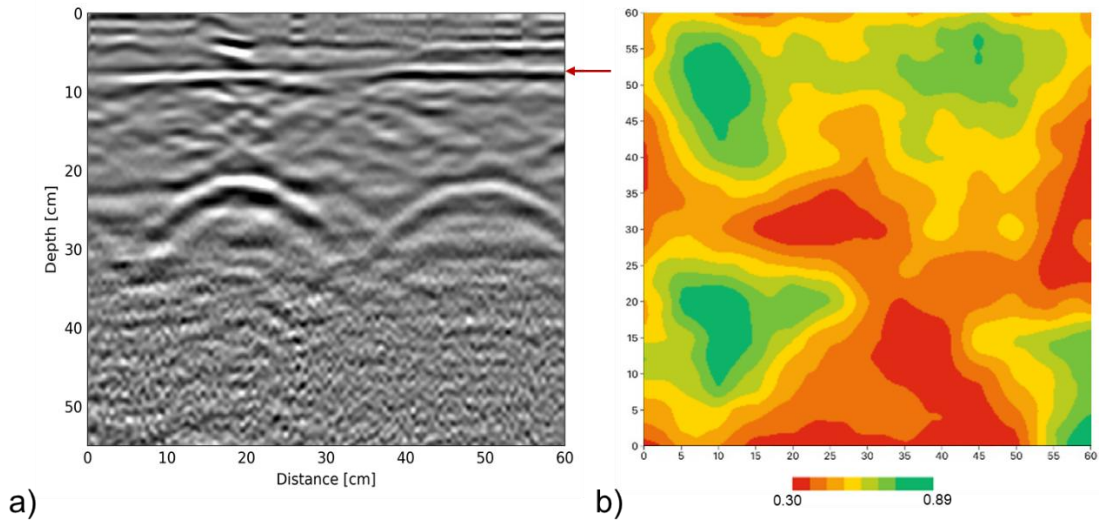

Figure 29. a) Flat response around 6 cm depth and b) Amplitude map of the response showing weaker and stronger regions.

5.3.3. GPR + ECT labour productivity

This baseline assessment establishes current performance metrics for the scanning task through workflow documentation and comprehensive cost analysis. Table 23 describes the overall workflow and quantifies costs across five key areas: tool transport, worker transport, labour hours, operational hours, and additional expenses. This systematic analysis provides the foundational benchmark for measuring future process improvements and enables informed cost-benefit analyses for scanning operation optimization.

Table 23: Details about the cost's quantification for GPR+ECT

Workflow	Prior to visit, review site plans and images Check equipment and charge before visit Determine scanning locations On-site data scanning On-site data verification (basic processing) Data post-processing and interpretation in the office 3 workers
Cost – tool transport	Included in workers transport
Cost – workers transport	526€ travel + 650€ accommodation + 600€ allowances
Cost – labour hours	Included in the operational hours cost
Cost – operational hours	120€/h * 15 hours = 1800€
Any other expense	N/A

Amount of time for the whole scan process

The total time required for conducting the scans in the Jolastokieta building was approximately 4.5 hours and all scans were performed on the same day.

Table 24: Details about the scans with the GPR and ECT sensors

SUM UP TIMES		
Jolastokieta building		
	GPR	ECT
Acquisition time	2h	1.5h
Preprocessing time	30 minutes	30 minutes
Number of scans	4	3

5.4. FOS by TECN

5.4.1. Methodology and objectives

Based on the research framework described in this deliverable, the fibre optic sensing (FOS) monitoring methodology applied in this task represents an innovative approach to structural health monitoring (SHM). It integrates advanced sensing technology with conventional

structural testing methods in the broader context of construction and demolition waste (CDW) reuse.

The central objective is to establish a calibrated and validated finite element model (FEM) that provides the foundation for ongoing condition assessment and enables informed decisions regarding the future reuse of steel beams in new construction projects. This approach recognises that effective SHM requires capturing both static and dynamic behaviour of structural elements, generating reliable, high-quality data to evaluate integrity, remaining service life, and reuse potential.

The use of FOS as the primary monitoring method is strategically motivated by its alignment with SUM4Re's objectives and long-term vision of continuous monitoring across multiple reuse cycles. Key advantages include:

- Superior measurement quality compared to conventional sensors.
- Immunity to electromagnetic interference, ensuring reliability in complex construction environments.
- Flexible installation and deinstallation, enabling both temporary assessment and permanent monitoring.
- Lower lifecycle costs, making continuous monitoring economically viable for reused elements.

The experimental program focused on two steel beams originating from a crane displacement system—a deliberate choice to study real-world elements with load conditions representative of construction applications. Their detailed characterisation under diverse boundary and loading conditions provides the dataset required for developing robust FEMs capable of predicting behaviour in future reuse scenarios.

Figure 30. Steel beams selected for the testing

The methodology employs a dual testing strategy:

- Static three-point bending tests monitored with FOS strain sensors to capture load–strain relationships, deflection patterns, and stress distributions. These datasets calibrate material properties, boundary conditions, and load-transfer mechanisms in the FEM.
- Dynamic modal analysis, using impact hammer excitation and optical accelerometers, to determine natural frequencies, damping, and mode shapes. This information calibrates the FEM's dynamic response.

Together, these components provide a comprehensive dataset that supports calibration of both the linear and nonlinear aspects of the FEM. Load scenarios are carefully controlled with feedback from FOS sensors, creating a closed loop testing environment that maximises precision and repeatability. The calibrated FEM is thus capable of predicting structural

performance under both service loads and ultimate capacity, enhancing confidence in reuse decisions.

The testing program is structured into four scenarios, systematically varying boundary conditions to understand their influence on structural behaviour:

- Original configuration as part of the crane system, preserving realistic support conditions and complex load transfer.
- Simply supported configuration using removable pillars, creating idealised conditions for reference calibration.
- 3–4. Replications across both beams, enabling comparison and quantification of boundary condition effects.

Figure 31. Left: Three-point loading testing installed on site. Right: Proposed testing modelled in ANSYS.

This systematic approach enables development of FEM calibration procedures that account for different support assumptions, reflecting the variety of potential reuse applications.

Throughout all scenarios, FOS sensors provide continuous, distributed deformation measurements, offering much higher spatial resolution than traditional point-based instrumentation. This capability enables robust model validation across the entire beam rather than at a limited set of points.

The long-term vision extends beyond initial testing: once the beams are reused in new structures, the FOS system can remain in place to provide continuous monitoring. This allows comparison with FEM predictions to detect early signs of degradation—such as fatigue, corrosion, or connection deterioration—and supports proactive maintenance strategies. In this way, calibrated FEMs and FOS monitoring jointly contribute to extending the service life of reused structural elements while ensuring safety and reliability.

5.4.2. Preliminary FEM modelling for monitoring plan

A preliminary inspection of the pilot area was carried out to select and measure two representative steel beam specimens for testing. Based on these measurements, a first ANSYS finite element model was created to reproduce the expected behaviour of the beam under loading conditions.

The model simulated the three-point bending test that would later be applied experimentally. This virtual scenario served two purposes:

- Definition of safe load levels: ensuring that the applied maximum load would not exceed the allowable stress in the beam and avoiding plastic damage or collapse.
- Sensor dimensioning: predicting the magnitude of the expected deformations in order to correctly select the fibre optic deformation sensors and their measurement range.

In addition, a preliminary modal analysis of the steel beam was performed. This analysis provided the expected natural frequencies and corresponding mode shapes. These results were essential to:

- Define the accelerometer specifications (sensitivity, frequency range) for the experimental campaign.
- Establish an optimal testing procedure by identifying where vibration amplitudes would be maximum (sensor placement strategy).

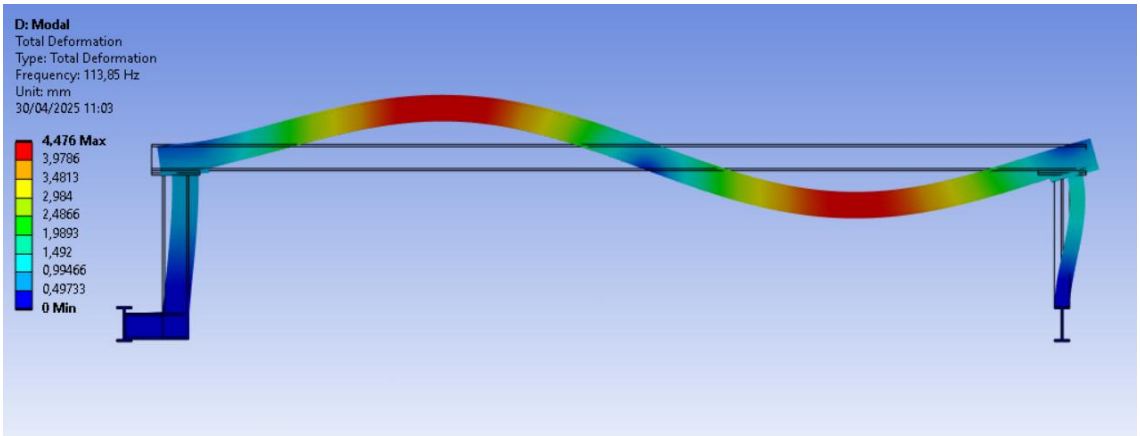

Figure 32. Preliminary mode shapes obtained

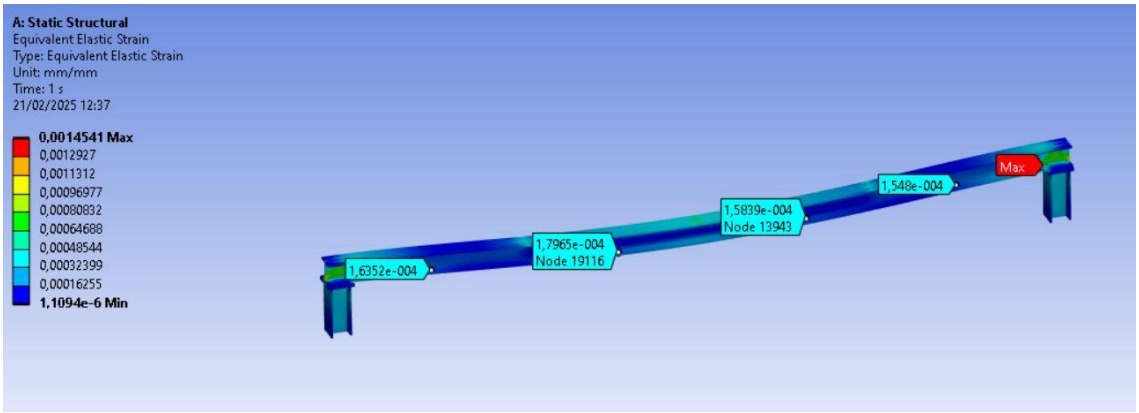

Figure 33. Preliminary expected strain values at the deformation sensors

5.4.2.1. Sensor placement strategy

The objective for the preliminary modelling is to identify the most critical regions for installing deformation sensors (strain FOS) and vibration sensors (FOS accelerometers). The FEM simulations guided the placement of fibre optic sensors as follows:

- Deformation (strain) sensors were installed at the mid-span between each loading point application, installing a total of 4 deformation sensors. The reason why installing not exactly under the point loading application, is to avoid peak stress due to the point loading application. Below it is presented the deformation sensors scheme, maximum stress expected applying 10kN as maximum at each loading point, and the expected microstrains at each sensor location.

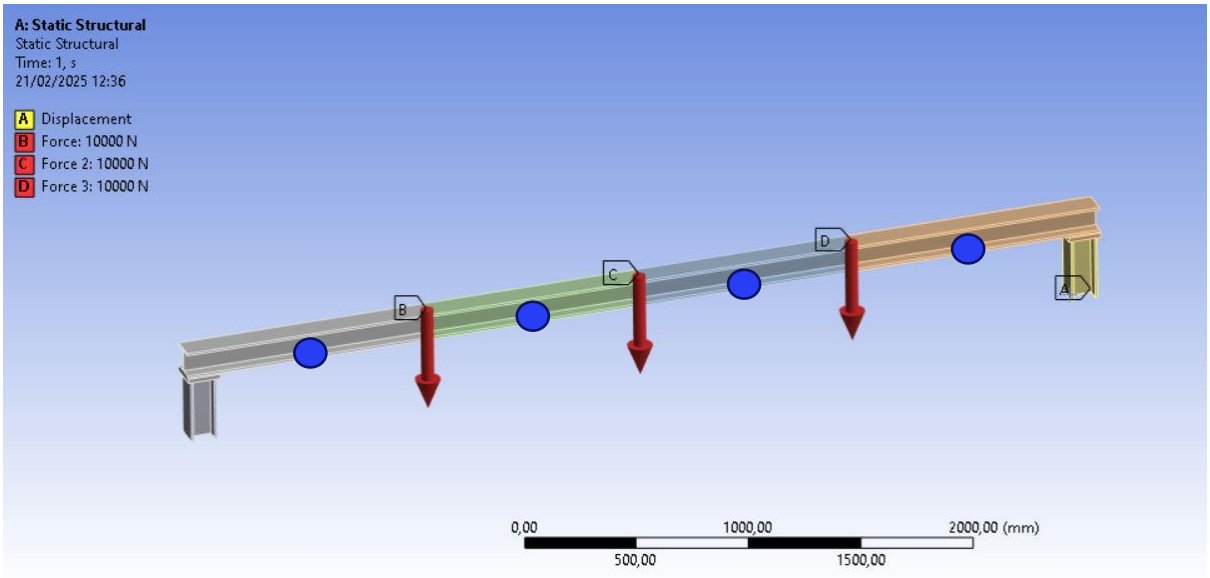

Figure 34. Blue circles: Location of the installed FOS deformation sensors

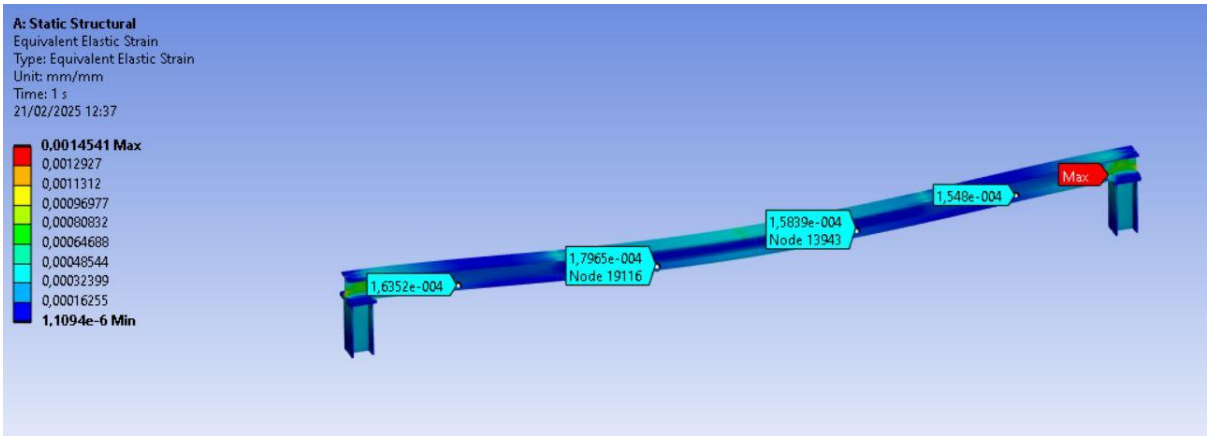

Figure 35. Expected strain values for the sensors

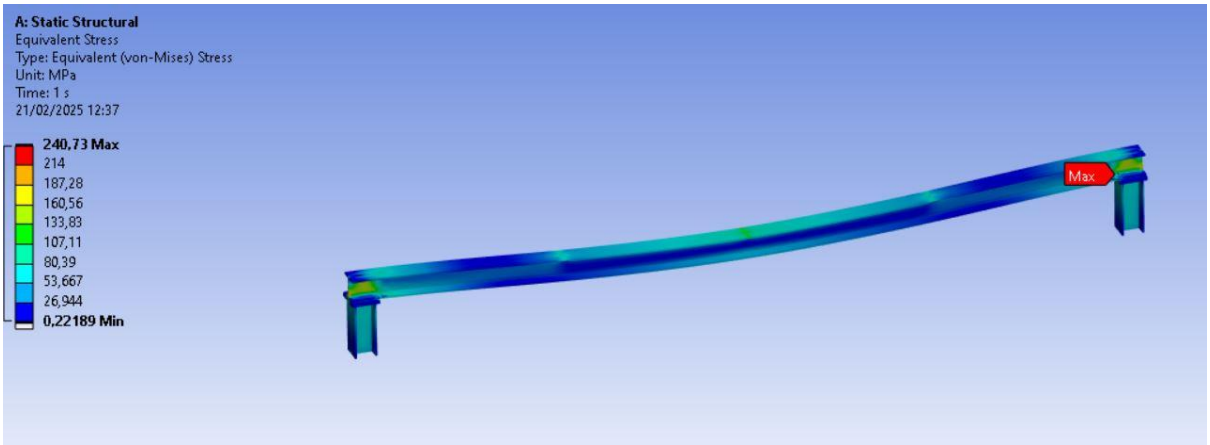

Figure 36. Expected stress values for the steel beam

- Vibration (accelerometer) sensors were placed at locations with maximum modal displacements for both vertical bending modes and horizontal bending/torsional modes, as identified by the modal analysis. This ensured high signal quality and reliable capture of the natural frequencies. The main mode shapes were obtained are:

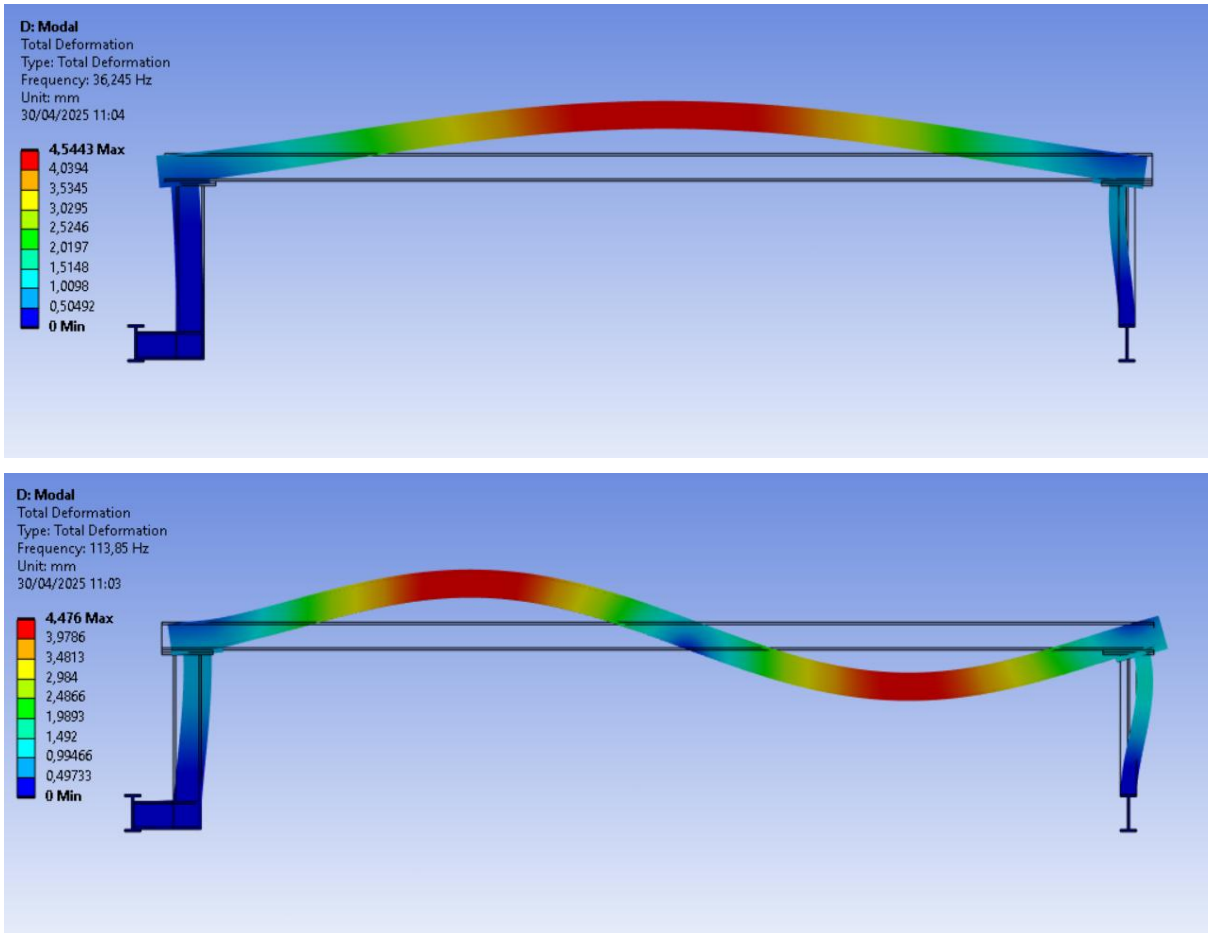

Figure 37. Top: 1st vertical mode, 36.45 Hz. Bottom: 2º vertical mode, 113.85 Hz

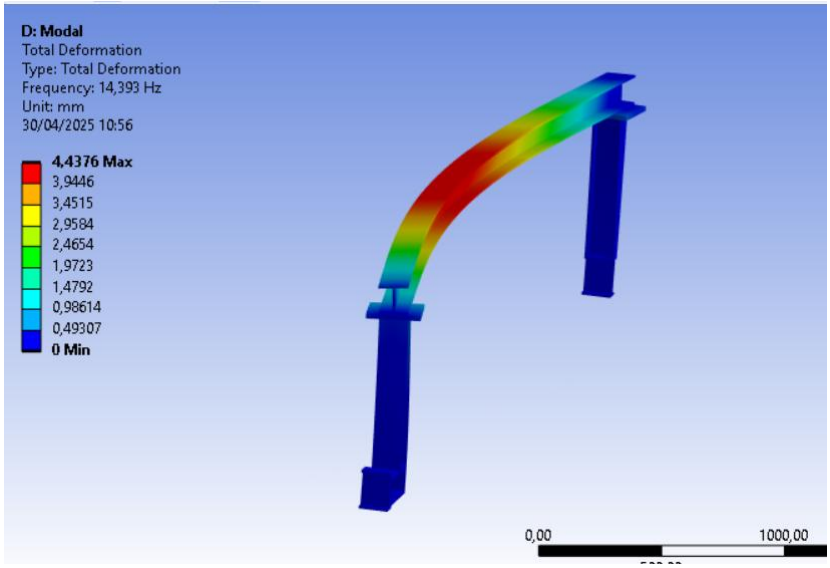

Figure 38. 1º horizontal mode, 14.39 Hz

Following the obtained mode shapes, the accelerometers position defined to be able of capturing these mode shapes is as follows, being these located at the mid-span point (capture of 1st vertical mode, and 1st horizontal mode) and at L/4 of the beam (to capture the 2nd vertical mode and possible torsional modes):

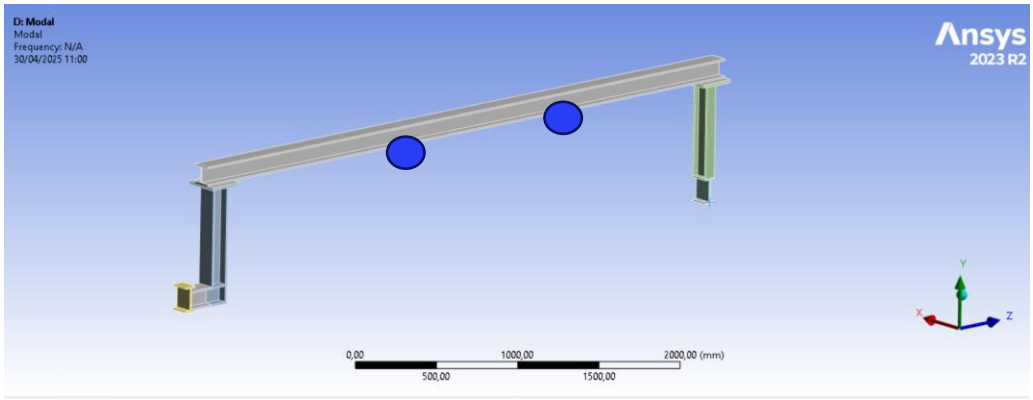

Figure 39. Blue circles: Position of accelerometers at L/2 and L/4

5.4.2.2. Calibration baseline

The calibration strategy is based on combining static and dynamic datasets:

- From the three-point bending tests, load–strain curves will be obtained using the fibre optic deformation sensors.
- From the dynamic vibration testing, the natural frequencies of the beam will be determined experimentally.

Together, these two sources of data allow the adjustment of the FEM model, in particular to estimate the effective Young's modulus of the steel beams. This procedure will later be continued in task 11.1 and 3.6, where transfer learning techniques will be applied to refine the calibration and extrapolate to similar structural elements.

5.4.3. Static behaviour – Testing

Static loading tests were performed on the steel beams to record strain evolution and validate FEM predictions. FOS strain sensors (FS62 type) were installed at the predetermined locations to capture distributed deformation profiles under controlled incremental loads.

Figure 40. Installed FOS deformation sensors

The following graphs present the results of the static loading campaign. Each curve represents the strain measured by the FOS sensors at their respective positions along the beam, plotted against the applied load. These results are compared against the FEM predictions to validate the deformation response.

STEEL BEAM 1

With removable pillars (simply supported condition)

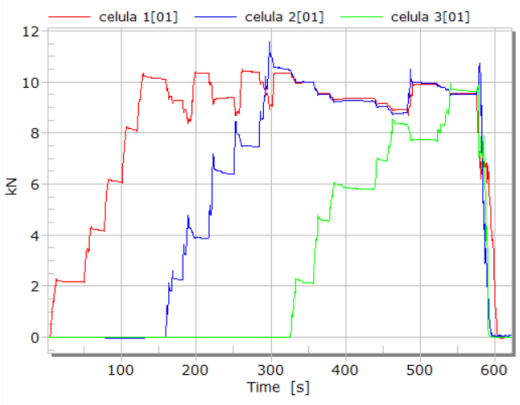

BEAM 1 – TEST 1 – Load cells (KN)

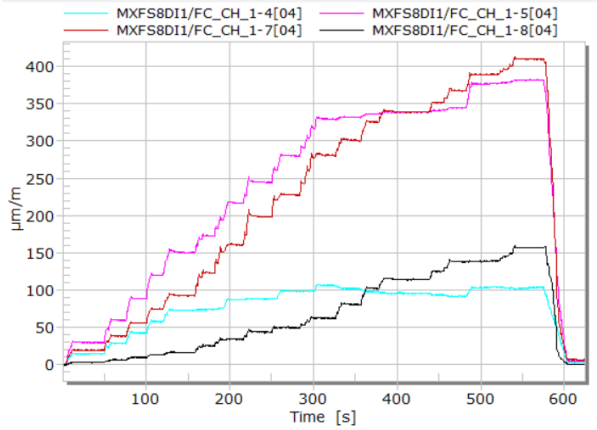

BEAM 1 – TEST 1 – Strain (µm/m)

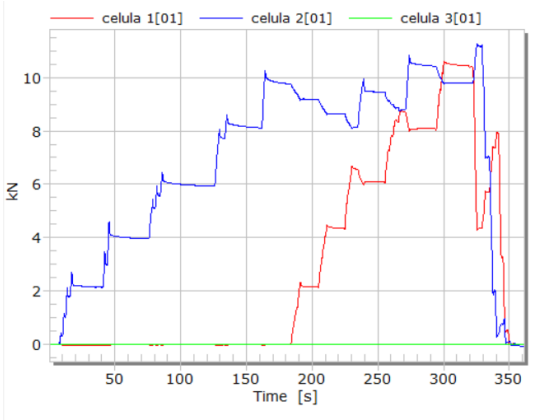

BEAM 1 – TEST 2 – Load cells (KN)

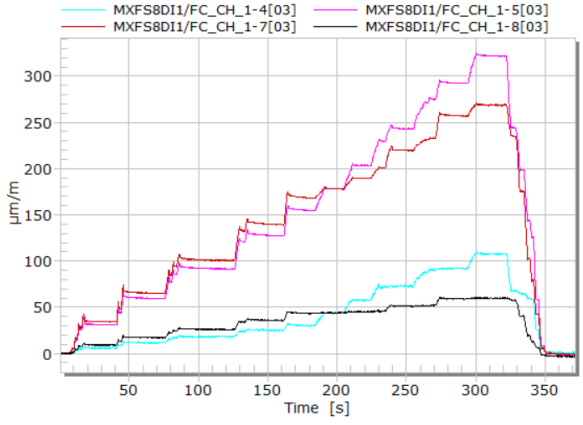

BEAM 1 – TEST 2 – Strain (µm/m)

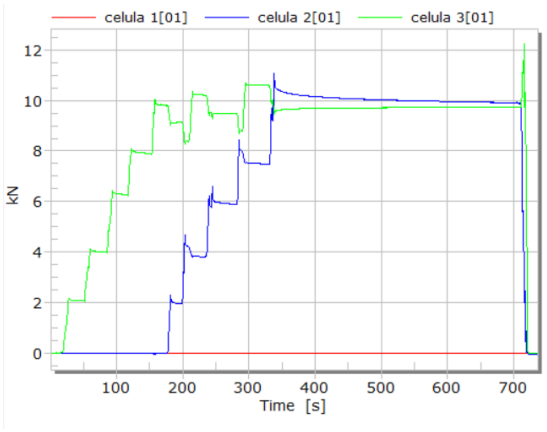

BEAM 1 – TEST 3 – Load cells (KN)

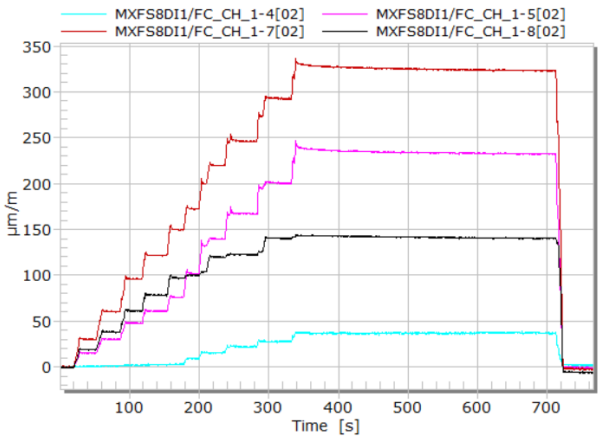

BEAM 1 – TEST 3 – Strain (µm/m)

Without removable pillars

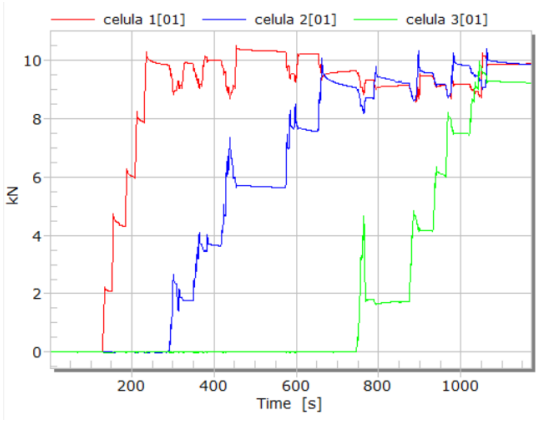

BEAM 1 – TEST 1 – Load cells (KN)

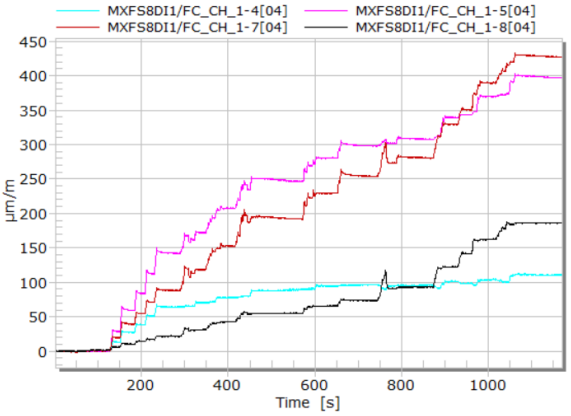

BEAM 1 – TEST 1 – Strain (µm/m)

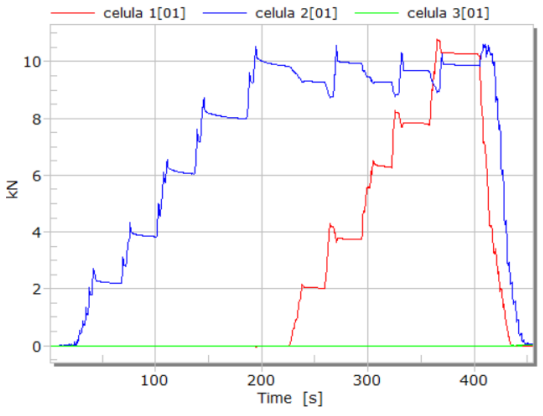

BEAM 1 – TEST 2 – Load cells (KN)

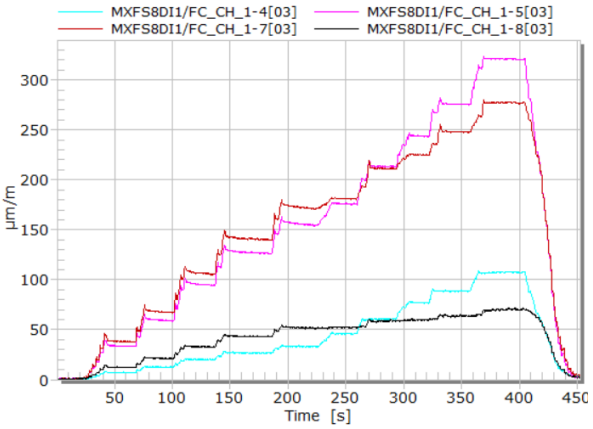

BEAM 1 – TEST 2 – Strain (µm/m)

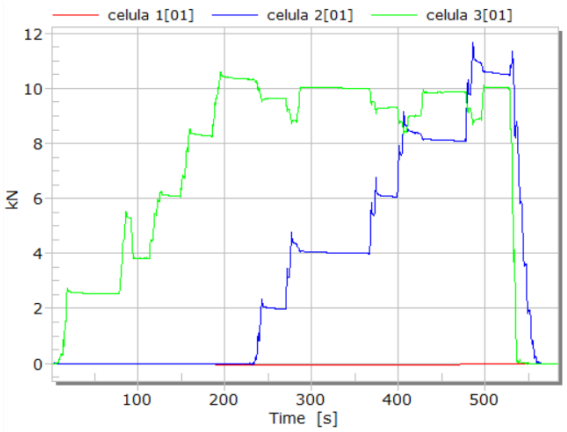

BEAM 1 – TEST 3 – Load cells (KN)

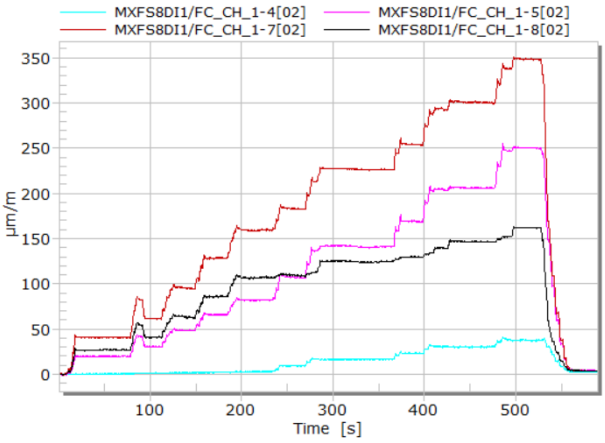

BEAM 1 – TEST 3 – Strain (µm/m)

Figure 41. Results obtained for static testing in steel beam 1

STEEL BEAM 2

With removable pillars (simply supported condition)

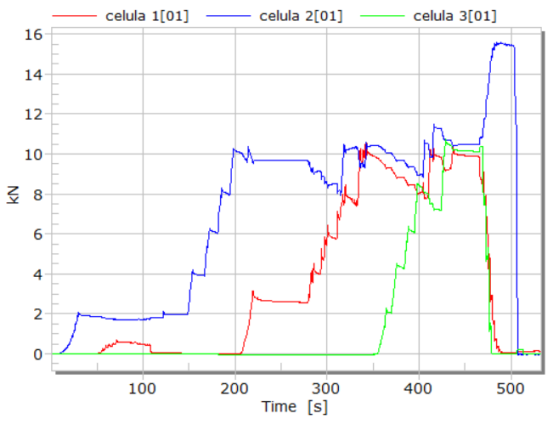

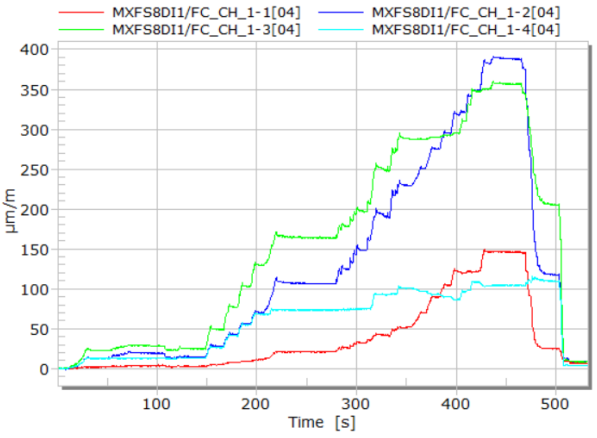

BEAM 2 – TEST 1 – Load cells (KN)

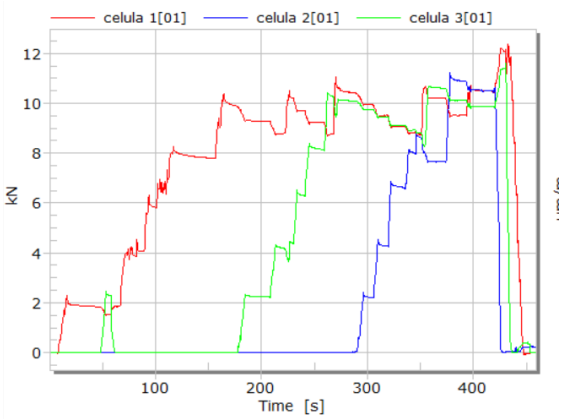

BEAM 2 – TEST 1 – Strain (µm/m)

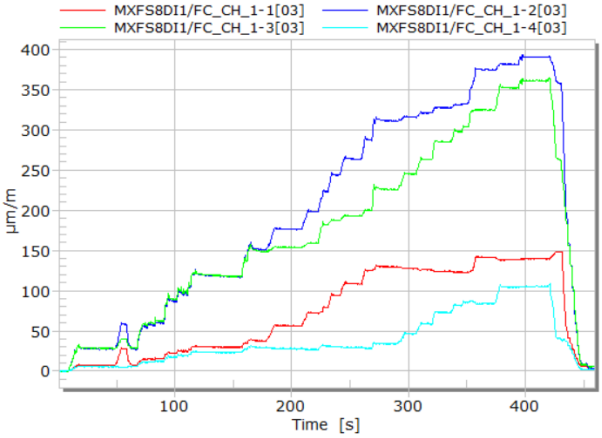

BEAM 2 – TEST 2 – Load cells (KN)

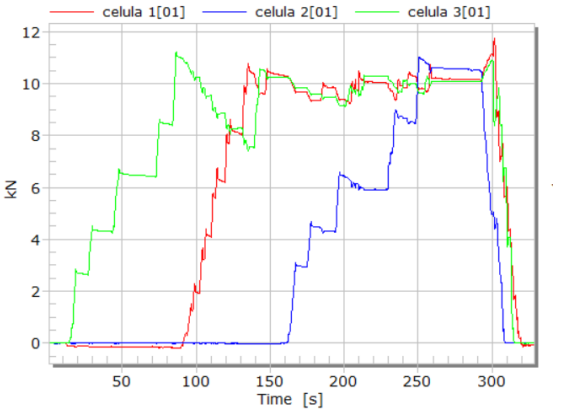

BEAM 2 – TEST 2 – Strain (µm/m)

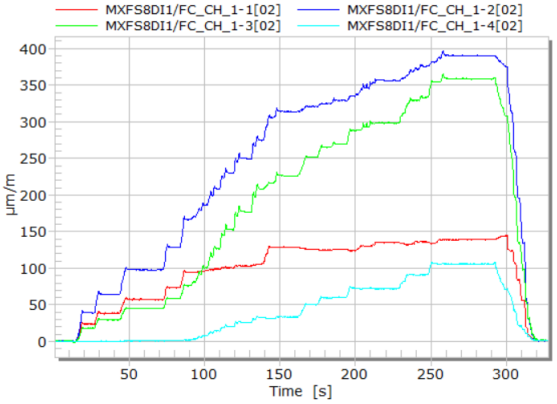

BEAM 2 – TEST 3 – Load cells (KN)

BEAM 2 – TEST 3 – Strain (µm/m)

Without removable pillars

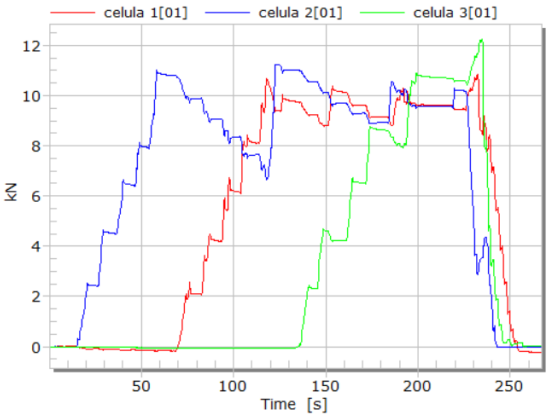

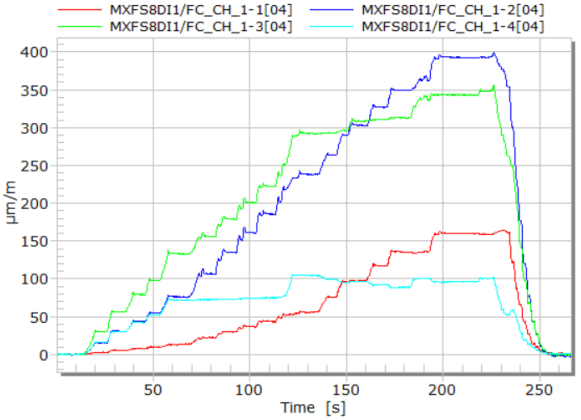

BEAM 2 – TEST 1 – Load cells (KN)

BEAM 2 – TEST 1 – Strain (µm/m)

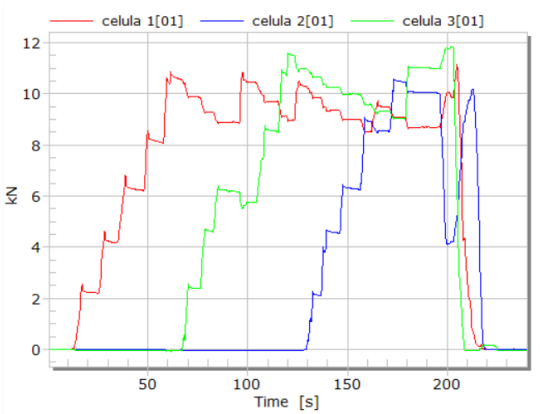

BEAM 2 – TEST 2 – Load cells (KN)

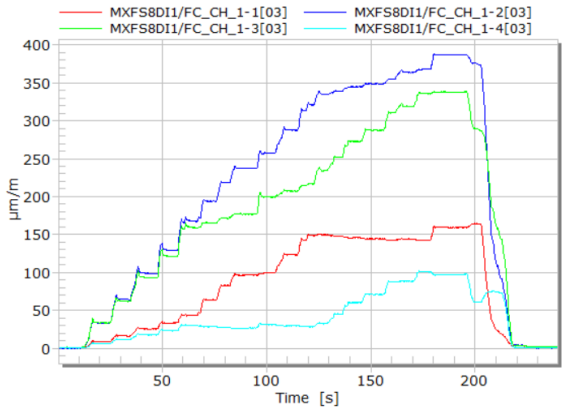

BEAM 2 – TEST 2 – Strain (µm/m)

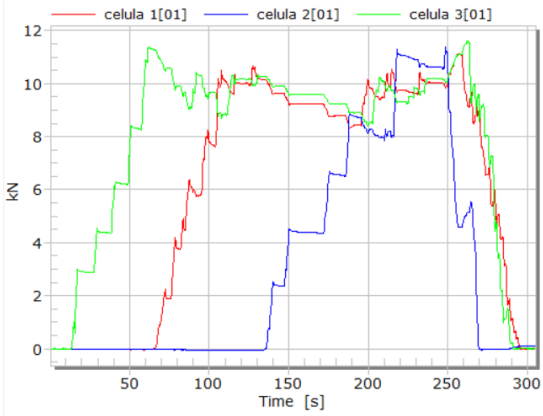

BEAM 2 – TEST 3 – Load cells (KN)

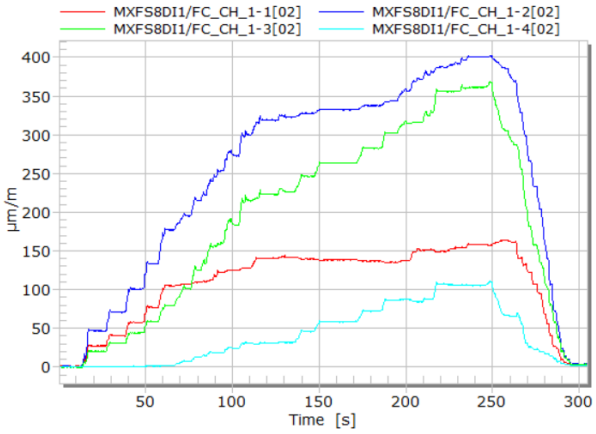

BEAM 2 – TEST 3 – Strain (µm/m)

Figure 42. Results obtained for static testing in steel beam 2

5.4.4. Dynamic behaviour – Testing

Dynamic behaviour was evaluated through vibration testing under both vertical and horizontal excitations. Optical accelerometers (FS65 type) recorded structural response at different excitation levels. The results allowed the identification of natural frequencies, damping ratios, and mode shapes, which will be later compared with FEM outputs. The acceleration response was measured with FOS accelerometers placed at critical locations:

- Vertical excitation: to identify vertical bending modes (Z axis).
- Horizontal excitation: to identify lateral or torsional modes (X axis).

The following figures show the time-history responses of the accelerometers under each excitation scenario, and for each steel beam. ACEL1 refers to the one installed at L/4 and ACEL2 refers to the one is at the middle of the beam.

STEEL BEAM 1

With removable pillars (simply supported condition)

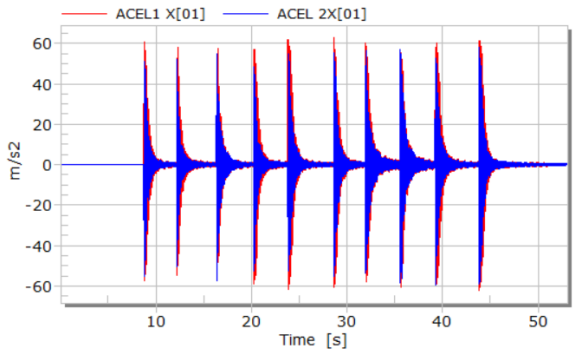

BEAM 1 – Horizontal excitation / X axis

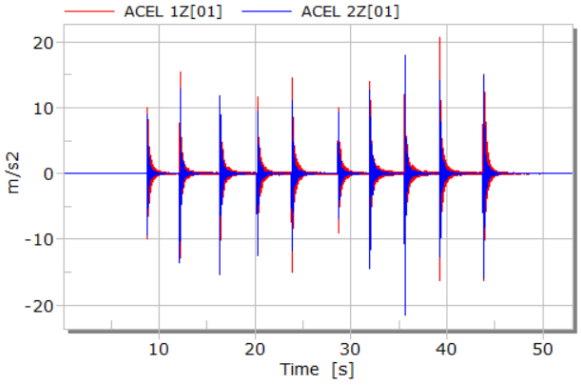

BEAM 1 – Horizontal excitation / Z axis

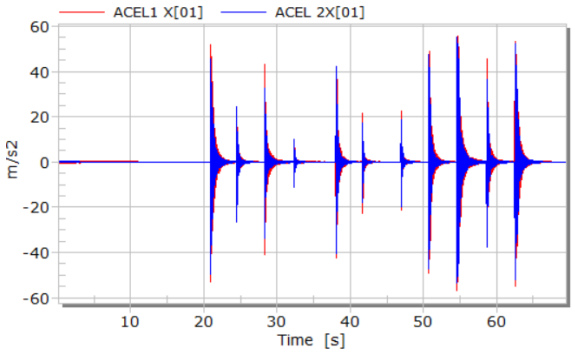

BEAM 1 – Vertical excitation / X axis

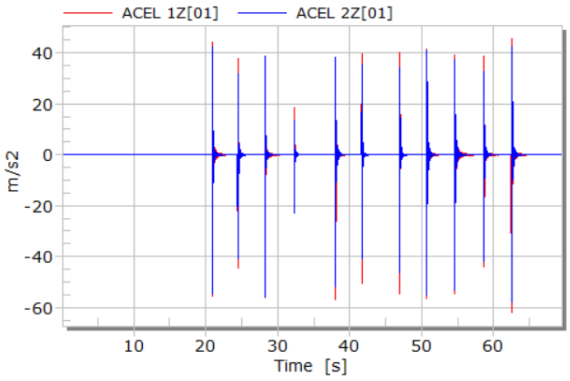

BEAM 1 – Vertical excitation / Z axis

Without removable pillars

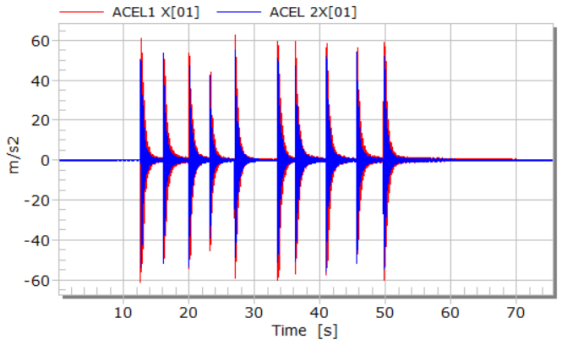

BEAM 1 – Horizontal excitation / X axis

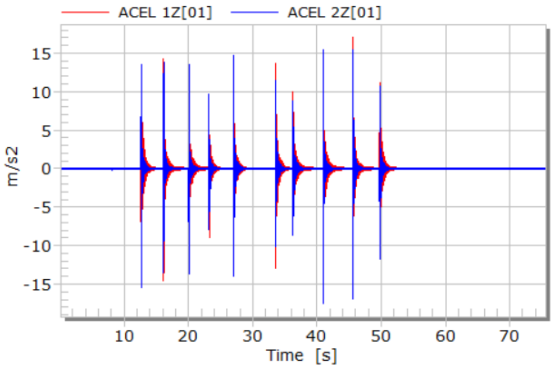

BEAM 1 – Horizontal excitation / Z axis

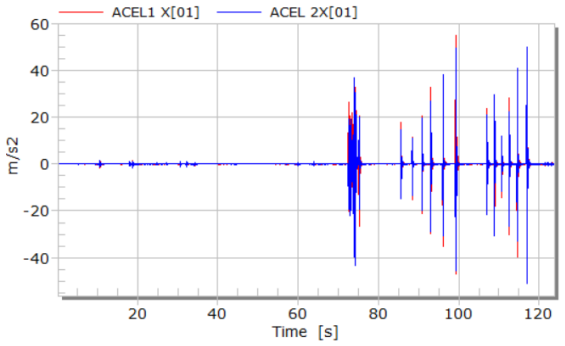

BEAM 1 – Vertical excitation / X axis

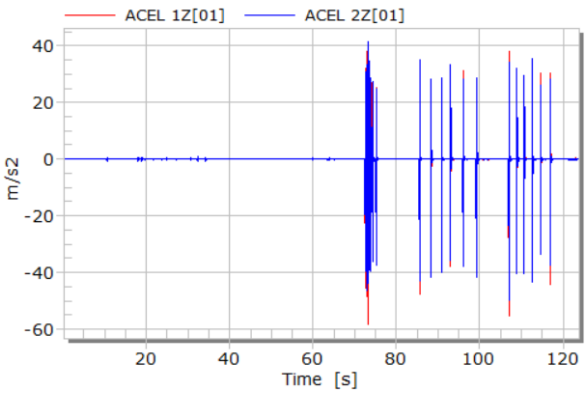

BEAM 1 – Vertical excitation / Z axis

Figure 43. Results obtained for dynamic testing in steel beam 1

STEEL BEAM 2

With removable pillars (simply supported condition)

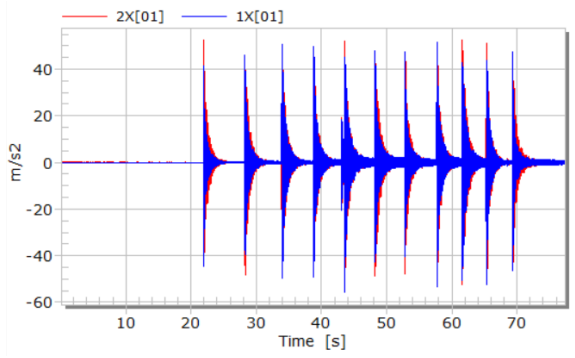

BEAM 2 – Horizontal excitation / X axis

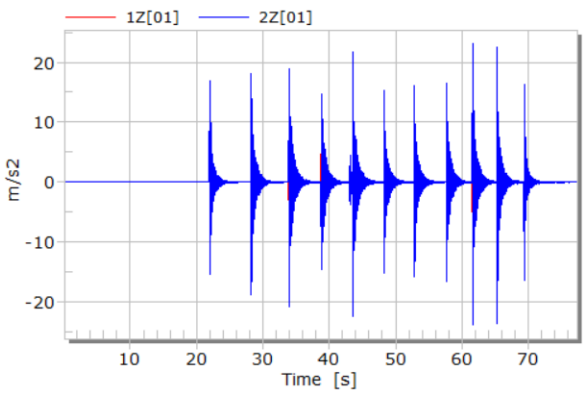

BEAM 2 – Horizontal excitation / Z axis

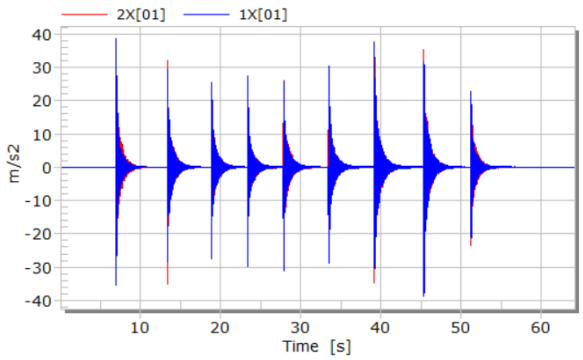

BEAM 2 – Vertical excitation / X axis

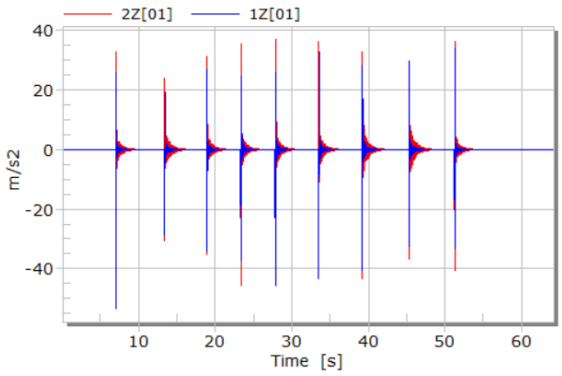

BEAM 2 – Vertical excitation / Z axis

Without removable pillars

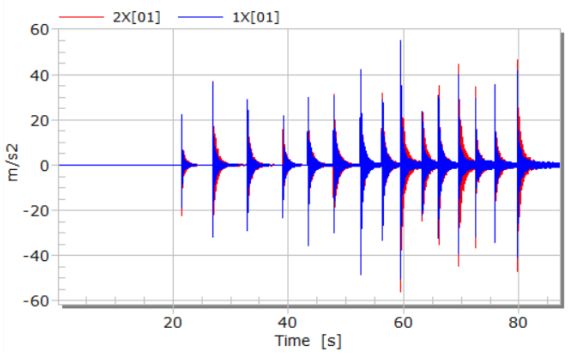

BEAM 2 – Horizontal excitation / X axis

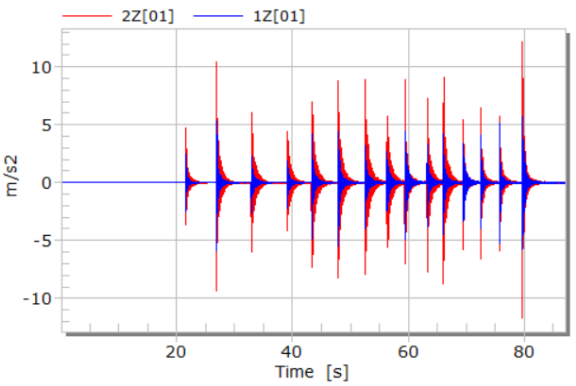

BEAM 2 – Horizontal excitation / Z axis

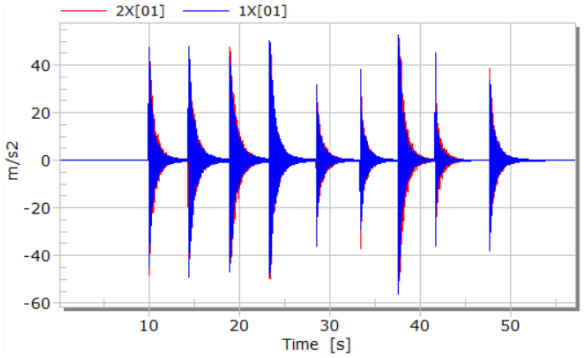

BEAM 2 – Vertical excitation / X axis

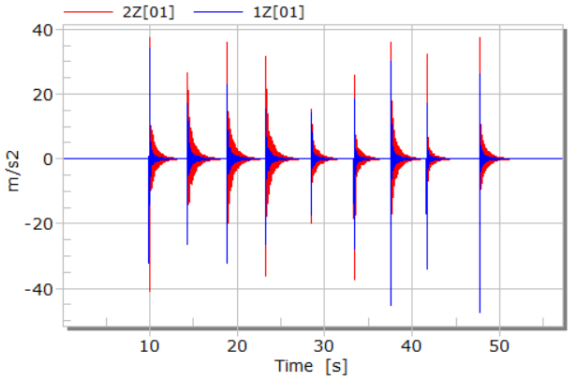

BEAM 2 – Vertical excitation / Z axis

Figure 44. Results obtained for dynamic testing in steel beam 2

5.4.5. Modal Analysis

The vibration records obtained during the dynamic tests were post-processed in the frequency domain to identify the main modal properties of the monitored structural elements. Fast Fourier Transform (FFT) analysis was applied to the acceleration time histories collected by the fibre optic system and reference accelerometers, enabling the detection of resonance frequencies and a preliminary assessment of structural condition.

Figure 45 shows the FFT corresponding to the vertical accelerations of the simply supported beam. A clear peak can be observed at approximately f_1 = 31,05 Hz, which corresponds to the fundamental bending mode of the beam. Higher-order modes appear as secondary peaks with lower amplitudes, in agreement with the expected behaviour obtained from the preliminary FEM simulations.

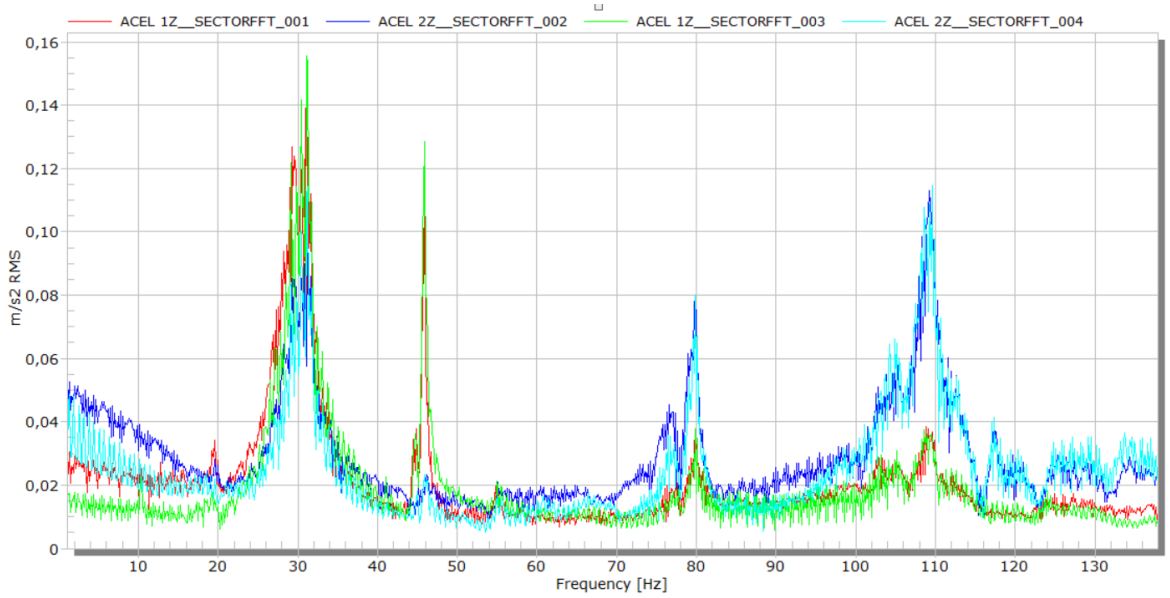

Figure 45. FFT of vertical axis vibration (composition of two vertical tests, simply supported condition).

Subsequently, FFT processing was carried out for the horizontal accelerations of the same beam, as illustrated in Figure 46. In this case, the frequency content is dominated by lower-energy peaks associated with lateral vibrations and local effects, with a first bending horizontal mode of 10.4 Hz. These results highlight the sensitivity of the horizontal axis to secondary response components, while confirming the dominance of the vertical response in capturing the global flexural behaviour of the element.

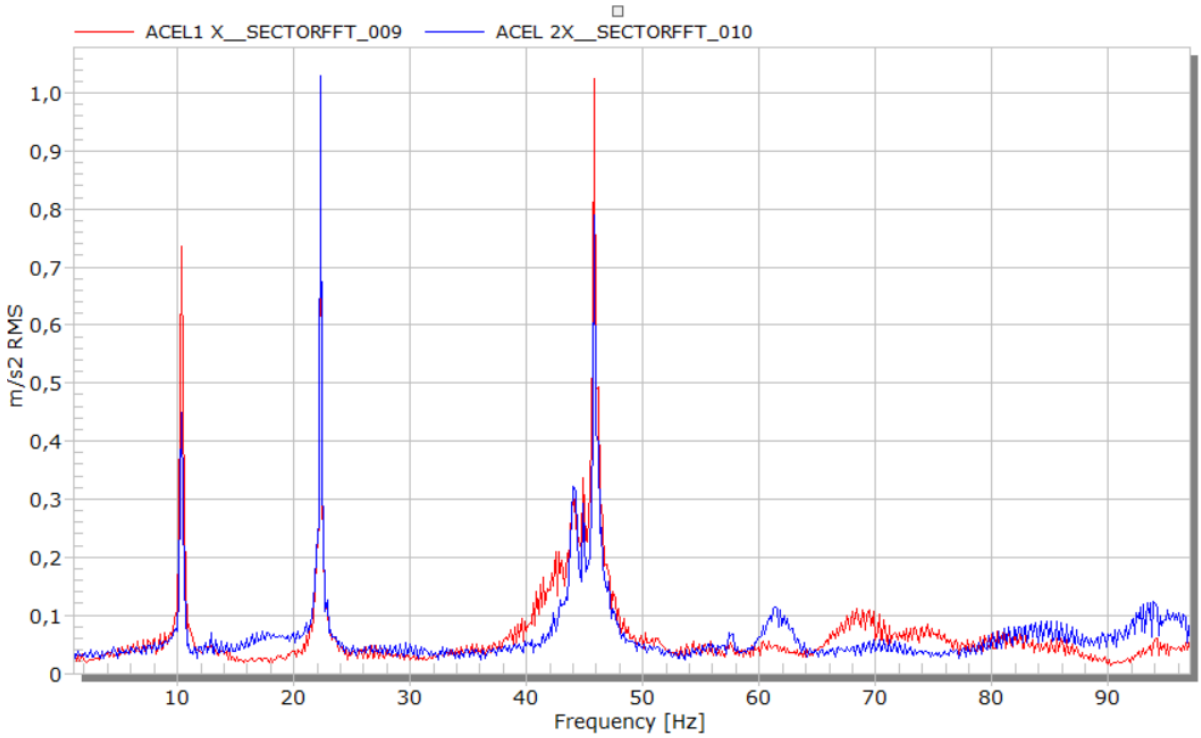

Figure 46. FFT of horizontal axis vibration (simply supported condition)

Finally, additional testing was performed in the configuration without the removable pillars, to evaluate its impact on the modal response. The corresponding FFT spectrum (Figure 47) exhibits a noisier response with less clearly defined peaks, although the main frequency content remains consistent with the tests performed with the pillars in place. Given the reduced

signal-to-noise ratio and lower reliability of the extracted modal parameters, this testing configuration was discarded for subsequent analysis.

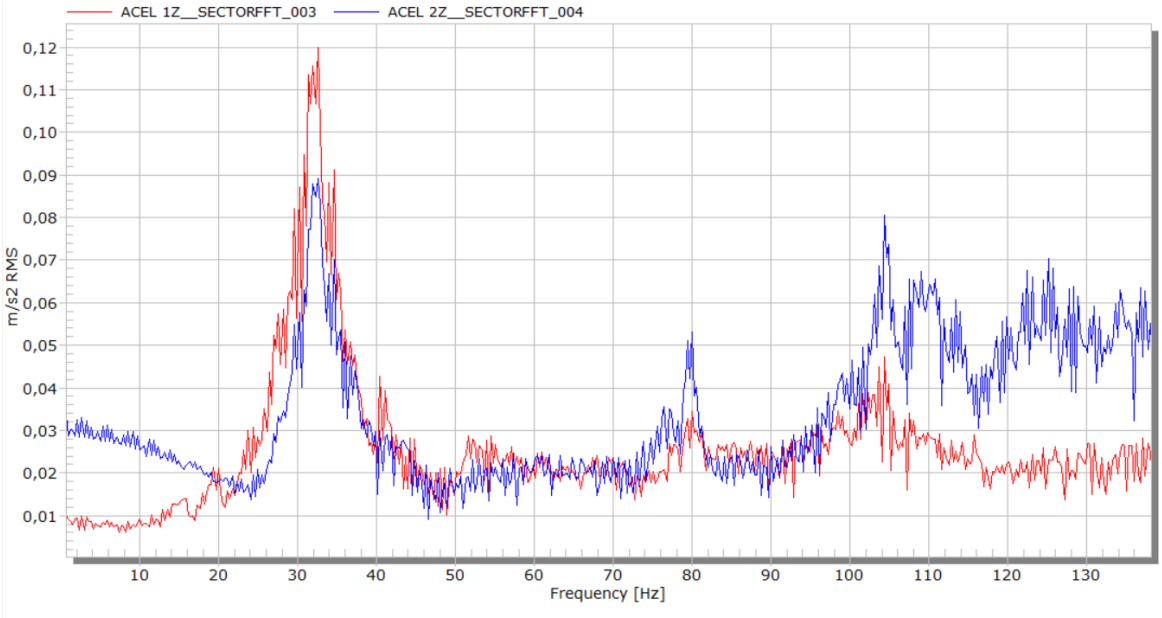

Figure 47. FFT of vertical axis vibration (composition of two vertical tests, simply supported condition).

Overall, the FFT-based modal analysis confirms the feasibility of using the developed sensing and processing approach to capture the dynamic characteristics of reinforced concrete elements under realistic boundary conditions. The identified frequencies will serve as a reference for subsequent calibration of the FEM models and for assessing stiffness degradation in future rehabilitation scenarios.

5.4.6. Labour productivity

This baseline assessment establishes current performance metrics for the scanning task through workflow documentation and comprehensive cost analysis. Table 25 describes the overall workflow and quantifies costs across five key areas: tool transport, worker transport, labour hours, operational hours, and additional expenses. This systematic analysis provides the foundational benchmark for measuring future process improvements and enables informed cost-benefit analyses for scanning operation optimization.

Table 25. FOS Labour productivity assessment

Workflow	Equipment preparation & calibration Transport to site On-site installation of sensors Data acquisition Data processing & validation
Cost – tool transport	Equipment preparation & calibration €50 Transport to site€60 (vehicle, fuel, loading) Total €110

Cost – workers transport	€40 (2 workers)
Cost – labour hours	Equipment preparation & calibration 2 h (€80) On-site installation (sensors, setup) 4 h (€160) Data acquisition (static + dynamic) 3 h (€120) Data processing & validation 3 h (€120) Total 12 h (€480)
Cost – operational hours	Equipment preparation & calibration 1 h (€40) Data acquisition (static + dynamic) 3 h (€120) Data processing & validation 2 h (€80) Total 6 h (€240)
Any other expense	Equipment preparation & calibration Adhesives, protective gear (€30) Transport to siteParking/tolls (€10) On-site installation (sensors, setup) Safety equipment (€25) Data acquisition (static + dynamic) Power supply (generator, €20) Data processing & validation Software licence (€15) Total €100

5.5. TRACLINE by TECN

5.5.1. Results

The measurement campaign combined multisensory punctual spectroscopy, RGB imaging, and hyperspectral imaging (HSI) to comprehensively characterize the CDW samples. First, punctual measurements were performed by applying matrices of acquisition points on the prepared samples. At each coordinate, the four spectrometers integrated in the TRAZIA platform—Raman, NIR, UV-Vis, and LIBS—were sequentially triggered, generating spectral signatures that capture complementary chemical and mineralogical information. Each point matrix was designed to cover representative areas of the sample surface, providing both spatial diversity and internal replicates.

In parallel, RGB images of each sample were recorded, capturing visual features such as colour, brightness, texture, and particle distribution. These images are essential for segmentation tasks, enabling individual particles to be isolated and linked with the corresponding spectral responses. To complement this dataset, hyperspectral imaging (HSI) was applied over the same sample sets. The HSI camera produced hypercubes with hundreds of contiguous spectral bands (ranging into the short-wave infrared), providing pixel-level reflectance information that combines spatial resolution with chemical specificity.

The raw outputs of each sensor were stored in structured formats:

- **Spectral data (Raman, NIR, UV-Vis, LIBS):** exported as 2D arrays (wavelength × intensity), either in .csv or .py format, with metadata including acquisition parameters and point coordinates.

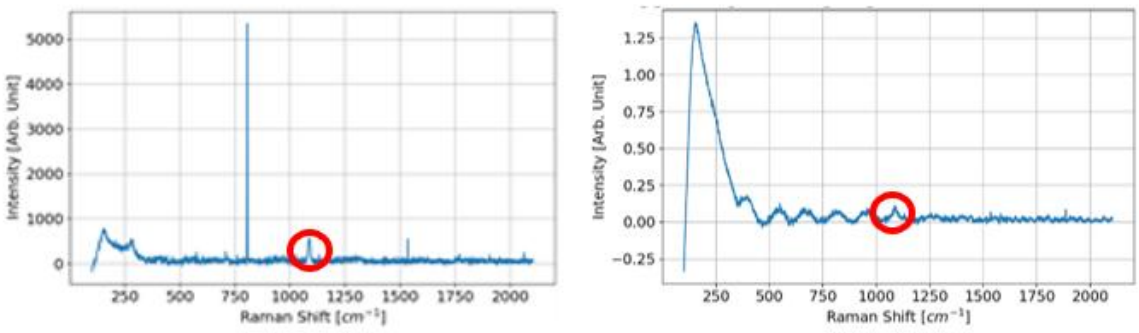

Figure 48. TRACLINE spectrometer signal examples

- **RGB images:** stored as high-resolution .tiff or .png files, associated with segmentation masks when available.

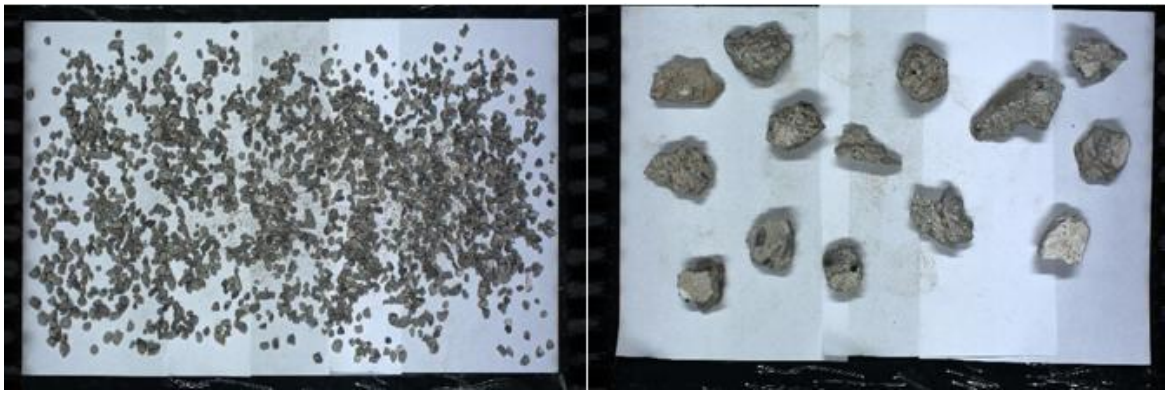

Figure 49. TRACLINE RGB examples

- **HSI cubes:** saved as .hdr/.raw or .dat files, containing full spectral information for each pixel.

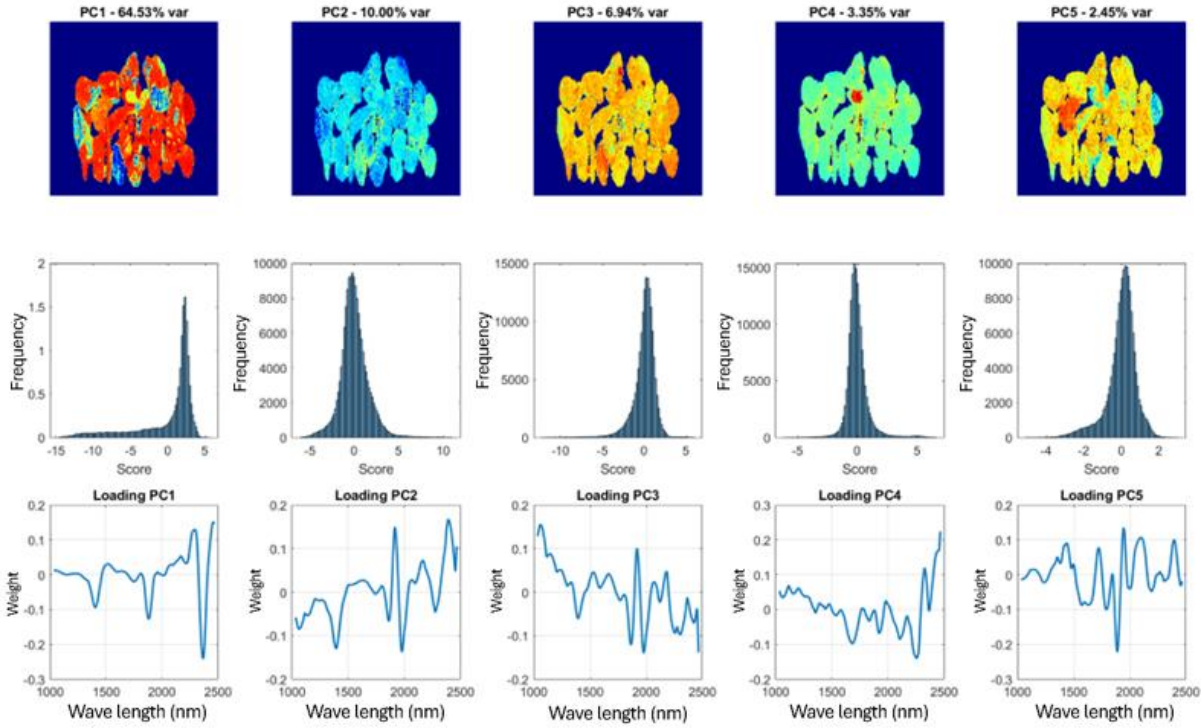

Figure 50. TRACLINE HSI hypercube analysis

After preprocessing (dark subtraction, normalization, SNV, baseline correction, clustering, etc.), the processed datasets were integrated into predictive models. The models return simplified and application-ready outputs, such as:

- Binary or multi-class masks (e.g., cement paste vs. aggregate vs. impurities).
- Numerical indicators (e.g., moisture %, intensity of characteristic peaks, elemental composition ratios).
- Confidence scores or probabilities associated with each classification.

This approach ensures that, although the raw data can be massive (thousands of spectra per sample and hundreds of spectral bands per image), the final model outputs are reduced to actionable results. The rest of the results and explanations related to them are in *D4.2_Report_on_multisensory_functional_algorithms.*

5.5.2. Labour productivity

This baseline assessment establishes current performance metrics for the scanning task through workflow documentation and comprehensive cost analysis. Table 26 describes the overall workflow and quantifies costs across five key areas: tool transport, worker transport, labour hours, operational hours, and additional expenses. This systematic analysis provides the foundational benchmark for measuring future process improvements and enables informed cost-benefit analyses for scanning operation optimization.

Table 26. TRACLINE Labour productivity assessment

Workflow	Sample preparation Laboratory analysis of the samples Equipment calibration Data acquisition Data processing & validation

Cost – labour hours	Sample preparation 16h – 640€ Laboratory analysis of the samples 17h – 680€ Equipment calibration 1h – 40€ Data acquisition (static + dynamic) 15h – 600€ Data processing & validation 15h – 600€ Total 2560€
Cost – operational hours	Equipment calibration 1h – 40€ Data acquisition (static + dynamic) 15h – 600€ Data processing & validation 15h – 600€ Total 1240€
Any other expense	Maintenance and calibrations of lenses – 2400€

Amount of time for the whole scan process

Table 27. Details about the scans with the different HW

SUM UP TIMES						
Anoeta + Jolastokieta						
	RAMAN	NIR	LIBS	UV-VIS	RGB	HSI
Acquisition time	30s	10ms	10ms	10ms	5s	-
Preprocessing time	2h	2h	4h	1h	6h	-
Number of scans	200 spectra	200 spectra	200 spectra	200 spectra	5 images	-
UTE Bajo-Añarbe + Moyua Gabierrota (61Kg)						
	RAMAN	NIR	LIBS	UV-VIS	RGB	HSI
Acquisition time	30s	10ms	10ms	10ms	5s	8h
Preprocessing time	4h	4h	6h	2h	6h	8h
Number of scans	1911 spectra	1911 spectra	1911 spectra	1911 spectra	5 images	30 images

6. Evaluation

This chapter makes a comparison with the key performance indicators and the results of this deliverable. This gives an overview of the impact we have made within this research document.

Key Performance indicator	Goal approved	Description
KPI 2: SUM4Re will address the most relevant construction entities, at least 3 different typologies of buildings (residential, tertiary & industrial) and 1 typology of infrastructure assets.	Yes	The pilot activities included different building typologies: residential and industrial (Jolastokieta current industrial area, future residential urbanization) and infrastructure (Anoeta station). This ensures that the technologies are tested across diverse use cases.
KPI 5: SUM4Re will be demonstrated through 3 case studies addressing 5Re of circularity: O7 (Reuse&Recycle), O8 (Reduce&Renovate) and O9 (Reuse&Repair), including service life extension and material banks creation.	Yes	The pilot cases focused on renovation and reuse, applying the Reduce & Renovate (O8) and Reuse & Recycle (O7) strategies. Materials from Spanish pilot buildings were characterised and reused to extend service life and contribute to material bank creation.
KPI8: The reuse of large structural components will be assessed through the structural condition index (FOS in combination with transfer learning) to detect structural alterations, reducing time for assessing mechanical behaviour by over 60%, when involving repetitive structural patterns.	To be confirmed.	FOS sensors were applied to beams for static and dynamic testing. Combined with FEM calibration and transfer learning, a preliminary indication shows that a reduction of the time required for condition assessment by more than 60% can be demonstrated in SUM4Re use cases. This statement will be proven in the next related tasks T11.1 – T12.1, demonstrating efficiency gains in evaluating large structural elements.
KPI9: One plugin to extend GENIA platform for data acquisition & integration of all the techniques included and for the assessment of structural components in accordance with their recyclability potential.	Yes	A new plugin is being developed to allow seamless integration of sensor outputs (iMMS, XRF, GPR-ECT, FOS, TRACLINE) into the GENIA platform. This will enable automated data ingestion and improved evaluation of recyclability within C-BIM workflows.
KPI10: For heterogeneous CDW composed by multiple mineral fractions, all-in-one TRACLINE will characterize material composition and mineral stream. It is composed by LIBS, Raman, RGB-D, NIR, UV. AI will be used to process (identify, quantify and classify) construction materials and assets for a C-BIM. CDW quality control process and/recycled materials with with capacity to process 1-3 t/h will be developed and tested in a real case study.	Yes	The TRACLINE prototype, combining LIBS, Raman, RGB-D, NIR, and UV sensors, was successfully deployed for classification of mixed CDW. AI models processed the data to identify, quantify, and classify materials, achieving throughput of 1–3 t/h in real case testing.

KPI 18: Reduction of 10% of time needed for circular assessment of the construction project (SUM4Re's solutions vs manual approach).	To be confirmed	The employed technologies in this use case enriched manual inspections, supporting the process of circular assessment in construction projects. The process added value through more detailed datasets, and once future tasks of this use case are completed, the full circular assessment of the construction materials will be possible to be measured the time reduction compared to baseline manual approaches.
KPI 19: Increased supply of secondary materials in pilots in 25% and reduction in construction CDW in 25% (SUM4Re's solutions vs manual).	Yes	By combining digital acquisition with material passports, the pilots will enable the recovery and reuse of secondary materials. The evaluation of KPI19 requires the completion of future WP11 tasks to be measured, with the release of the related D11.3 – CDW values.

Table 28. SUM4Re KPIs evaluation

7. Conclusions and further research

Deliverable D10.1 has demonstrated the feasibility and effectiveness of integrating advanced sensing technologies and data acquisition methodologies into SUM4Re's pilot sites. The coordinated use of iMMS/AR scanning, XRF, GPR+ECT, fibre optic sensing (FOS), and TRACLINE has provided a multi-layered dataset capturing geometry, material composition, and structural behaviour of demolition and rehabilitation environments.

The outcomes confirm several key conclusions:

- Data acquisition efficiency: Indoor Mobile Mapping Systems (iMMS) and AR-enabled HoloLens scanning proved highly efficient, delivering directly usable point clouds with minimal post-processing. When compared to traditional TLS workflows, this reduced the time and labour required for registration and alignment, accelerating the generation of BIM-ready datasets. With the GPR sensors, areas can be scanned fast within minutes to detect hidden components and layers, no cables are required, and data collection is performed via an iPad app where the acquisition software has also AR capabilities and 3D view of detected objects.
- Material characterisation: Portable XRF measurements at Anoeta Station and Jolastokieta Urbanization confirmed the capability of in situ chemical analysis for distinguishing between concrete, asphalt, masonry and metallic elements. The method provided rapid insights into heterogeneity, contamination and hazardous compounds, supporting circularity assessments at pre-demolition stages. In addition, with the GPR measurements the concrete condition (e.g. moisture content and possible voids) from the GPR responses themselves and dielectric estimations could be determined.
- Hidden elements detection: With GPR+ECT, the metallic reinforcement mesh can be identified with information regarding the location and depth. Apart from the rebar mesh, other features where identified, possibly different types of reinforcement or pipes and potential voids in the walls and floor.
- Georeferencing robustness: The successful alignment of SUM4Re point clouds with national PNOA LiDAR data underscores the potential for integrating pilot-scale datasets with national-scale repositories, thereby enhancing interoperability, traceability and scalability of SUM4Re workflows.
- Structural assessment with FOS: Fibre optic sensing demonstrated clear productivity advantages over conventional electrical instrumentation. Simplified installation, multiplexing capacity and the ability to remain attached across reuse cycles reduced both installation effort (≈40–50%) and reassessment times (>60%). This validates FOS as a transformative enabler for lifecycle-based monitoring of structural components within circular construction schemes.

Collectively, these findings reinforce the central hypothesis of SUM4Re: that multi-sensor integration can accelerate data collection, improve reliability of material and structural assessments, and enable digital workflows that underpin circular economy strategies in construction.

Despite these achievements, several challenges and research gaps remain:

- Data integration across modalities: Harmonising outputs from heterogeneous sensors (iMMS, XRF, GPR, FOS, TRACLINE) into coherent, standardised datasets suitable for C-BIM and Digital Product Passports (DPPs) remains complex. Future work should focus on automated data fusion pipelines and uncertainty quantification.
- Scalability and representativeness: While promising at pilot scale, further validation is needed across larger and more diverse infrastructures to ensure robustness under varied environmental and operational conditions.

- AI-driven interpretation: The integration of advanced machine learning models for material classification, anomaly detection and predictive maintenance is still at an early stage. Expanding training datasets and embedding uncertainty-aware algorithms will be critical.
- Standardisation and regulatory alignment: Alignment with evolving EU frameworks for circularity, waste management and digital product passports will require continuous engagement with regulatory bodies and standardisation committees.

In conclusion, Deliverable D10.1 establishes a solid baseline for SUM4Re pilot demonstrations, proving both the feasibility and added value of digital, sensor-driven approaches. The insights gained provide a foundation for subsequent tasks in WP10 and beyond, where emphasis will shift toward AI-enhanced modelling, long-term monitoring and large-scale replication. These future directions will be essential to fully realise the project's ambition of transforming demolition and rehabilitation workflows into catalysts for a circular construction economy.

BIBLIOGRAPHY

[1] Askar, C., Scheider, A., & Sternberg, H. (2023). Evaluation of a State-of-the-Art Indoor Mobile Mapping System in a Complex Indoor Environment. ZfV-Zeitschrift für Geodäsie, Geoinformation und Landmanagement, (zfv 5/2023).

[2] Sarlin, P. E., Dusmanu, M., Schönberger, J. L., Speciale, P., Gruber, L., Larsson, V., ... & Pollefeys, M. (2022, October). Lamar: Benchmarking localization and mapping for augmented reality. In European Conference on Computer Vision (pp. 686-704). Cham: Springer Nature Switzerland.

[3] Bortolon, M., Bazzanella, L., & Poiesi, F. (2021). Multi-view data capture for dynamic object reconstruction using handheld augmented reality mobiles. Journal of Real-Time Image Processing, 18(2), 345-355.

[4] Manni, A., Oriti, D., Sanna, A., De Pace, F., & Manuri, F. (2021). Snap2cad: 3D indoor environment reconstruction for AR/VR applications using a smartphone device. Computers & Graphics, 100, 116-124.

[5] Tang, R., Ma, L. F., Rong, Z. X., Li, M. D., Zeng, J. P., Wang, X. D., ... & Dong, J. H. (2018). Augmented reality technology for preoperative planning and intraoperative navigation during hepatobiliary surgery: A review of current methods. Hepatobiliary & Pancreatic Diseases International, 17(2), 101-112.

[6] Liu, H., Wu, Y., Li, A., & Deng, Y. (2024). Precision detection and identification method for apparent damage in timber components of historic buildings based on portable LiDAR equipment. Journal of Building Engineering, 98, 111050.

[7] Navares-Vázquez, J. C., Arias, P., Díaz-Vilariño, L., & Balado, J. (2024). Mixed reality head mounted displays for enhanced indoor point cloud segmentation with virtual seeds. Resilient Cities and Structures, 3(3), 43-52.

[8] Adan, A., & Huber, D. (2011, May). 3D reconstruction of interior wall surfaces under occlusion and clutter. In 2011 International Conference on 3D Imaging, Modeling, Processing, Visualization and Transmission (pp. 275-281). IEEE.

[9] Yu, X., Salimpour, S., Queralta, J. P., & Westerlund, T. (2023). General-purpose deep learning detection and segmentation models for images from a LiDAR-based camera sensor. Sensors, 23(6), 2936.

[10] Wu, S. C., Tateno, K., Navab, N., & Tombari, F. (2020, November). Scfusion: Real-time incremental scene reconstruction with semantic completion. In 2020 International Conference on 3D Vision (3DV) (pp. 801-810). IEEE.

[11] Shih, N. J., & Wu, Y. C. (2022). AR-based 3D virtual reconstruction of brick details. Remote sensing, 14(3), 748.

[12] Bock, A., Axelsson, E., Costa, J., Payne, G., Acinapura, M., Trakinski, V., ... & Ynnerman, A. (2019). OpenSpace: A system for astrographics. IEEE transactions on visualization and computer graphics, 26(1), 633-642.

[13] Directive 2008/98/EC of the European Parliament and of the Council of 19 November 2008 on waste and repealing certain Directives. Special edition in Croatian: Chapter 15 Volume 034 P. 99 – 126. https://eur-lex.europa.eu/eli/dir/2008/98/oj/eng

[14] Fundamentals of X-ray Absorption Fine Structure. Matt Newville. Consortium for Advanced Radiation Sources. University of Chicago. https://web.mit.edu/course/5/5.062/oldwww/Fall04/XAS%20Fundamentals.pdf

[15] Silicon Drift Detectors Keith Thompson, Thermo Fisher Scientific, Madison, WI, USA. https://documents.thermofisher.com/TFS-Assets/CAD/Warranties/TN52342_E_0512M_SiliconDrift_H.pdf

[16] Joshua T. Padilla, Josef Hormes, H. Magdi Selim. Use of portable XRF: Effect of thickness and antecedent moisture of soils on measured concentration of trace elements, Geoderma, Volume 337,2019, Pages 143-149, ISSN 0016-7061, https://doi.org/10.1016/j.geoderma.2018.09.022.

[17] Richard M. Roussea. Corrections for matrix effects in X-ray fluorescence analysis—A tutorial, Spectrochimica Acta Part B: Atomic Spectroscopy, Volume 61, Issue 7, 2006, Pages 759-777, ISSN 0584-8547, https://doi.org/10.1016/j.sab.2006.06.014.

[18] McComb, J.Q., Rogers, C., Han, F.X. et al. Rapid Screening of Heavy Metals and Trace Elements in Environmental Samples Using Portable X-Ray Fluorescence Spectrometer, A Comparative Study. Water Air Soil Pollut 225, 2169 (2014). https://doi.org/10.1007/s11270-014-2169-5

[19] A comparison of XRFS and ICP-OES methods for soil trace metal analyses in a mining impacted agricultural watershed. Amy L. Sikora, Lane W. Maguire, Robert W. Nairn, Robert C. Knox. https://link.springer.com/content/pdf/10.1007/s10661-021-09275-9.pdf

[20] Roozbeh Ravansari, Susan C. Wilson, Matthew Tighe, Portable X-ray fluorescence for environmental assessment of soils: Not just a point and shoot method, Environment International, Volume 134, 2020, 105250, ISSN 0160-4120, https://doi.org/10.1016/j.envint.2019.105250.

[21] Nevenka Mijatović, Anja Terzić, Lato Pezo, Ljiljana Miličić, Dragana Živojinović. Validation of energy-dispersive X-ray fluorescence procedure for determination of major and trace elements present in the cement based composites, Spectrochimica Acta Part B: Atomic Spectroscopy, Volume 162, 2019, 105729, ISSN 0584-8547, https://doi.org/10.1016/j.sab.2019.105729.

[22] José Vinícius Ribeiro, Tiago Rodrigues Tavares, José Francirlei de Oliveira, Graziela M.C. Barbosa, Fábio Luiz Melquiades, Impact of calibration set size for predicting soil fertility attributes using local pXRF spectral libraries, Soil Advances, Volume 3, 2025, 100031, ISSN 2950-2896, https://doi.org/10.1016/j.soilad.2024.100031.

[23] Lobo, A.; Garcia, E.; Barroso, G.; Martí, D.; Fernandez-Turiel, J.-L.; Ibáñez-Insa, J. Machine Learning for Mineral Identification and Ore Estimation from Hyperspectral Imagery in Tin–Tungsten Deposits: Simulation under Indoor Conditions. *Remote Sens.* **2021**, *13*, 3258. https://doi.org/10.3390/rs13163258

[24] Bardia Yousefi, Clemente Ibarra Castanedo, Xavier P.V. Maldague, Georges Beaudoin, Assessing the reliability of an automated system for mineral identification using LWIR Hyperspectral Infrared imagery, Minerals Engineering, Volume 155, 2020, 106409, ISSN 0892-6875, https://doi.org/10.1016/j.mineng.2020.106409.

[25] Inaudi, D. & Glisic, B. (2010). Long-range pipeline monitoring by distributed fibre optic sensing. Journal of Pressure Vessel Technology.

[26] Measures, R. (2001). Structural Monitoring with Fiber Optic Technology. Academic Press.

[27] Kinet, D. et al. (2014). Fiber Bragg Grating Sensors toward Structural Health Monitoring in Composite Materials. Sensors.

[28] Liu, Q. et al. (2021). Ultra-weak FBG arrays for large-scale strain monitoring. Optics Express.

[29] Henault, J.M. et al. (2012). Quantitative strain measurement and crack detection in RC structures using DFOS. Sensors.

[30] Bao, X. & Chen, L. (2012). Recent progress in Brillouin scattering based fibre sensors. Sensors.

[31] Hartog, A.H. (2017). An Introduction to Distributed Optical Fibre Sensors. CRC Press.

[32] Dervilis, N. et al. (2015). Machine learning in SHM: challenges and opportunities. Philosophical Transactions of the Royal Society A.

[33] Bassil, A. et al. (2019). Durability of optical fibres embedded in concrete. Cement and Concrete Composites.

[34] Glisic, B. & Inaudi, D. (2007). Fibre Optic Methods for Structural Health Monitoring. Wiley.

[35] Li, C. et al. (2021). Big data analytics for DFOS in civil engineering. Automation in Construction.

[36] IEEE Standard 2067-2021. IEEE Standard for Fiber Bragg Grating Sensors.

[37] https://www.hbm.com/es/8427/interrogador-optico-quantumx-mxfs/?product_type_no=Interrogador%20%C3%B3ptico%20QuantumX%20MXFS

[38] Daniels, D. J. (2004). Ground penetrating radar, 2nd edition. The Institution of Engineering and Technology

[39] Solla, M., Novo, A., Elseicy, A. & Prego, J. F. (2024). Rebar detection: Comparison of stepped frequency continuous wave and pulsed GPR. Procedia Structural Integrity, vol.64, 293-300.

[40] Goodman, D., Piro, S. (2013). Multi-channel GPR. In: GPR Remote Sensing in Archaeology. Geotechnologies and the Environment, vol 9. Springer, Berlin, Heidelberg.

[41] Faris, N. et al. (2024). Automated rebar recognition and corrosion assessment of concrete bridge decks using ground penetrating radar. Automation in Construction.

[42] Warren, C., Giannopoulos, A., & Giannakis, I. (2016). gprMax: Open source software to simulate electromagnetic wave propagation for Ground Penetrating Radar. In Computer Physics Communications, 209, 163-170

[43] Patsia, O., Giannopoulos, A. & Giannakis, I. (2023). Background Removal, Velocity Estimation, and Reverse-Time Migration: A Complete GPR Processing Pipeline Based on Machine Learning. In IEEE Transactions on Geoscience and Remote Sensing, vol. 61, 1-11.

[44] Elseicy, A., Solla, M. and Novo, A. (2025). Preliminary Study on Automating Rebar Detection in Reinforced Concrete Structures Using YOLOv11 and GPR Data. In the 13th International Workshop on Advanced Ground Penetrating Radar (IWAGPR), Thessaloniki, Greece, 2025, pp. 1-6

SUM4Re

Creating materials banks
from digital urban mining

APPENDICES

Funded by the European Union. Views and opinions expressed are however those of the author(s) only and do not necessarily reflect those of the European Union. Neither the European Union nor the granting authority can be held responsible for them.

Funded by
the European Union

LIST OF APPENDICES

APPENDIX A : XRF results

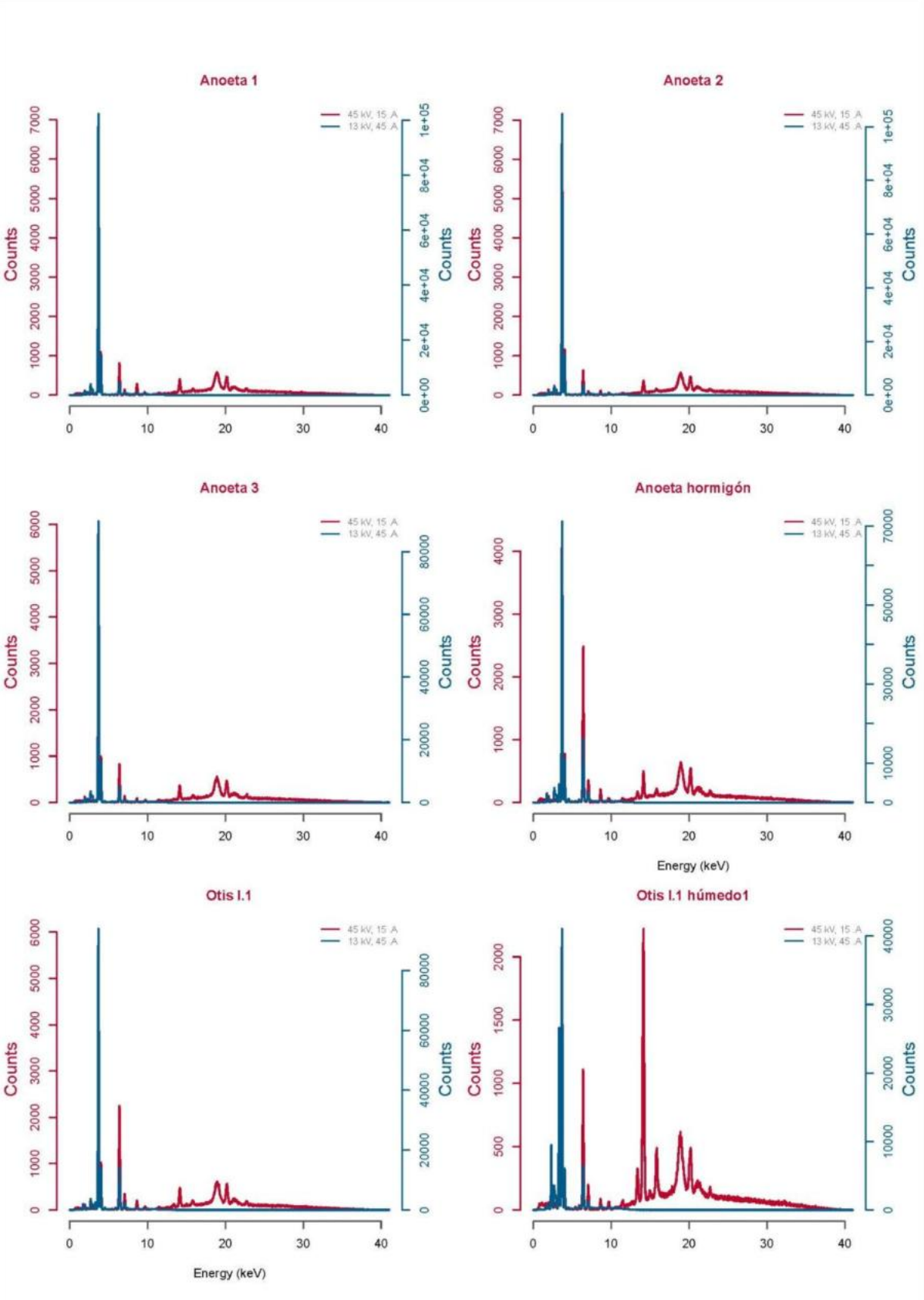

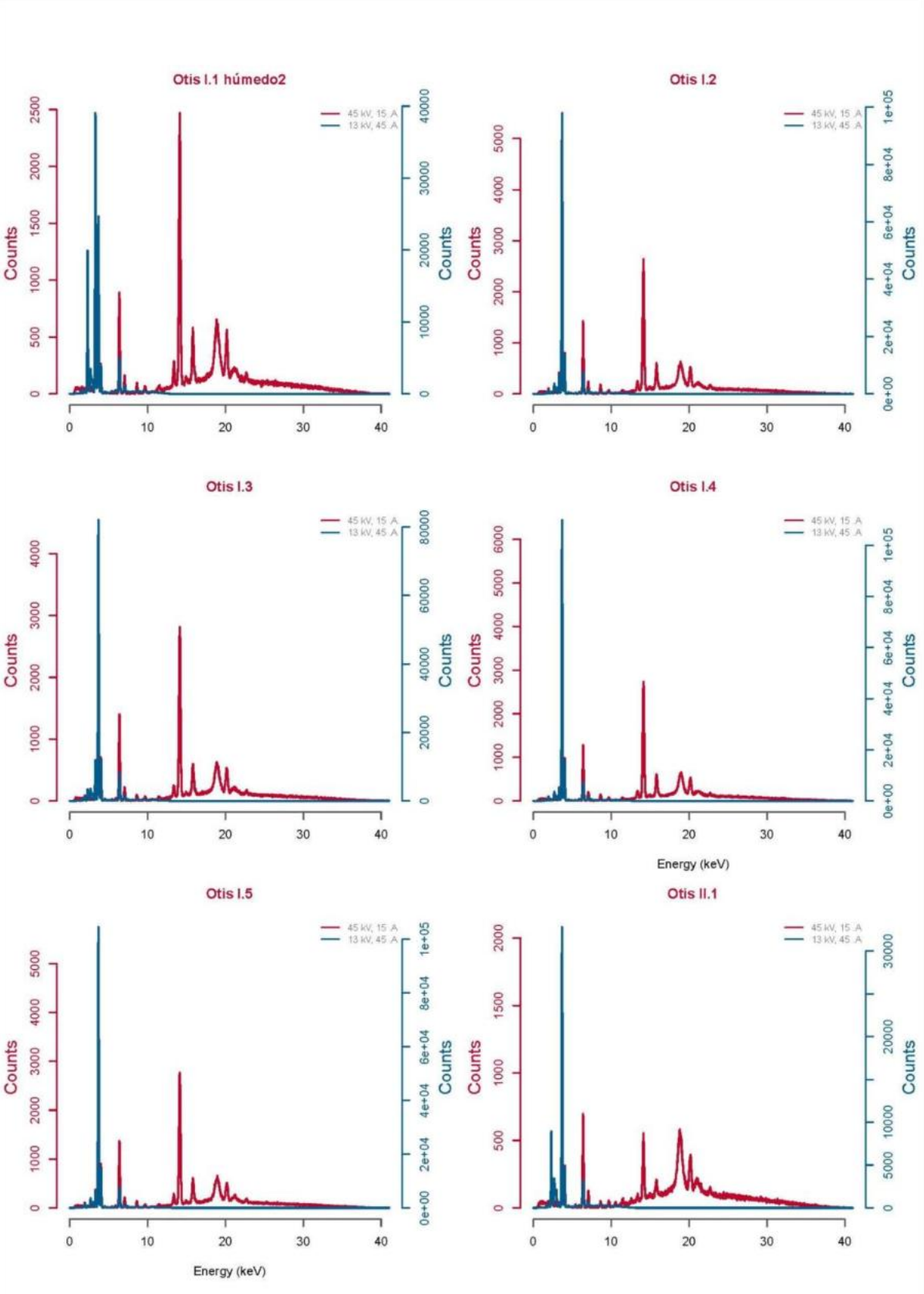
Otis I.1 húmedo2
Otis I.2
Otis I.3
Otis I.4
Otis I.5
Otis II.1
45 kV, 15 A
13 kV, 45 A
Counts
Energy (keV)

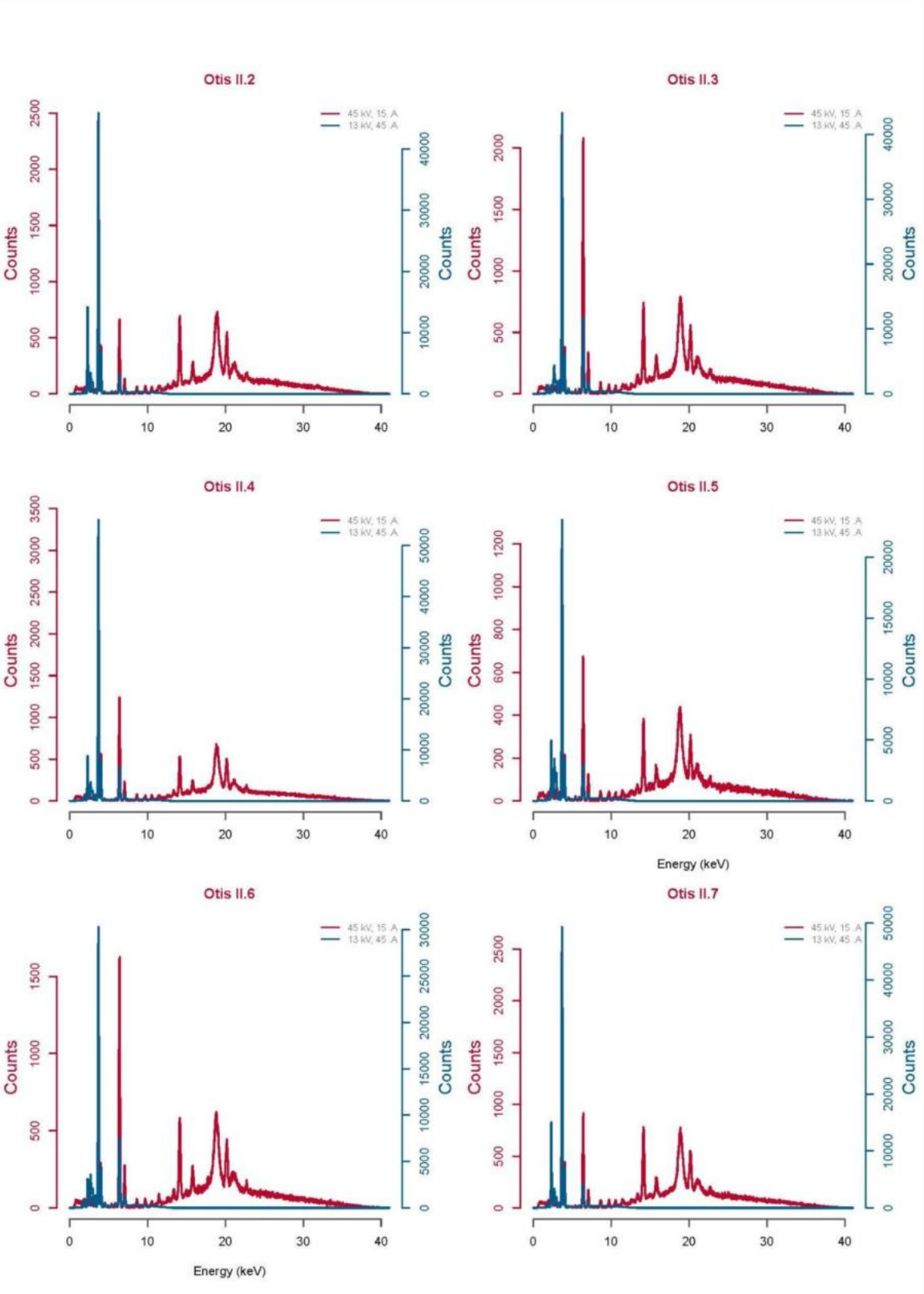
Otis II.2
Otis II.3
Otis II.4
Otis II.5
Otis II.6
Otis II.7
45 kV, 15 .A
13 kV, 45 .A
Counts
Energy (keV)

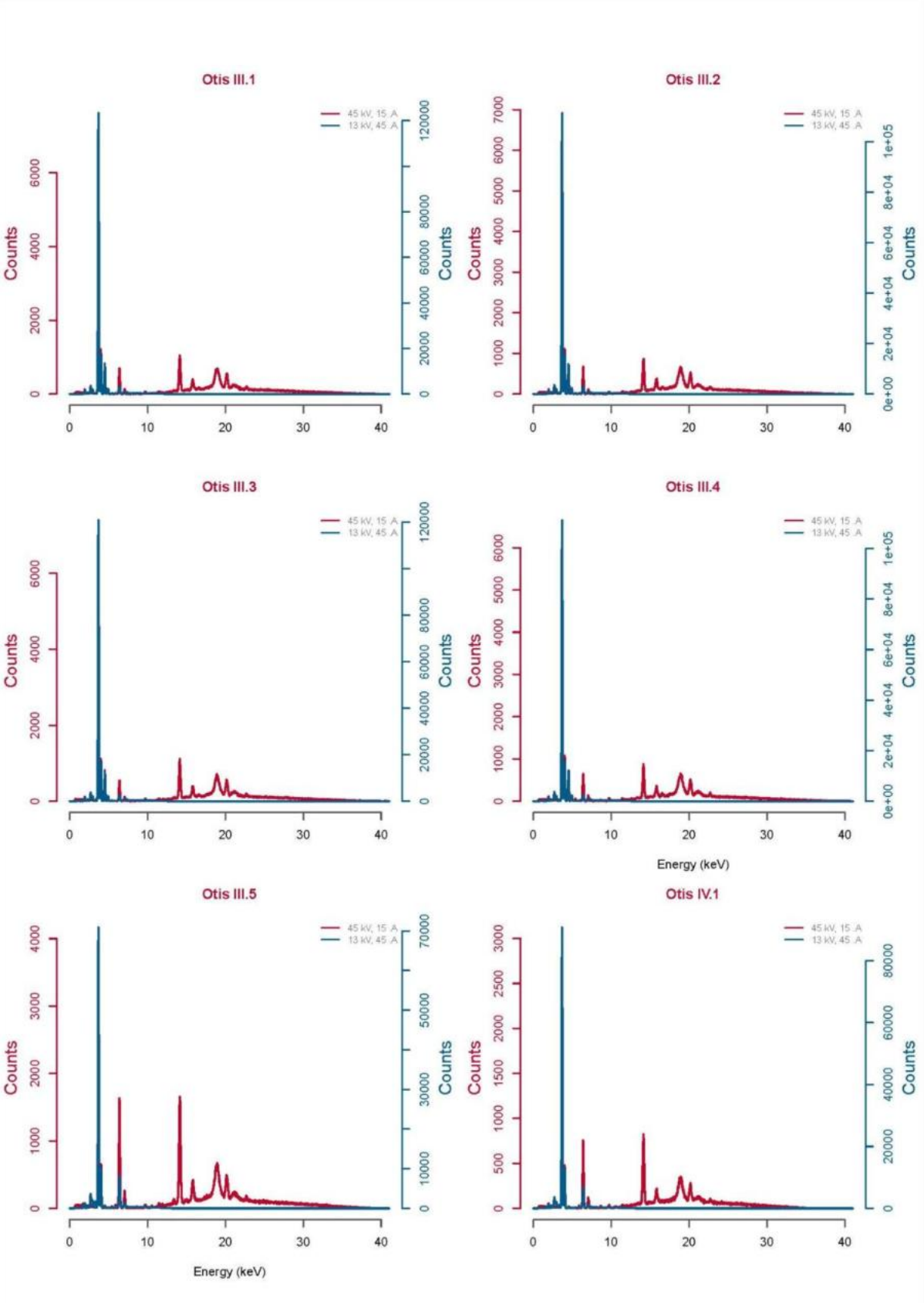

Figure A-1 XRF spectra of the measurements done on the pilot site

SUM4Re

Creating materials banks
from digital urban mining

www.sum4re.eu sum4re@uvigo.gal SUM4Re SUM4Re_EU

Funded by the European Union. Views and opinions expressed are however those of the author(s) only and do not necessarily reflect those of the European Union. Neither the European Union nor the granting authority can be held responsible for them.

Funded by the European Union